DESIGN OF BENCH-SCALE METHANE PROCESSING REACTORS FOR HYDROGEN-DRIVEN PEM FUEL CELLS

by

Emre Maşalacı

B.S., Chemical Engineering, Istanbul Technical University, 2005

Submitted to the Institute for Graduate Students in
Science and Engineering in partial fulfilment of
the requirements for the degree of
Master of Science

Graduate Program in Chemical Engineering

Boğaziçi University

2007

DESIGN OF BENCH-SCALE METHANE PROCESSING REACTORS FOR HYDROGEN-DRIVEN PEM FUEL CELLS

APPROVED BY:

Prof. Zeynep İlsen Önsan ……
(Thesis Supervisor)

Assist. Prof. Ahmet Kerim Avcı ……
(Thesis Co-Supervisor)

Prof. Ayşe Nilgün Akın ……

Prof. Mehmet C. Çamurdan ……

Assoc. Prof. Ramazan Yıldırım ……

DATE OF APPROVAL: …….

dedicated to

my family

ACKNOWLEDGEMENTS

I would like to express my sincere gratitude to my thesis supervisors, Professor Zeynep İlsen Önsan and Assistant Professor Ahmet Kerim Avcı for their invaluable guidance and understanding in me. I would like to mention their patience to my questions, giving me hope when I was stuck at dead-ends. It was a great opportunity for me to work with them on catalysis and reactor engineering.

I would like to thank Mustafa Karakaya who shares his scientific background with me. I would also thank to Özgür Tan, my best friend during my undergraduate and graduate education, for his friendship and partnership who provided a great deal of support in this project.

I would also like to thank to my permanent friends from Saint Joseph; Burak Evren, Onur Kürüm and Deniz Bolayır, also my sister Burcu Maşalacı for their friendship and morale support before and during my graduate education.

Finally I have to express my infinite thanks to my family who gives all their moral and material support. Their patience and encouragement provided me the courage of being an engineer.

The financial support for this research was provided by TÜBİTAK through project 104M163 and by Boğaziçi University Research Fund (BAP) through project 06HA501.

ABSTRACT

DESIGN OF BENCH-SCALE METHANE PROCESSING REACTORS FOR HYDROGEN-DRIVEN PEM FUEL CELLS

The steady state behaviour of conversion of methane to hydrogen in the fuel processor system is investigated using computer-based modeling/simulation techniques for use in small scale fuel cell applications. The fuel processor system is consisted of a catalytic indirect partial oxidation reactor, (combined of total oxidation, steam reforming and water gas shift reactions), a water-gas shift converter, and a preferential oxidation reactor. Steady-state simulation and sizing of packed-bed tubular type reactors are carried out for six different feed ratio configurations: ((methane/oxygen, steam/methane) = (2.24, 1.17), (1.89, 1.56))/PEMFC power output (10, 50, 100 W). Material balance calculations have been carried out to obtain boundary conditions used in the reactor simulations which have been carried out using one-dimensional pesudohomogeneous reactor model. The model equations give the size of reactors in terms of catalyst weight. Reactor dimensions and catalyst particle diameter are then estimated by using a set of criteria to quantify intraparticle mass and interfacial heat transfer resistances and flow behaviour in packed beds. Total pressure change along the reactor tube is also checked such that the dimensions do not lead to excessive pressure drop. At both feed compositions, catalyst quantity in each reactor is found to increase linearly with respect to power output size of PEMFC. Consequently, lengths and diameters for IPOX, WGS and PROX reactors are also observed to increase with growing PEMFC output. Total reactor volumes to operate 10, 50, 100 W of PEM fuel cell, are estimated to be 7.36 cm^3, 38.05 cm^3, 83.52 cm^3 respectively. In addition, a bench scale laboratory prototype to operate 10W PEMFC has been proposed using simulation results.

ÖZET

HİDROJENLİ PEM TİPİ YAKIT PİLİ İÇİN METAN DÖNÜŞMELİ REAKTÖRLERİN LABORATUVAR ÖLÇEKLİ TASARIMI

Küçük ölçekli yakıt pili uygulamalarında kullanmak üzere metan gazının yakıt dönüşüm sisteminde hidrojene dönüşümünün durağan davranışı bilgisayar destekli modelleme/benzetim yöntemleriyle incelenmiştir. Yakıt dönüşüm sistemi dolaylı kısmi oksidasyon (toplam oksidasyon + buhar reformlama) reaktörü, su-gazı değişim reaktörü ve seçimli karbon monoksit oksidasyon reaktöründen oluşmaktadır. Dolgulu yataklı tipte ve tüp şeklinde olduğu kabul edilen reaktörlerin kararlı durum benzetimleri ve boyutlandırılmaları altı değişik besleme oranı ((metan/oksijen, buhar/metan) = (2.24, 1.17), (1.89, 1.56))/yakıt pili çıkış gücü (10, 50, 100 W) düzeninde yapılmıştır. Reaktörlerin boyutlarının katalizör miktarı cinsinden bulunmasıyla sonuçlanan reaktör benzetimlerinde kullanılacak sınır değerlerini elde etmek amacıyla kütle dengesi hesaplamaları yürütülmüştür. Modelleme ve benzetim çalışmaları bir boyutlu türdeş reaktör modeli kullanılarak yapılmıştır. Uzunluk cinsinden reaktör boyutları ve katalizör parçacığının çapı, katalizör parçacığının içindeki kütle iletimini, akışkan ve katalizör arayüzündeki ısı iletimini, ve dolgulu yataklı reaktörlerdeki akış rejimini belirleyen kriterler kullanılarak bulunmuştur. Boyutlandırmanın aşırı basınç düşüşüne sebep olmaması için reaktör tüpü boyunca toplam basınç değişimi ayrıca kontrol edilmiştir. İki farklı besleme oranı için ve bütün reaktörlerde katalizör miktarının PEM tipi yakıt pili nin gücüyle doğrusal olarak arttığı bulunmuştur. Bunun sonucu olarak, her reaktörün uzunluk ve çap değerlerinin de artan yakıt pili gücüyle birlikte arttığı gözlemlenmiştir. 10, 50 ve 100W lık yakıt pillerini çalıştaracak toplam reaktör hacimleri 7.36 cm^3, 38.05 cm^3, 83.52 cm^3 olarak hesaplanmıştır. Bunun yanısıra benzetim sonuçları kullanılarak 10W lık yakıt pilini çalıştırmak üzere laboratuvar ölçekli bir esas model önerilmiştir.

TABLE OF CONTENTS

ACKNOWLEDGMENTS iv
ABSTRACT v
ÖZET vi
LIST OF FIGURES ix
LIST OF TABLES xiii
LIST OF SYMBOLS/ABBREVATIONS xix
1. INTRODUCTION 1
2. LITERATURE SURVEY 4
2.1. Fuel Cell Technology 4
2.1.1. Fuel Cell Operation 4
2.1.2. PEM Fuel Cells 5
2.2. Methane-to-hydrogen conversion routes for driving PEM fuel cells 7
2.2.1. Thermal Cracking 9
2.2.2. Steam Reforming 10
2.2.3. Partial Oxidation 11
2.3. Partial Oxidation 12
2.3.1. Direct Partial Oxidation 12
2.3.2. Indirect Partial Oxidation 13
2.3.2.1. Catalysts 15
2.3.2.2. Reaction Kinetics 17
2.4. Water-Gas Shift Reaction 21
2.4.1. Catalysts 22
2.4.2. Kinetics 23
2.5. Selective CO Oxidation in H_2-Rich Streams 25
2.5.1. Catalysts 27
2.5.2. Reaction Kinetics 29
3. FUEL PROCESSOR DESIGN AND MOLE BALANCE CALCULATIONS . . . 32
3.1. Fuel Processor Design 32
3.1.1. Fuel Processor System 32

3.1.2. Temperatures and Stream Properties 36
3.2. Mole balance Calculations 37
3.2.1. Mole balance Assumptions 44
3.2.2. Mole balance results 45
4. STEADY-STATE MODELING AND SIMULATION OF REACTORS 53
4.1. Modeling of the Fuel Processor System 53
4.1.1. Modeling Procedure 53
4.1.1.1. Rate Equations 53
4.1.1.2. Model Equations 56
4.1.1.3. Equations for Heat and Mass Transfer Criteria 58
4.1.2. Computational Results 61
4.1.2.1. Results for 10W PEMFC 62
4.1.2.2. Results for 50W PEMFC 70
4.1.2.3. Results for 100W PEMFC 78
4.1.3. Discussion 86
4.2.Reactor Sizing 88
4.2.1. Sizing for 10W PEMFC 89
4.2.2. Sizing for 50W PEMFC 92
4.2.3. Sizing for 100W PEMFC 95
4.3. Results and Discussions 98
5. PROPOSAL FOR BENCH SCALE LABORATORY PROTOTYPE 103
5.1. Description of the Prototype System 103
5.2. Proposed Bench-Scale Fuel Processor System 106
6. CONCLUSIONS AND RECOMMENDATIONS 110
6.1. Conclusions 110
6.2. Recommendations 111
APPENDIX A: PHYSICAL PROPERTIES OF THE SPECIES 113
REFERENCES 114

LIST OF FIGURES

Figure 2.1. Fuel Cell operation 5

Figure 2.2. CO Effect over PEMFC performance 6

Figure 2.3. Performance comparisons of PEMFC anodes and cathodes 7

Figure 3.1. Fuel processor system 32

Figure 4.1. Temperature profile along IPOX reactor for CH_4/O_2=1.89, H_2O/CH_4=1.56 at 10W PEMFC 63

Figure 4.2. Flow rates along IPOX reactor for CH_4/O_2=1.89, H_2O/CH_4=1.56 at 10W PEMFC 63

Figure 4.3. Temperature profile along WGS reactor for CH_4/O_2=1.89, H_2O/CH_4=1.56 at 10W PEMFC 64

Figure 4.4. Flow rates along WGS reactor for CH_4/O_2=1.89, H_2O/CH_4=1.56 at 10W PEMFC 64

Figure 4.5. Temperature profile along PROX reactor for CH_4/O_2=1.89, H_2O/CH_4=1.56 at 10W PEMFC 65

Figure 4.6. Flow rates along PROX reactor for CH_4/O_2=1.89, H_2O/CH_4=1.56 at 10W PEMFC 65

Figure 4.7. Temperature profile along IPOX reactor for CH_4/O_2=2.24, H_2O/CH_4=1.17 at 10W PEMFC 67

Figure 4.8. Flow rates along IPOX reactor for CH_4/O_2=2.24, H_2O/CH_4=1.17 at 10W PEMFC 67

Figure 4.9. Temperature profile along WGS reactor for CH_4/O_2=2.24, H_2O/CH_4=1.17at 10W PEMFC 68

Figure 4.10. Flow rates along WGS reactor for CH_4/O_2=2.24, H_2O/CH_4=1.17 at 10W PEMFC 68

Figure 4.11. Temperature profile along PROX reactor for CH_4/O_2=2.24, H_2O/CH_4=1.17 at 10W PEMFC 69

Figure 4.12. Flow rates along PROX reactor for CH_4/O_2=2.24, H_2O/CH_4=1.17 at 10W PEMFC 69

Figure 4.13. Temperature profile along IPOX reactor for CH_4/O_2=1.89, H_2O/CH_4=1.56 at 50W PEMFC 71

Figure 4.14. Flow rates along IPOX reactor for CH_4/O_2=1.89, H_2O/CH_4=1.56 at 50W PEMFC 71

Figure 4.15. Temperature profile along WGS reactor for CH_4/O_2=1.89, H_2O/CH_4=1.56 at 50W PEMFC 72

Figure 4.16. Flow rates along WGS reactor for CH_4/O_2=1.89, H_2O/CH_4=1.56 at 50W PEMFC 72

Figure 4.17. Temperature profile along PROX reactor for CH_4/O_2=1.89, H_2O/CH_4=1.56 at 50W PEMFC 73

Figure 4.18. Flow rates along PROX reactor for CH_4/O_2=1.89, H_2O/CH_4=1.56 at 50W PEMFC 73

Figure 4.19. Temperature profile along IPOX reactor for CH_4/O_2=2.24, H_2O/CH_4=1.17 at 50W PEMFC 75

Figure 4.20. Flow rates along IPOX reactor for CH_4/O_2=2.24, H_2O/CH_4=1.17 at 50W PEMFC 75

Figure 4.21. Temperature profile along WGS reactor for CH_4/O_2=2.24, H_2O/CH_4=1.17at 50W PEMFC 76

Figure 4.22. Flow rates along WGS reactor for CH_4/O_2=2.24, H_2O/CH_4=1.17 at 50W PEMFC 76

Figure 4.23. Temperature profile along PROX reactor for CH_4/O_2=2.24, H_2O/CH_4=1.17 at 50W PEMFC 77

Figure 4.24. Flow rates along PROX reactor for CH_4/O_2=2.24, H_2O/CH_4=1.17 at 50W PEMFC 77

Figure 4.25. Temperature profile along IPOX reactor for CH_4/O_2=1.89, H_2O/CH_4=1.56 at 100W PEMFC 79

Figure 4.26. Flow rates along IPOX reactor for CH_4/O_2=1.89, H_2O/CH_4=1.56 at 100W PEMFC 79

Figure 4.27. Temperature profile along WGS reactor for CH_4/O_2=1.89, H_2O/CH_4=1.56 at 100W PEMFC 80

Figure 4.28. Flow rates along WGS reactor for CH_4/O_2=1.89, H_2O/CH_4=1.56 at 100W PEMFC 80

Figure 4.29. Temperature profile along PROX reactor for CH_4/O_2=1.89, H_2O/CH_4=1.56 at 100W PEMFC 81

Figure 4.30. Flow rates along PROX reactor for CH_4/O_2=1.89, H_2O/CH_4=1.56 at 100W PEMFC 81

Figure 4.31. Temperature profile along IPOX reactor for CH_4/O_2=2.24, H_2O/CH_4=1.17 at 100W PEMFC 83

Figure 4.32. Flow rates along IPOX reactor for CH_4/O_2=2.24, H_2O/CH_4=1.17 at 100W PEMFC 83

Figure 4.33. Temperature profile along WGS reactor for CH_4/O_2=2.24, H_2O/CH_4=1.17at 100W PEMFC 84

Figure 4.34. Flow rates along WGS reactor for CH_4/O_2=2.24, H_2O/CH_4=1.17 at 100W PEMFC 84

Figure 4.35. Temperature profile along PROX reactor for CH_4/O_2=2.24, H_2O/CH_4=1.17 at 100W PEMFC 85

Figure 4.36. Flow rates along PROX reactor for CH_4/O_2=2.24, H_2O/CH_4=1.17 at 100W PEMFC 85

Figure 5.1. Basic flow diagram for fuel processor system prototype 105

Figure 5.2. Elements used in Figure 5.3 107

Figure 5.3. Bench scale prototype for the fuel processor system 108

LIST OF TABLES

Table 2.1. Temperature ranges of steam reforming for different fuels 8

Table 2.2. Light-off temperatures of methane oxidation at different CH_4/O_2 ratios 17

Table 2.3. Rate equations for steam reforming of methane 18

Table 2.4. Rate equations for water-gas shift side reaction 18

Table 2.5. Parameters of k_i and K_j 19

Table 2.6. Power-law rate equation parameters for methane steam reforming . . . 19

Table 2.7. Catalyst properties 20

Table 2.8. Rate equations for oxidation of methane for Pt-based catalysts 21

Table 2.9. Five models describing rate expressions 24

Table 2.10. Adsorption heats and apparent activation energies of model III 24

Table 2.11. Parameter comparison for empirical expressions 25

Table 2.12. Catalysts used in selective CO oxidation 27

Table 2.13. Parameters of the two kinetic models of CO oxidation in H_2-rich stream 30

Table 2.14. Power-law rate constants for Au/α-Fe_2O_3 and Pt/γ-Al_2O_3 catalyst Systems 31

Table 3.1. Light-off temperatures of methane oxidation at different CH_4/O_2 ratios over Pt/Al_2O_3 catalysts 37

Table 3.2. Feed conditions 38

Table 3.3. Mole Balance Terms 39

Table 3.4. Hydrogen Requirements of PEMFC 43

Table 3.5. Mole Balance Results for 10W PEMFC (CH_4:O_2= 1.89 and H_2O:CH_4=1.56) 46

Tanle 3.6. Mole Balance Results for 50W PEMFC (CH_4:O_2= 1.89 and H_2O:CH_4=1.56) 47

Table 3.7. Mole Balance Results for 100W PEMFC (CH_4:O_2= 1.89 and H_2O:CH_4=1.56) 48

Table 3.8. Mole Balance Results for 10W PEMFC (CH_4:O_2= 2.24 and H_2O:CH_4=1.17) 49

Table 3.9. Mole Balance Results for 50W PEMFC (CH_4:O_2= 2.24 and H_2O:CH_4=1.17) 50

Table 3.10. Mole Balance Results for 100W PEMFC (CH_4:O_2= 2.24 and H_2O:CH_4=1.17) 51

Table 3.11. Calculated Flow Rates of Species in the Feed Stream 52

Table 4.1. Adsorption constants used in Van't-Hoff equation 54

Table 4.2. Simulation results for 10W PEMFC system (CH_4/O_2=1.89, H_2O/CH_4=1.56) 62

Table 4.3. Simulation results of 10W PEMFC system (CH_4/O_2=2.24, H_2O/CH_4=1.17) 66

Table 4.4. Simulation results of 50W PEMFC system (CH_4/O_2=1.89, H_2O/CH_4=1.56) 70

Table 4.5. Simulation results of 50W PEMFC system (CH_4/O_2=2.24, H_2O/CH_4=1.17) 74

Table 4.6. Simulation results of 100W PEMFC system (CH_4/O_2=1.89, H_2O/CH_4=1.56) 78

Table 4.7. Simulation results of 100W PEMFC system (CH_4/O_2=2.24, H_2O/CH_4=1.17) 82

Table 4.8. Catalyst weight requirements for all reactors and feed ratio combinations 86

Table 4.9. Comparison between PR and SR for 1.89 & 1.56 ratio combination on 10W fuel system 87

Table 4.10. Comparison between PR and SR for 2.24 & 1.17 ratio combination on 100W fuel system 88

Table 4.11. IPOX reactor sizing for 10W PEMFC system (CH_4/O_2=1.89, H_2O/CH_4=1.56) 89

Table 4.12. IPOX reactor sizing for 10W PEMFC system (CH_4/O_2=2.24, H_2O/CH_4=1.17) 89

Table 4.13. WGS reactor sizing for 10W PEMFC system (CH_4/O_2=1.89, H_2O/CH_4=1.56) 90

Table 4.14. WGS reactor sizing for 10W PEMFC system (CH_4/O_2=2.24, H_2O/CH_4=1.17) 90

Table 4.15. PROX reactor sizing for 10W PEMFC system (CH_4/O_2=1.89, H_2O/CH_4=1.56) 91

Table 4.16. PROX reactor sizing for 10W PEMFC system (CH_4/O_2=2.24, H_2O/CH_4=1.17) 91

Table 4.17. IPOX reactor sizing for 50W PEMFC system (CH_4/O_2=1.89, H_2O/CH_4=1.56) 92

Table 4.18. IPOX reactor sizing for 50W PEMFC system (CH_4/O_2=2.24, H_2O/CH_4=1.17) 92

Table 4.19. WGS reactor sizing for 50W PEMFC system (CH_4/O_2=1.89, H_2O/CH_4=1.56) 93

Table 4.20. WGS reactor sizing for 50W PEMFC system (CH_4/O_2=2.24, H_2O/CH_4=1.17) 93

Table 4.21. PROX reactor sizing for 50W PEMFC system (CH_4/O_2=1.89, H_2O/CH_4=1.56) 94

Table 4.22. PROX reactor sizing for 50W PEMFC system (CH_4/O_2=2.24, H_2O/CH_4=1.17) 94

Table 4.23. IPOX reactor sizing for 100W PEMFC system (CH_4/O_2=1.89, H_2O/CH_4=1.56) 95

Table 4.24. IPOX reactor sizing for 100W PEMFC system (CH_4/O_2=2.24, H_2O/CH_4=1.17) 95

Table 4.25. WGS reactor sizing for 100W PEMFC system (CH_4/O_2=1.89, H_2O/CH_4=1.56) 96

Table 4.26. WGS reactor sizing for 100W PEMFC system (CH_4/O_2=2.24, H_2O/CH_4=1.17) 96

Table 4.27. PROX reactor sizing for 100W PEMFC system (CH_4/O_2=1.89, H_2O/CH_4=1.56) 97

Table 4.28. PROX reactor sizing for 100W PEMFC system (CH_4/O_2=2.24, H_2O/CH_4=1.17) 97

Table 4.29. Design parameters for 10W fuel cell system 99

Table 4.30. Design parameters for 50W fuel cell system. 99

Table 4.31. Design parameters for 100W fuel cell system. 100

Table 4.32. Feed ratios for reactor design 100

Table 4.33. Design parameters for the fuel processing reactors 101

Table 5.1. Calculated Catalyst weights for 10W fuel processor system 103

Table 5.2. Flow rates at the inlet of IPOX reactor for 10W fuel processor (Feed conditions: CH_4/O_2 = 2.24, H_2O/CH_4=1.17) 104

Table 5.3. Stream temperatures for 10W fuel cell processor prototype 105

Table 5.4. Volumetric flowrates along the 10W fuel cell processor prototype . . . 105

Table 5.5. Maximum flow rates for mass flow controllers on the fuel processor system 107

Table 5.6. Specifications of gas chromatographs 109

Table A.1. Constants of the heat capacity equation 113

LIST OF SYMBOLS/ABBREVIATIONS

A_c	Cross-sectional area of the reactor
$c_{p,j}$	Heat capacity of species *j*
E_i	Activation energy of reaction *i*
D_e	Effective diffusivity inside catalyst
D_{kj}	Binary diffusivity of component *k* into component *j*
D_{km}	Diffusivity of component *k* diffusing into a homogeneous gas mixture
D_p	Catalyst particle diameter
D_t	Diameter of the reactor tube
$F_{j,k}$	Flow rate for stream j and for specie k
G	Superficial mass velocity
h_s	Particle-to-fluid heat transfer coefficient
i	Reaction index
j	Species index
k	Species index
k_i	Rate constant for reaction *i*
$k_{0,i}$	Pre-exponential factor of reaction *i* in Arrhenius equation
K_j	Adsorption constant for species *j* (reforming)
$K_{0,j}$	Pre-exponential factor of species *j* in van't Hoff equation
$K_{eq,SR}$	Equilibrium constant for steam reforming reaction
$K_{eq,WGSS}$	Equilibrium constant for water-gas shift side reaction (in IPOX)
$K_{eq,WGS}$	Equilibrium constant for water-gas shift reaction
$K^c_{CH_4}$	Adsorption constant for methane (oxidation)
$K^c_{O_2}$	Adsorption constant for oxygen (oxidation)
L	Length of the reactor tube

P	Pressure
P_j	Partial pressure of species *j*
r_i	Rate of reaction *i*
R	Universal gas constant
Pr	Prandtl number
Re	Reynolds number
T	Temperature
X_i	Conversion for reaction i
W	Catalyst weight
Y_j	Mole fraction of component *j*
α_j	Constant in heat capacity equation
β_j	Constant in heat capacity equation
γ_j	Constant in heat capacity equation
δ_j	Constant in heat capacity equation
ΔH^o_{298}	Standard heat of reaction at 298 K
ΔH_i	Heat of reaction *i* at *T*
ΔH_j	Heat of adsorption of species *j*
ε_p	Pellet porosity
λ_f	Thermal conductivity of the bulk fluid
λ_{N_2}	Thermal conductivity of nitrogen
μ	Viscosity of the gas mixture
v	Velocity of the gas mixture
v_a	Atomic diffusion volume
v_{ij}	Stoichiometric coefficient of species *j* in reaction *i*
ρ_b	Bulk density of the catalyst
ρ_c	Solid density of the catalyst
ρ_m	Density of the gas mixture

ρ_p	Particle density of the catalyst
σ	Constriction factor
τ	Tortuosity
ϕ	Porosity

AFC	Alkaline fuel cell
ATR	Autothermal reforming
BDFs	Backward differentiation formulas
CG	Carrier gas
CtOr	CH_4 toO_2 ratio
ehtc	external heat transfer criterion
GC	Gas Cromotographer
HPLC	High Performance Liquid Chromatography
HTS	High-temperature shift
imtc	internal mass transfer criterion
IPOX	Indirect partial oxidation
LPG	Liquefied petroleum gas
LTS	Low-temperature shift
MCFC	Molten carbonate fuel cell
MFC_i	Mass flow controller for stream i
MS	Mass spectrometer
NDFs	Numerical differentiation formulas
PAFC	Phosphoric acid fuel cell
PEMFC	Polymer electrolyte/Proton exchange fuel cell
PROX	Preferential oxidation of carbon monoxide
ppm	Parts per million
SOFC	Solid oxide fuel cell
SR	Steam reforming
StCr	H_2O to CH_4 ratio
TOX	Total oxidation
WGS	Water-gas shift
WGSS	Water-gas shift as a side reaction

1. INTRODUCTION

Significant increase in carbon dioxide and other hazardous gas emission levels and depletion of the conventional fossil-based fuels in recent years have led to the development of renewable energy technologies (Trimm and Önsan, 2001). Hydrogen based fuel cell technology is one of the most promising options to replace conventional fossil fuel based energy conversion systems and offers the potential of complete removal of hazardous emissions with a more efficient operation (Muradov, 2003).

A fuel cell is an electrochemical conversion device. In a typical fuel cell, on the anode side hydrogen splits into electrons and protons via electrochemical oxidation, while on the cathode side oxygen molecules are reduced to oxide or hydroxide ions. The electrolyte between the two electrodes conducts positive ions selectively from anode to cathode. Conversely, by means of an external circuit in which the electrical power is generated, electrons are transferred from anode to cathode. Oxygen molecules, protons and electrons react at the cathode to give the products of the fuel cell conversion process. (Avcı, 2003; Karakaya, 2006). Fuel cell technology is considered as an alternative to the batteries used in mobile applications and to the internal-combustion engines used in automobiles (Zaidi *et al.,* 2007). However, it is also reported that, in order to achieve a desired performance level in hydrogen-based energy consumption at acceptable costs, further technological advances in hydrogen production, storage and distribution are required (Seymour, *et al.,* 2007).

Proton Exchange/Polymer Electrolyte Membrane Fuel Cell (PEMFC), using perfluorinated sulphonic acid membrane as the electrolyte, and operating with pure hydrogen or a hydrogen-rich mixture, is attracting much more attention among other fuel cell systems such as Alkaline Fuel Cells (AFC), Phosphoric Acid Fuel Cells (PAFC), Molten Carbonate Fuel Cells (MCFC) and Solid Oxide Fuel Cells (SOFC), due to its low temperature operation, affordability, compactness, fast start-up technology and higher power density (Karakaya, 2006; Zalc and Löffler, 2002; Shao *et. al.* 2007). However, there are also some disadvantages in the use of PEMFC such as low-energy density of

today's hydrogen storage technology and the lack of hydrogen distribution infrastructure which is a handicap for the need of continuous hydrogen availability. Also, as a method of having hydrogen on-board, storage of hydrogen on-board needs excessive volumes and when the current technological status is considered, it is still an expensive way. In spite of it all, it is an option very likely to be commercialized in the long term (Satyapal *et al.*, 2007). Consequently, compact, efficient devices that convert hydrocarbon fuels into hydrogen-rich gas mixture on-board the vehicle with a system called fuel processor seems to be a promising alternative (Trimm and Önsan, 2001).

Fuel processor considered in this study includes three main catalytic reactors (Avcı *et al.,* 2002). Avcı (2003) has investigated several fuel types such as natural gas, LPG, gasoline, methanol for use in this fuel processor system. In this study, natural gas, mainly composed of methane, is considered as the hydrocarbon fuel. The system starts-up with an indirect partial oxidation (IPOX) process which includes exothermic total oxidation (TOX) and endothermic steam reforming (SR) of methane coupled with water gas shift as a side reaction (WGSS) (Avcı *et al.,* 2001b). In IPOX process, heat released by total oxidation is consumed by endothermic steam reforming reaction and a hydrogen-rich gas mixture is produced (Ma and Trimm, 1996).

The fuel processor system includes a PEM type of fuel cell and requires a hydrogen-rich gas mixture almost free of carbon monoxide. Therefore, carbon monoxide has to be reduced below a level to which PEMFC can tolerate (ca. 10 ppm) (Kamarudin *et al.,* 2004). In order to decrease carbon monoxide level produced during steam reforming reaction, a separate water gas shift (WGS) reactor has to be used. This unit can reduce the CO level to ca. 2 mol percent but cannot bring it down to the ppm levels (ca. 10 ppm) (Avcı *et. al.* 2001b). Such a reduction can be achieved by using a catalytic reactor that can preferentially oxidize (PROX) carbon monoxide present in the hydrogen-rich gas mixture (Kamarudin *et al.,* 2004).

The objective of this study is to estimate the sizes of the reactors of the fuel processor system that will produce hydrogen such that the PEM fuel cell delivers a desired electrical power output. For this purpose, a material balance is formulated first and solved using the conversion values reported in the literature to calculate the feed flow rate that

gives the desired hydrogen production rate. The values obtained from material balance are then used as boundary conditions to estimate catalyst weight requirements of the reactors, which are assumed to be packed-bed tubular type, using a one-dimensional pseudohomogeneous reactor model. Calculations have been done for two different feed compositions, CH_4/O_2=2.24 with H_2O/CH_4=1.17 and CH_4/O_2=1.89 with H_2O/CH_4=1.56, and for three different fuel cell power output values, 10, 50 and 100 W. Therefore, catalyst weights in the IPOX, WGS and PROX reactors are estimated using six different feed ratio/power output combinations. Once the catalyst weights are known, length and diameter of each reactor and corresponding catalyst particle size are determined using a set of criteria that quantifies the importance of particle-to-fluid (interfacial) heat and intraparticle mass transfer resistances and axial dispersion. In addition, pressure drop along the reactors is also considered in evaluating reactor and particle dimensions. These dimensional parameters are evaluated such that they will help in minimizing axial dispersion, pressure drop and transport resistances mentioned above.

A literature survey about fuel cell technology has been presented in Chapter 2 with proposed reaction rates for methane total oxidation, methane steam reforming, water gas shift and preferential oxidation reactions. Material balance calculations and their solutions are presented in Chapter 3. Chapter 4 includes differential equations used in reactor simulations, the simulation process and results obtained from the computational work. In the light of results obtained in Chapter 4, a bench-scale fuel processor system prototype to operate a 10W PEM fuel cell is proposed in Chapter 5. Major conclusions of this study and the future recommendations are presented in Chapter 6.

2. LITERATURE SURVEY

2.1. Fuel Cell Technology

2.1.1. Fuel Cell Operation

A fuel cell is an electrochemical energy conversion device. It produces electricity from external supplies of fuel and oxidant. Fuel cell technology has experienced a rapid development in recent years in both stationary and vehicular applications (Galvita and Sundmacher, 2005). Electrochemical fuel cell process is a simpler, cleaner and more efficient operation compared to fuel conversion in conventional internal combustion engines (Song, 2002).

A fuel cell consists of electrodes, i.e. an anode, a cathode and an electrolyte which is placed between these porous electrodes. In a fuel cell operation, fuel is sent to the anode where the fuel is oxidized to give positive ions and electrons. The electrolyte between the two electrodes conducts positive ions selectively from anode to cathode. Conversely, by means of an external circuit in which the electrical power is generated, electrons are transferred from anode to cathode. Oxygen molecules (that is generally supplied in the form of air), protons and electrons react at the cathode to give the products of the fuel cell conversion process. A typical fuel cell operation is given in Figure 2.1 in which the operation of a hydrogen-driven fuel cell with a positively charged-hydrogen ion conducting electrolyte is demonstrated (Karakaya, 2006).

In general, a single fuel cell plate produces an electrical potential about 0.6-0.7 volts, which is usually insufficent. Therefore, individual fuel cell plates are combined in the form of stacks to produce the desired electrical power output (Trimm and Önsan, 2001).

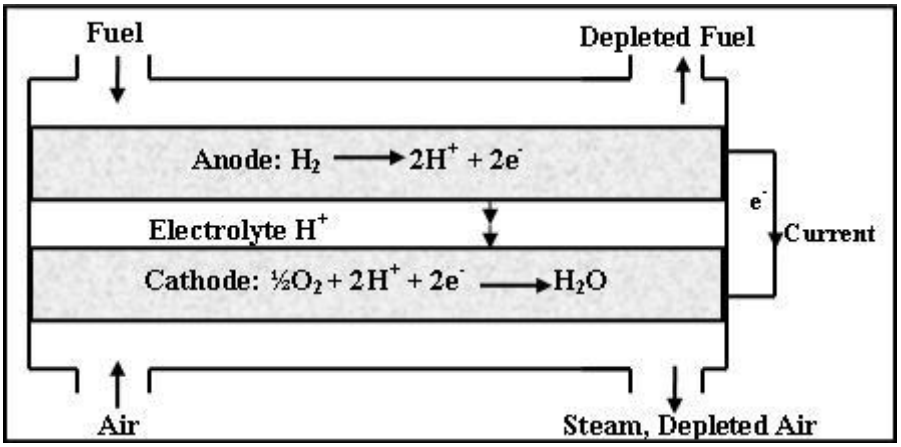

Figure 2.1. Fuel Cell operation (Karakaya, 2006)

2.1.2. PEM Fuel Cells

Fuel cells can be categorized as low temperature fuel cells, and high temperature fuel cells. Proton Exchange/Polymer Electrolyte Membrane Fuel Cells (PEMFC), Alkaline Fuel Cells (AFC) and Phosphoric Acid Fuel Cells (PAFC) operate at low temperatures. On the other hand, Molten Carbonate Fuel Cells (MCFC) and Solid Oxide Fuel Cells (SOFC) operate at high temperatures (Örücü, 2005).

Each type of fuel cell has a set of specific features that are associated with their efficiencies, electrolyte materials, operating temperatures and costs. PAFC has high efficiency of power generation, and also it has a tolerance of carbon monoxide concentration of about 1.5 percent. AFC's power generating efficiency is up to 70 per cent and has advantages of having simple design and low cost (Hirschenhofer *et al.*, 1998). On the other hand, it requires pure hydrogen as feed, and can not tolerate high carbon monoxide concentration. MCFC and SOFC promise high fuel-to-electricity efficiencies, they can process hydrocarbon fuels. However, they operate at elevated temperatures about 923 K and 1273 K (Örücü, 2005). Higher operating temperatures cause higher energy demands, and relatively high capital cost as the consequences of the need of materials of construction having improved thermal resistances.

Pure hydrogen is used to operate a PEM fuel cell. Also it uses a perfluorinated sulphonic acid membrane as the electrolyte. Compared to other types of fuel cells, PEMFC has a high power density, quick start-up ability and low operating temperatures around

333-363 K (Ralph and Hards, 1998). Due to these advantages, PEM fuel cells are preferred for residential, transportation and commercial applications.

PEM fuel cells can show good performance if the proper conditions, such as humidity, low impurities and low temperatures are provided. Zeng (2007) reported that, using organic/inorganic composite is one way to improve water-holding property of the membrane to keep it hydrated. Another important issue in the PEMFC usage is the strict tolerances of impurities such as carbon monoxide and sulphur. PEMFC can only tolerate 10 ppm of carbon monoxide as platinum-based electrolytes are highly sensitive to it (Avcı, 2003). The effect of carbon monoxide concentration on PEMFC performance can be seen clearly in Figure 2.2 (Cheng *et al.,* 2007). This information is based on the IPEE data for platinum anode catalyst (1mg/cm^2). Here, T-stack=80, p-anode=2.2 atm, p-cathode=2.4 atm and A=4 cm^2.

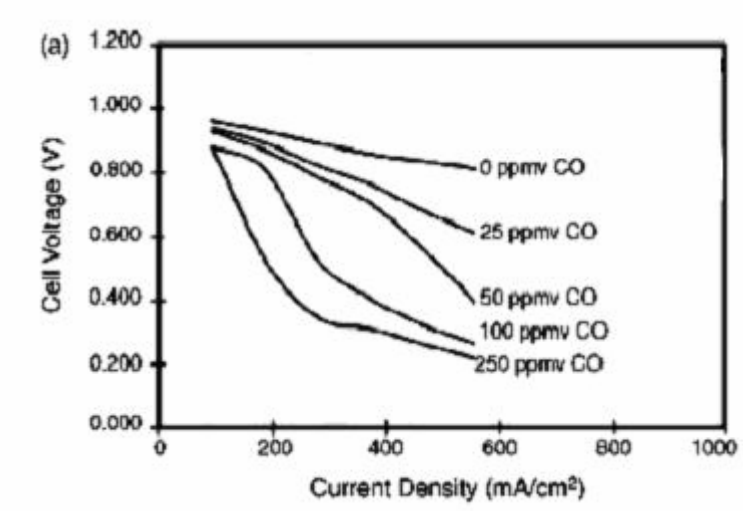

Figure 2.2. CO Effect over PEMFC performance (Cheng *et al.,* 2007)

The usage of expensive materials in the anode and the cathodes of PEMFC is one of the major drawbacks of this technology, as these electrodes contain of certain amounts of platinum, palladium and rhodium which are very expensive materials and therefore increase the cost for commercial use (Larminie and Dicks 2003). Several methods have been used to increase the activity of platinum while minimizing its usage, such as reducing metal loading, development of biological catalysts, using non-platinum catalysts based on porphyrins of metal or mixed catalysts, i.e. PtRu and PtSn, with reduced Pt content

(Grigoriev *et al.,* 2007). In another study, Yong-hun and co-workers (2007) increased palladium/platinum ratio to 19:1 to minimize the cost of PEMFC electrolytes. They also investigated three different types of single cells with electrodes containing (PdPt/C:Pt/C), (Pt/C:PdPt/C) and (PdPt/C:PdPt) as their anode and cathode catalysts (Cho *et al.,* 2007). Comparisons of these anode-cathode couples are shown in Figure 2.3. It has seen that electrodes which are doped with Pt/C on anode and PdPt/C in cathode gives similar performances with electrodes doped with PdPt/C on anode and PdPt/C on cathode, while electrodes doped with PdPt/C on anode and Pt/C on cathode achieves higher voltages and power density on same current density.

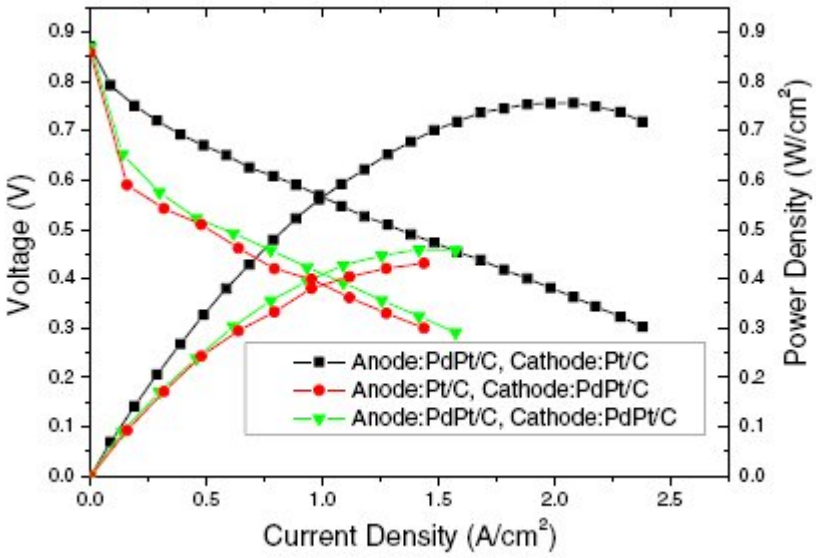

Figure 2.3. Performance comparisons of PEMFC anodes and cathodes (Cho *et al.,* 2007)

2.2. Methane-to-hydrogen conversion routes for driving PEM fuel cells

Many different types of fuels such as natural gas, methanol, LPG, ethanol and methane are considered for their conversion into hydrogen (Brown, 2001; Pukrushpan *et al.,* 2006). Between these fuels only methanol, diesel and gasoline can be kept in liquid form, which is a great advantage for use in vehicles. On the other hand diesel can deposit coke easily during the fuel conversion process which creates the requirements of well-controlled conditions. Nevertheless diesel may be considered as an important choice due to its availability, price advantage and well-established on-board storage (Avcı, 2003).

When compared with other fuels, methanol has received most interest for on-board conversion, since it has a high energy density; it can be stored in liquid form at ambient temperatures and can be reformed at lower temperatures, when compared to other fuel types, as seen in Table 2.1 (Brown, 2001). Another advantage of methanol is related with the level of carbon monoxide produced after its reforming: after methanol steam reforming reaction, CO level is around 0.8 mol percent, while the same reaction with methane gives ca. 11.2 mol percent of CO (Brown, 2001). Although many studies reported successful demonstration of on-board methanol conversion, methanol has problems about its production volume and a lacking-distribution network; current supply of methanol can only meet the demands of a certain number of fuel cell vehicles (Thomas *et al.*, 2000). Furthermore, methanol is a highly toxic chemical, which may cause serious health issues, even death in case of inhalation (Avcı, 2003).

Table 2.1. Temperature ranges of steam reforming for different fuels (Brown, 2001)

Fuel	Temperature Range (K)
Ethanol	800 – 1000
Methane	1000 – 1100
Methanol	500 – 560
Multi-carbon Hydrocarbons	1000 – 1150

Gasoline is another type of fuel which can be used for on-board hydrogen production. It is currently used as fuel for internal combustion engines and has a widespread refuelling infrastructure. Gasoline has also a high energy density, and differs from methanol, since it does not requiring an extra synthesis step (Avcı, 2003). In spite of coke formation and catalyst deactivation in the hydrogen generation step, car prototypes with gasoline driven fuel cell vehicles are being developed by major companies (Springman *et al.*, 2004).

Liquefied petroleum gas, also known as LPG, is a well-known and widely used fuel. It can be stored in liquid form in pressurized vessels for mobile and portable use. LPG is by-product of crude oil processing in refineries and is a mixture of propane and n-

butane, whose amounts change with the processed crude oil. Moreover, LPG has very low sulphur content, high power density and is a cheaper fuel compared to others. Therefore, its on-board conversion for use in small-scale applications has been also investigated by Ahmed and Krumpelt (2001).

Natural gas, being mainly composed of 75 to 85 percent methane, with the remainder being composed of ethane, propane and carbon dioxide, is the cleanest hydrocarbon-based energy source used worldwide (Selen, 2005). However, its use in on-board hydrogen production requires the presence of large and heavy pressurized gas cylinders. Furthermore, natural gas is the most stable hydrocarbon fuel and needs a considerable energy input to trigger and to sustain its conversion during the hydrogen generation step (Avcı, 2003; Rostrup-Nielsen, 1984).

Different methods are suggested for the conversion of hydrocarbon fuels to hydrogen such as thermal cracking, carbon dioxide reforming, autothermal reforming (ATR), partial oxidation and steam reforming (Jamal and Wyszynski, 1994). Details of these techniques are summarized in the following section.

2.2.1. Thermal Cracking

Thermal cracking is the direct decomposition of hydrocarbons to carbon and hydrogen under the effect of heat (Abanades and Flamant, 2006):

$$C_nH_m \longrightarrow nC + \tfrac{1}{2}mH_2 \qquad (2.1)$$

$$CH_4 \longrightarrow C + 2H_2, \qquad \Delta H^o_{298} = 74.8 \text{ kJ/mol} \qquad (2.2)$$

In this technique, hydrogen is produced in a single step and there is no need for an extra stage to reduce carbon monoxide concentration, since it is not generated in the process. The major advantages of thermal cracking are fuel flexibility, relative simplicity and compactness, production of clear carbon byproduct, and significant reduction in CO_2 emissions (Muradov *et al.,* 2005). However, some difficulties appear associated with thermal cracking: However, due to its endothermic nature, requirement of high energy

input and need of high temperatures (ca. 1670 K in case of methane (Muradov, 2003)) are the major drawbacks of thermal cracking. Li and co-workers (2005) have studied Ni/CeO_2 catalyst for this reaction, while Muradov and co-workers (2005) have studied stable carbon catalysts. However, in the literature, Ni based catalysts have been widely used to achieve thermal cracking reaction.

2.2.2. Steam Reforming

Steam reforming of hydrocarbons is a well-known route for hydrogen production and used in commercial applications, especially for large-scale ones (Avcı *et al.,* 2001a):

$$C_nH_m + nH_2O \longleftrightarrow nCO + (½m+n)H_2, \qquad (2.3)$$

$$CH_4 + H_2O \longleftrightarrow CO + 3H_2 \qquad \Delta H^{\circ}_{298} = 206.2 \text{ kJ/mol} \qquad (2.4)$$

Steam reforming gives the highest hydrogen amount per fuel converted among the other hydrocarbon conversion routes. The process runs over Ni-Mg based catalysts (Ma and Trimm, 1996; Ma, Trimm and Jiang, 1996). During the steam reforming reaction, water gas shift reaction (Reaction (2.5)) is occurring as a side reaction which decreases carbon monoxide concentration and increases hydrogen production:

$$CO + H_2O \longleftrightarrow CO_2 + H_2, \qquad \Delta H^{\circ}_{298} = -41.2 \text{ kJ/mol} \qquad (2.5)$$

One of the drawbacks of steam reforming is its high energy demand: heat must be added to the system to sustain the steam reforming reaction it is endothermic. Heat is introduced into the reactors by means of external heating which is added to this system by exothermic total oxidation and an additional heat exchanger. In the industrial applications steam reforming process is used on high pressure tubes, ca. 20 atm, (Avcı, 2003). Although steam reforming reaction is widely used to produce hydrogen, it causes to form very heavy fuel processor system (Hoang *et al.,* 2006). In addition, on steam reforming of hydrocarbons, temperatures above 673K, provides a suitable environment for catalyst deactivation (Reuse *et al.,* 2004).

2.2.3. Partial Oxidation

In spite of the fact that steam reforming is widely preferred, its high energy demand is an important disadvantage, because in the fuel cell system, hydrogen generation is used to operate fuel processor which needs smaller reactor volumes, compared to steam reforming reactors used in the industry; in addition, partial oxidation process is faster than steam reforming, and it can sustain itself once triggered. Partial oxidation of hydrocarbons is reported to occur via two routes (Avcı, 2003):

- Indirect Partial Oxidation, which involves the coupling of total oxidation and steam reforming reactions

- Direct Partial Oxidation, which involves hydrocarbon conversion to synthesis gas – a mixture of carbon monoxide and hydrogen

Carbon dioxide reforming, also known as dry reforming can be considered as an alternative route to steam reforming due to its high heat demand (Larentis *et al.,* 2001).

$$CH_4 + CO_2 \longleftrightarrow 2CO + 2H_2 \quad \Delta H^{o}_{298} = 247 \text{ kJ/mol} \qquad (2.6)$$

Autothermal reforming is the combination of two reactions, which are steam reforming and partial oxidation. It can be accepted as the most common and traditional hydrogen production way, especially on industrial scale. Autothermal reforming process can yield a high concentration of hydrogen up to 70 percent on a dry basis (Hoang *et al.,* 2006). In addition heat generated by partial oxidation can be used on endothermic steam reforming reaction without an extra heater or burner which provides important system efficiency (Cipiti *et al.,* 2006).

2.3. Partial Oxidation

2.3.1. Direct Partial Oxidation

Direct partial oxidation is a reaction in which hydrocarbons are directly converted to hydrogen and carbon monoxide in a single step (Trimm and Önsan, 2001). For methane, this reaction is shown below:

$$CH_4 + \tfrac{1}{2}O_2 \longrightarrow CO + 2H_2, \qquad \Delta H^{o}_{298} = -35.7 \text{ kJ/mol} \qquad (2.7)$$

Direct partial oxidation is thermodynamically favored at high temperatures around 1023 K and at short residence times around 1-5 ms. (Avcı *et al.,* 2001b). Therefore, once triggered, it is a fast reaction and required small reactor volumes which is a desired feature for mobile and portable fuel processing applications.

Direct partial oxidation of hydrocarbons has been investigated on different types of catalysts such as platinum group metals Pt, Pd, Rh on alumina, ceria, titania supports and on NiO-MgO. Schmidt and co-workers have studied the partial oxidation of various hydrocarbons such as methane, n-hexane, cyclohexane, isooctane and decane (Hickman and Schmidt, 1992; Hickman and Schmidt, 1993; Bharadwaj and Schmidt, 1995; Schmidt *et al.*, 2003). In these studies, it has been reported that high conversions (~80 per cent) and high selectivity (~90 per cent) to hydrogen was achieved on Pt and Rh-coated monoliths at very low contact times (ca. 10^{-4} and 10^{-2} s) and at near stoichiometric hydrocarbon-to-oxygen feed ratios, without any carbon formation over the catalysts (Hickman and Schmidt, 1992).

Direct partial oxidation is also investigated over different catalysts. Choudhary and coworkers (1998) have studied methane direct partial oxidation on $Ni/AlPO_4$ between the temperatures of 773 and 1173 K. Jin *et al.* (2000) reported investigation about the direct partial oxidation of methane on Ni/Al_2O_3. In addition Jun and co-workers (2006) have investigated nickel-calcium hydroxyapatite catalyst, for partial oxidation. Ru/TiO_2 is another catalyst that has been investigated for its possible use in direct partial oxidation of

methane at lower temperatures. For 773K, conversion appears as ~65 per cent, while it's ~94 per cent at 973K (Yan *et al.,* 2004).

2.3.2. Indirect Partial Oxidation

The concept of combustion of part of the fuel for methane has received attention in many practices and applications. Indirect partial oxidation (IPOX) is basically based on the same concept as the one mentioned above. It is the combination of exothermic total oxidation and endothermic steam reforming, and heat needed to drive the latter reaction is generated by combusting part of the fuel by the former reaction (Trimm and Önsan, 2001). Although steam reforming yields highest hydrogen production compared to the other conversion routes; during the process, high temperature need appears. By means of IPOX process, i.e. heat generated by TOX reaction is harnesses by steam reforming reaction, latter is a self-sustaining reaction once it is triggered. The concept of indirect partial oxidation has commercial applications such as the Johnson Matthey Hot Spot^{TM} reactors (Golunski, 1998).

IPOX has potential problems such as possibility of coke formation and need of water injection. Water injection is needed for temperature control of the catalyst bed and for meeting the water demand for steam reforming reaction. To avoid coke formation, indirect partial oxidation process must be realized with careful control. Furthermore, coke formation can be decreased by keeping the steam-to-carbon ratio (defined in Equation (2.8)) around 2.5, when reaction takes place over Ni-based catalysts (Rostrup-Nielsen, 1984).

$$steam/carbon\ ratio = \frac{moles\ of\ water\ fed + moles\ of\ water\ produced\ by\ TOX}{moles\ of\ methane\ fed - moles\ of\ methane\ consumed\ in\ TOX} \quad (2.8)$$

In indirect partial oxidation operation, various types of fuels such as natural gas (simulated by methane) may be considered for their conversion to a hydrogen-rich stream. Reactors for indirect partial oxidation of methanol are reported to be widely available (Trimm and Önsan, 2001). Hydrogen production from hydrocarbons via indirect partial oxidation is a well-established process which is used in industrial processes (Pena *et al.*,

1996). However, except in the case of methanol, conversion of hydrocarbons cannot be initiated at room temperature and they have to be heated up to their light-off temperatures. Light-off temperature is defined as the temperature at which ca. 10 percent of the oxidation conversion of the fuel is reached (Ma *et al.,* 1996). Ma (1995) has suggested a solution for this purpose in which hydrocarbons can reach to their light-off temperatures by the heat generated by methanol or by hydrogen combustion, both of which can be initiated at room temperatures.

Indirect partial oxidation is based on two major reactions: total oxidation and steam reforming of the hydrocarbon fuel. Ma (1995) has proposed using two different catalysts specific to these reactions and placed a Pt based catalyst (for total oxidation) and a Ni based catalyst (for steam reforming) into the same reactor. Various placing configurations of these catalysts, named as mixed-bed, dual-bed, and uniform-bed (in the form of a bimetallic catalyst), have been investigated to see their effect on conversion and product selectivity (Ma, 1995; Ma and Trimm, 1996).

The mixed-bed system corresponds to a physical mixture of two catalysts where the total oxidation and steam reforming is believed to take place simultaneously. In the dual-bed system, Ni-based steam reforming catalyst is placed downstream and Pt-based total oxidation catalyst is placed upstream of a tubular reactor. In such a system, total oxidation and steam reforming is assumed to occur consecutively where the steam reforming is thought to be triggered by the heat released by total oxidation reaction (Karakaya, 2006). In the uniform-bed configuration, both reactions occur over a bifunctional catalyst having Pt and Ni metals on the same support. Investigations on these catalyst bed configurations came up with different hydrogen production efficiencies (Ma, 1995; Trimm and Önsan, 2001).

Steam reforming reaction is endothermic and requires heat input, which can be supplied in several ways. Electric heaters or burners could be considered as heaters; however, due to its high cost and low overall efficiency, other options should be investigated. Total oxidation methane is a possible way to generate necessary heat for endothermic steam reforming reaction (Avcı *et al.,* 2001b). For example, methane is oxidized and converted to carbon dioxide and water in total oxidation:

$$CH_4 + 2O_2 \longrightarrow CO_2 + 2H_2O, \quad \Delta H^{o}_{298} = -802 \text{ kJ/mol} \qquad (2.9)$$

Heat released by exothermic total oxidation reaction is the utilized by endothermic steam reforming reaction.

Steam reforming, which is the other major reaction of IPOX, is used widely in commercial applications at industrial scale (Twigg, 1989; Armor, 1999). Hydrogen requirement of PEM fuel cells is produced by steam reforming which is defined of two resembling reactions:

$$C_nH_m + (2n)H_2O \longleftrightarrow nCO_2 + (½m+2n)H_2 \qquad (2.10)$$

$$C_nH_m + nH_2O \longrightarrow nCO + (½m+n)H_2, \qquad (2.3)$$

In addition to hydrogen yield, carbon dioxide and carbon monoxide production appears in reaction 2.10 and 2.3 respectively.

Moreover, water-gas shift (WGS) reaction occurs simultaneously as a side reaction in steam reforming which converts carbon monoxide to carbon dioxide using steam which is present in the medium. Also, additional hydrogen is produced:

$$CO + H_2O \longleftrightarrow CO_2 + H_2, \qquad \Delta H^{o}_{298} = -41.2 \text{ kJ/gmol} \qquad (2.5)$$

2.3.2.1. Catalysts. Compared with the precious metal catalysts such as Rh-based ones, Ni-based catalyst are currently being used in the conventional steam-reforming processes since they are cheaper but still offer sufficient activity (Rostrup-Nielsen, 1984; Twigg, 1989; Trimm and Önsan, 2001). Rh-based catalysts are more expensive, but, on the other hand, they offer activities higher than Ni-based ones with almost no carbon formation. Coking is a possible phenomenon during steam reforming over Ni-based catalyst, but can be minimized by careful control of the operating conditions such as the steam-to-carbon ratio defined in Equation (2.8). It is reported that, this ratio should not be below ca. 2.5 during steam reforming of methane over Ni-based catalysts. It is worth noting that the

value of this ratio changes with the type of hydrocarbon (Rostrup-Nielsen, 1984; Trimm and Önsan, 2001; Avcı *et al.*, 2002).

Supports used for Ni-based catalysts have also been investigated to minimize coke formation. Ross (1974) reported that magnesia or potassium, both of which are alkaline components, eliminates coke formation. Additionally, Trimm (1999) reported that ceria can reduce coke formation. Bradford and Vannice (1996) mentioned that Ni-based catalysts demonstrate steam reforming activities in the order of $Ni/TiO_2 > Ni/C > Ni/SiO_2 > Ni/MgO$. A comprehensive summary about coke formation during steam reforming can be found in the literature (Rostrup-Nielsen, 1998; Ma, 1995).

As explained above, coke formation is much less on Ru and Rh (Rostrup-Nielsen, 1984). However, their high cost makes it difficult for commercial use. The specific activities of several metals doped on alumina or magnesia are reported to be in the order of Rh, Ru > Ni, Pd, Pt > Re > Co (Avcı, 2003).

Methane oxidation reaction can be achieved on very strict conditions, since it is the most stable hydrocarbon. For this reason use of precious metals such as Platinum and Palladium, or a combination of both is reported to drive this reaction. Mostly, palladium-based catalysts are preferred, since light-off temperature of methane oxidation is the lowest for this choice (Ciaparu and Pfefferle 2001). Additionally, rhodium-based (Burch *et al.,* 1999), and platinum-based (Michalkiewitz 2006; Ma *et al.,* 1996) catalysts are being utilized.

Light-off temperature is another characteristic of total oxidation (TOX) and depends on the hydrocarbon/oxygen ratio (Veser and Schmidt 1996). A list of light-off temperatures at different methane/oxygen ratio values obtained over a $Pt/\delta\text{-}Al_2O_3$ catalyst is given in Table 2.2. It can be seen from Table 2.2 that as methane/oxygen ratio increases, light-off temperature decreases. Avcı and co-workers (2003) have studied the relation between light-off temperatures and fuel:oxygen ratio. Relation between the fuel:oxygen ratio and minimum light-off temperatures relation between n-butane and propane reacting on Pt-Ni catalyst has been explained by the possible interaction between two sites (Avcı *et al.,* 2003).

Table 2.2. Light-off temperatures of methane oxidation at different CH_4/O_2 ratios (Ma *et al.*, 1996)

CH_4/O_2	Light-off Temperature (K)
0.27	724
0.9	641
2.53	623
5.04	589

2.3.2.2. Reaction Kinetics. Several studies have been reported on steam reforming kinetics of methane. Xu and Froment (1989) reported Langmuir-Hinshelwood type of rate equations determined using elementary-step kinetic model proposal for a $Ni/MgAl_2O_4$ catalyst. They also reported rate expressions for water-gas shift side reaction. The rate expressions for methane steam reforming and water gas shift are given in Table 2.3 and Table 2.4, respectively. Numaguchi and Kikuchi (1988) have proposed a kinetic model for steam reforming of methane and water-gas shift reactions over a Ni/Al_2O_3 catalyst. In their kinetic model, surface reaction is considered as the rate-determining step. The resulting rate laws are of Langmuir-Hinshelwood type and are given in Table 2.3 and Table 2.4 for steam reforming and water-gas shift, respectively. They reported rate equation for methane steam reforming towards formation of carbon monoxide, thus the parallel reaction, i.e. steam reforming of methane towards carbon dioxide is not taken into account (Numaguchi and Kikuchi, 1988). Ma (1995) also proposed an empirical rate expression for methane steam reforming over a Ni/MgO catalyst (Table 2.3).

Table 2.3. Rate equations for steam reforming of methane

Rate Equation	Reference
$-r_{SR} = \frac{k_{SR}(P_{CH_4} - P_{H_2O}^3 P_{CO} / K_{eq,SR})}{P_{CH_4}^{\alpha_2} P_{H_2O}^{\beta_2}}$	Numaguchi and Kikuchi (1988)
$-r_{SR} = \frac{k_{SR} / P_{H_2}^{2.5}(P_{CH_4} P_{H_2O} - P_{H_2}^3 P_{CO} / K_{eq,SR})}{(1 + K_{CO} P_{CO} + K_{H_2} P_{H_2} + K_{CH_4} P_{CH_4} + K_{H_2O} P_{H_2O} / P_{H_2})^2}$	Xu and Froment (1989)
$-r_{SR} = \frac{k_{SR} K_{CH_4} K_{H_2O} P_{CH_4} P_{H_2O}}{P_{H_2}^{1.5}(1 + K_{CH_4} \frac{P_{CH_4}}{P_{H_2}^{0.5}} + K_{H_2O} \frac{P_{H_2O}}{P_{H_2}})^2}$	Ma (1995)

Table 2.4. Rate equations for water-gas shift side reaction

Rate Equation	Reference
$-r_{WGSS} = \frac{k_{WGSS}(P_{CO} - P_{H_2} P_{CO_2} / K_{eq,WGSS})}{P_{CH_4}^{\alpha_3} P_{H_2O}^{\beta_3}}$	Numaguchi and Kikuchi (1988)
$-r_{WGSS} = \frac{k_{WGSS} / P_{H_2}(P_{CO} P_{H_2O} - P_{H_2} P_{CO2} / K_{eq,WGSS})}{(1 + K_{CO} P_{CO} + K_{H_2} P_{H_2} + K_{CH_4} P_{CH_4} + K_{H_2O} P_{H_2O} / P_{H_2})^2}$	Xu and Froment (1989)

In Tables 2.3 and 2.4, k_i is the reaction rate constant for reaction i (i = TOX – total oxidation, SR – methane steam reforming, WGSS – water-gas shift running as a side reaction, WGS – Water-gas shift reaction) and is expressed as a function of temperature using Arrhenius functionality as follows:

$$k_i = k_{0,i} \exp\left(\frac{-E_i}{RT}\right) \tag{2.11}$$

K_j is the adsorption constant for species j whose temperature dependency is calculated by using van't-Hoff Equation:

$$K_j = K_{0,j} \exp\left(\frac{-\Delta H_j}{RT}\right) \tag{2.12}$$

In Tables 2.3, 2.4 and 2.5 $K_{eq,i}$ is the equilibrium constant for reaction i. Values of the parameters that appear in Equations (2.11) and (2.12) are given in Table 2.5.

Table 2.5. Parameters of k_i and K_j (Xu and Froment, 1989)

Reaction	$k_{0,i}$ (mol kgcat^{-1} s^{-1})		E_i (kJ kmol^{-1})
SR	1.17 x 10^{15} bar$^{-0.5}$		240,100
WGSS	5.43 x 10^{5} bar^{-1}		67,130
Species	$K_{0,j}$ (bar^{-1})	ΔH_j (kJ kmol^{-1})	Equilibrium Constants
CH_4	6.65 x 10^{-4}	- 38,280	$K_{eq,SR} = 4.707\times10^{12} \exp\left(\frac{-224{,}000}{RT}\right)$ bar^2
H_2O	1.77 x 10^{5}	88,680	
CO	8.23 x 10^{-5}	- 70,650	$K_{eq,WGSS} = 1.142\times10^{-2} \exp\left(\frac{-37{,}300}{RT}\right)$
H_2	6.12 x 10^{-9}	- 82,900	

Parameters of the empirical rate law proposed for methane steam reforming are given in Table 2.6.

Table 2.6. Power-law rate equation parameters for methane steam reforming (adapted from Avcı (2003))

Hydrocarbon	Catalyst	Temp. Range (K)	Pressure (MPa)	Orders			E_A (kJ/gmol)
				CH_4	H_2O	H_2	
CH_4	Ni/MgO	723-823	0.1	1	-	-	110
CH_4	Ni/MgO	623-673	0.1	0.96	0.17	0.25	60

Catalysts that are used in experiments conducted by Xu and Froment (1989) and Numaguchi and Kikuchi (1988) are both Ni-based ones. However, support materials are different. The catalyst properties are shown in Table 2.7. Metal surface areas are nearly identical, but nickel content of catalysts differs from each other.

Table 2.7. Catalyst properties

	Xu and Froment (1989)	Numaguchi and Kikuchi (1988)
Catalyst	$Ni/MgAl_2O_4$	Ni/Al_2O_3
Metal Content (wt per cent)	15.2	8.7
Metal Surface Area (m^2/g)	4.1	3.6
Density (kg/m^3)	1,870	1,970

Several studies about the kinetics of oxidation of hydrocarbons can be found in the literature. These studies report different rate expressions in the form of Langmuir-Hinshelwood and power-law types proposed for several ranges of operating conditions and catalysts. These studies indicate positive and negative dependencies of reaction rate on hydrocarbon and oxygen concentrations, respectively (Avcı, 2003). It is reported that, these orders vary between 0.22 and 3.4 for hydrocarbons; -2.9 and -0.17 for oxygen.

Langmuir-Hinshelwood and power-law type rate expressions describing methane oxidation over Pt-based catalysts are presented in Table 2.8 (Trimm and Lam, 1980; Ma, 1995). Rate expressions reported by Trimm and Lam (1980) are Langmuir-Hinshelwood type. Here the first term is based on the reaction between molecularly adsorbed methane and oxygen, while the second term describes the Elay-Rideal mechanism between and oxygen in the gas phase and molecularly adsorbed methane.

Table 2.8. Rate equations for oxidation of methane for Pt-based catalysts

Catalyst	Rate Equation	Reference
Pt/Al_2O_3	$-r_{TOX} = \frac{k_{TOXa} P_{CH_4} P_{O_2}^{0.5}}{1 + K_{CH_4}^c P_{O_2}^{0.5}} + \frac{k_{TOXb} P_{CH_4} P_{O_2}}{1 + K_{CH_4}^c P_{O_2}}$	Trimm and Lam, 1980
Pt/Al_2O_3	$-r_{TOX} = \frac{k_{TOX1a} P_{CH_4} P_{O_2}}{(1 + K_{CH_4}^c P_{CH_4} + K_{O_2}^c P_{O_2})^2} + \frac{k_{TOXb} P_{CH_4} P_{O_2}}{(1 + K_{CH_4}^c P_{CH4} + K_{O_2}^c P_{O_2})}$	Trimm and Lam, 1980
$Pt/\delta\text{-}Al_2O_3$	$-r_{TOX} = \frac{k_{TOX} K_{CH_4}^c P_{CH_4} \sqrt{K_{O_2}^c P_{O_2}}}{(1 + K_{CH_4}^c P_{CH_4} + \sqrt{K_{O_2}^c P_{O_2}})^2}$	Ma *et al.*, 1996
Pt/Al_2O_3	$-r_{TOX} = k^0{}_{TOX} * \exp(\frac{-E}{RT}) * P_{CH_4}{}^{0.95} * P_{O_2}{}^{-0.17}$	Ma, 1996

2.4. Water-Gas Shift Reaction

Water-gas shift (WGS) is a reaction in which carbon monoxide and water react to form carbon dioxide and hydrogen:

$$CO + H_2O \longleftrightarrow CO_2 + H_2, \qquad \Delta H^o{}_{298} = -41.2 \text{ kJ/mol} \tag{2.13}$$

As it is seen in Equation (2.13) WGS is exothermic and thermodynamically favoured at lower temperatures. Its mission is to reduce carbon monoxide level, and to increase the amount of hydrogen. With a conversion of 90-95 percent, Reaction (2.13) can decrease carbon monoxide level from 30000-100000 ppm to 1000-10000 ppm (Kamarudin, 2004).

WGS is the one of the stages in hydrogen production from natural gas, LPG and oil for ammonia synthesis and in other important industrial processes such as hydrotreating of

petroleum stocks and refining heavy oil. Recently, WGS achieves important roles in new application areas, mainly in hydrogen production in fuel processing systems for hydrogen fuel cells, especially for PEMFC (Saito *et al.*, 2003). In such processes, water-gas shift helps in decreasing carbon monoxide concentration at the exit of the hydrogen generation unit down to ca. 7000 ppm of 2 mol percent (Sun *et al*., 2005; Avcı, 2003). Moreover, in some systems, it may be used as the only CO clean-up mechanism instead of CO oxidation due its lower calorific value (Utaka *et al.*, 2000). Water-gas shift reaction can be carried out at two different temperatures: (a) Low Temperature Shift (LTS) taking place between 453 and 523 K and (b) High Temperature Shift (HTS) taking place between 623 and 673 K. The catalysts used in these processes are outlined below.

2.4.1. Catalysts

In fuel processing/PEM fuel cell systems, it has been reported that WGS reactor is the heaviest unit due to the (a) slow kinetics of the reaction, requiring higher catalyst quantitites and (b) prohibition of high temperature operation conditions (Choi and Stenger, 2004). Use of a catalyst whose activity and stability is high, such as MgO addition to Pt/CeO_2 (Farias, 2007), can provide a considerable decrease in the size of the WGS reactor.

Iron-based and copper-based catalysts are used on commercial basis to run high-temperature (623 K-673 K) (HTS) and low-temperature (453 K-523 K) (LTS) water-gas shift reactions on industrial scale, respectively. These catalysts are reported to be the most widely used catalysts in industry as water-gas shift catalysts (Amadeo and Laborde, 1995). Moreover, high activity and fewer side reactions at high temperatures are reported as extra advantages of these catalysts (Amadeo and Laborde, 1995). In recent studies, authors have tried to improve the activity of copper-based catalysts for water-gas shift reaction. Saito *et al.* (2003) investigated the effects of pretreatment of Cu/ZnO-based catalysts such as calcination temperature and treatment in H_2 at high temperatures to improve the activity of LTS catalysts.

Furthermore, the effect of promotion by precious metals of Fe_3O_4-Cr_2O_3 is investigated and found that rhodium doped Fe_3O_4-Cr_2O_3 to be effective on activity (Lei *et*

al., 2006). In addition, Radhakrishnan *et al.* (2006) have made investigations on rhenium promotion of ceria-zirconium supported platinum catalysts and found that catalyst used enhanced the WGS activity.

Sun *et al.,* (2005), demonstrated that in comparison with the conventional Cu/Zn catalyst, precious metal catalysts such as Au, Pd and Pt offer high activities, meanwhile eliminating self-heating issue. Pt offers high activity in a wide temperature range for WGS reaction (Lian *et al.*, 2006). Catalysts involving various noble metals, such as Au, Pd and Pt are reported to have high activities. Great attention has been given to the gold-based catalysts supported on different support materials such as CeO_2, Fe_2O_3 (Tabakova *et al.*, 2000) and TiO_2 (Idakiev *et al.*, 2004). In the studies of Andreeva *et al.* (2002), Au/Fe_2O_3 catalyst is demonstrated to have high catalytic activity for LTS because of the specific interaction between gold and the ferric oxide support. It is also reported that Au/ZnO may be an active catalyst for low-temperature WGS reaction; however, its catalytic activity is lower than those of Au/Fe_2O_3 and Au/ZrO_2 (Tabakova *et al.*, 2000).

2.4.2. Kinetics

Various kinetic studies have been made on water-gas shift reaction kinetics, still including disagreements, and controversies. Two kinetic mechanisms are proposed for water-gas shift reaction, which are adsorptive mechanism, and regenerative mechanism. In the adsorptive mechanism, CO and H_2O adsorb on the catalyst surface and form an intermediate which results in desorbed H_2 and CO_2 (Choi and Stenger, 2003). On the other hand, the regenerative, known also as the surface redox mechanism is based on the adsorption and dissociation of water on the catalytic surface (Amadeo and Laborde, 1995).

Various mechanistic rate expressions can be derived from these two mechanisms (Choi and Stenger, 2003). In addition, unlike the rate expressions derived from detailed mechanisms, there are also empirical, power-law type rate expressions which are found to be sufficient for most reactor design studies (Choi and Stenger, 2003; Lei *et al.*, 2005).

Amadeo and Laborde (1995) studied five different models that resulted with five different rate expressions for water-gas shift reaction on $Cu/ZnO/Al_2O_3$ between 453 and

503 K. Models I and II represent a redox mechanism, while models III-V are Langmuir-Hinshelwood type. These models are represented in Table 2.9.

It has been reported that among the five models, model III, which is a Langmuir-Hinshelwood type rate law, presents the best fit with the experimental data. In this model, adsorption constant of each species are taken into account (Amadeo and Laborde, 1995). Heats of adsorption and apparent activation energy of model III are shown in Table 2.10.

Table 2.9. Five models describing rate expressions (Amadeo and Laborde, 1995)

Model I	$r_{WGS} = \frac{k_{WGS} P_{H_2O}(1-\beta)}{A P_{H_2O} + P_{CO}}$
Model II	$r_{WGS} = \frac{k_1 k_2 P_{CO} P_{H_2O}(1-\beta)}{k_1 P_{CO} + k_2 P_{H_2O} + k_3 P_{CO_2}}$
Model III	$r_{WGS} = \frac{k_{WGS} P_{CO} P_{H_2O}(1-\beta)}{1+\sum K_i P_i}$
Model IV	$r_{WGS} = \frac{k_{WGS} P_{CO}(1-\beta)}{(1 + K_{H_2CO_2} P_{H_2} P_{CO_2} P_{H_2O}^{-1} + K_{H_2} P_{H_2} + K_{H_2O} P_{H_2O} + K_{CO_2} P_{CO_2}}$
Model V	$r_{WGS} = \frac{k_{WGS} P_{CO} P_{H_2O}(1-\beta)}{(1 + K_{CO_2} P_{CO_2} + K_{H_2} P_{H_2})}$

Where $\beta = P_{CO_2} P_{H_2} / (P_{CO} P_{H_2O} K_e)$

Table 2.10. Adsorption heats and apparent activation energies of model III (Amadeo and Laborde, 1995)

	CO	CO_2	H_2O	H_2
ΔH (kj/gmol)	-0.91	-24.72	-1.42	-14.4
$K_{0,j}$ (atm^{-1})	2.21	0.0047	0.40	0.052
E_{WGS}= 4.08 kJ/gmol $k_{0,WGS}$=0.92 mol/g.s.atm				

Choi and Stenger (2003) offered an empirical power-law rate expression derived from numerical fitting for water-gas shift reaction between 393 and 523 K running over $Cu/ZnO/Al_2O_3$ catalyst:

$$r_{WGS} = 2.96x10^5 \exp\left(-\frac{47{,}400}{RT}\right)\left(P_{CO}P_{H_2O} - \frac{P_{CO_2}P_{H_2}}{K_{eq,WGS}}\right) \tag{2.14}$$

In addition, a comparison of activation energies and frequency factors with other empirical power-law rate equations derived from different catalysts are given in Table 2.11 (Choi and Stenger, 2003).

Table 2.11. Parameter comparison for empirical expressions (Choi and Stenger, 2003)

$$r_{WGS} = k_{0,WGS} \exp(-E_{WGS} / RT) P_{CO}^m P_{H_2O}^n (1-\beta)$$

Catalyst	*m*	*N*	Lnk_0	*E* (kJ/gmol)
Cu/Al_2O_3	1	1.9	-	69.3
CuO/MnO_2	1	1	-	55.0
$Cu/ZnO/Al_2O_3$	0	1	-	41.8
$Cu/ZnO/Al_2O_3$	1	1	12.6	47.4
ICI-$Cu/ZnO/Al_2O_3$	1	1	15.2	52.8

2.5. Selective CO Oxidation in H_2-Rich Streams

Pure hydrogen is the main requirement of PEM fuel cells. In order to prevent poisoning of the fuel cell electrodes, it is reported that the CO concentration in hydrogen-rich streams should be below 10 ppm (Seo *et al.,* 2006; Rosa *et al.,* 2006; Cipiti *et al.,* 2006; Kamarudin *et al.,* 2004). Precious metals such as Platinum and Palladium are used in the electrolydes to provide purified hydrogen for the inlet of PEM fuel cells (Ralph *et al.*,

1998). In spite of this low temperature, i.e. maximum 500K, reaction behaviour can cause deactivation of these metals by carbon monoxide adsorption (Schmidt *et al.*, 1994).

Several methods have been proposed for decreasing carbon monoxide level in hydrogen-rich streams for fuel cell applications. Diffusing hydrogen through a Pd/Ag membrane is one of them, but this needs fairly high temperatures and pressures, which may not be practical for use in vehicular applications. Carbon monoxide methanation is another route for removal of CO. However, this method causes significant loss in hydrogen and results in the production of methane, which is a greenhouse gas (Trimm and Önsan, 2001). PEM fuel cells are very sensitive to carbon monoxide concentration even for trace amounts, i.e. <50 ppm (Zalc and Löffler, 2004). Another possible route for carbon monoxide removal is selective CO oxidation, or preferential CO oxidation (PROX) (Trimm and Önsan, 2001; Moretti *et al.,* 2007).

Among all possible methods, selective oxidation of carbon monoxide seems to be the most likely option (Choi and Stenger, 2004; Özkara and Aksoylu, 2003; Trimm and Önsan, 2001). It is reported that selective CO oxidation is convenient for small-scale operations and is particularly promising for transportation applications (Kahlich *et al*., 1999).

In the selective CO oxidation, two parallel reactions occur. Among these reactions, CO oxidation (Reaction (2.15)) is the desired one whereas H_2 oxidation (Reaction (2.16)) is undesired since it causes loss of efficiency due to hydrogen consumption.

$$CO + \tfrac{1}{2}\, O_2 \longleftrightarrow CO_2, \quad \Delta H^{o}_{298} = -283 \text{ kJ/mol} \tag{2.15}$$

$$H_2 + \tfrac{1}{2}\, O_2 \longleftrightarrow H_2O, \quad \Delta H^{o}_{298} = -242 \text{ kJ/mol} \tag{2.16}$$

Selectivity of carbon monoxide, defined in Equation (2.17), needs to be high for preferential oxidation (Chin *et al.*, 2005; Moretti et al., 2007):

$$Selectivity\ (\%) = \frac{0.5(n_{CO}^{in} - n_{CO}^{out})}{n_{O_2}^{in} - n_{O_2}^{out}} \times 100 \tag{2.17}$$

Additionally, the amount of oxygen to be injected into the system has to be carefully controlled since the excess O_2 may oxidize H_2. Hence, a catalyst that can selectively oxidize CO has to be chosen and stoichiometric amounts of oxygen have to be fed to the PROX system (Trimm and Önsan, 2001).

It is reported that there are three obvious possibilities to increase the selectivity of CO in preferential oxidation reaction: an appropriate catalyst that adsorbs CO but not H_2 or on which both CO and H_2 oxidized, but small amounts of H_2 oxidation and preferential CO oxidation is leaded by kinetic parameters and an operation temperature where CO is oxidized but H_2 is not. It is also recommended that in all cases, deterministic oxygen: carbon monoxide ratios and temperature have to be controlled carefully (Trimm and Önsan, 2001).

2.5.1. Catalysts

Various catalyst types are reported in several studies. A brief summary has been made by Choi and Stenger (2004), and the results are given in Table 2.12.

Table 2.12. Catalysts used in selective CO oxidation (Choi and Stenger (2004))

Catalyst Type	Catalyst use sequence*
Pt based	35.8
Ru, Rh or Pd based	24.5
Co, Fe or Cu based	17.0
Au based	13.2
Others(Mn, Cr, Mg or Zn based)	9.4

* Choi and Stenger have investigated on thirty different papers, catalysts used, suggested or accepted in selective oxidation of CO.

Most of the catalysts used for CO PROX are based on late transition metals such as Pt, Rh, Ru, or such as Au and Cu. Additionally, it is reported that non-precious transition metals such as Co, Cr, Ni are being used (Moretti *et al.,* 2007). Catalyst selection is very important in CO oxidation process since PEM fuel cells are highly sensitive to impurities.

CO concentration must be reduced below 10 ppm, hence oxidation reaction conversion must be better than 99.99 percent (Şimşek *et al.,* 2007).

Kahlich *et al.* (1999) reported that the commonly used PROX catalysts (alumina-supported Pt, Ru and Rh) operate at 423-473 K; because of high temperature operation they lose activity and selectivity. At low temperatures, i.e. 353-373 K, which is close to PEMFC operating temperature, oxide supported gold catalysts, are reported to be a promising alternative and show good performance (Kahlich *et al.*, 1999; Choi and Stenger, 2004). Gold-based catalysts are confirmed to be more active for carbon monoxide oxidation than hydrogen oxidation since they can operate at low temperatures, and are moisture-resistant (Trimm and Önsan, 2001).

Au-based catalysts, compared with well-known Pt-based PROX catalysts, demonstrate better activity and selectivity features. Gold-based catalysts exhibit different behaviour, depending on the type of support material. Besides, these catalysts differ from each other by the type of materials on which they are supported. A set of investigations shows that, among the gold catalysts supported on TiO_2, α-Fe_2O_3, ZrO_2 and Co_3O_4, Au/α-Fe_2O_3 gave the best activity and selectivity (Kahclich *et al.*, 1997; Rossignol *et al.*, 2005; Schumacher *et al.*, 2004). Moreover, Pt supported on various materials such as zeolites and TiO_2 are reported to give higher activity and selectivity than Pt/Al_2O_3 do (Watanabe *et al.*, 1997; Schumacher *et al.*, 2004).

Another CO oxidation study conducted in excess of H_2 over a nanostructured $Cu_{0.1}Ce_{0.9}O_{2-y}$ catalyst shows that higher activity with addition of 15 percent of CO_2 and hydrogen; and higher CO selectivity 100 percent between 318K and 363K which are much better than those obtained on Pt/γ-Al_2O_3 and Au/α-Fe_2O_3. It is also reported that nanostructure catalyst has also the price advantage when compared to others (Sedmak *et al.,* 2003; Moretti *et al.,* 2007).

Furthermore, it is reported that effects of CO_2 and H_2O is an important effect in the PROX process (Chin *et al*., 2005). As a result of their experimental study on Au/α-Fe_2O_3, Schubert *et al.* (2004) reported that addition of CO_2 to PROX reduces the rate of CO oxidation and the selectivity, whereas addition of H_2O increases the selectivity.

2.5.2. Reaction Kinetics

Several rate equations describing PROX over different catalysts have been reported. Although there are many studies that report kinetic rate expressions about carbon-monoxide oxidation, only a few of them consider hydrogen oxidation simultaneously with CO oxidation. Some of the studies that consider simultaneous H_2 oxidation with CO oxidation assume constant selectivity for carbon monoxide in PROX reactions at certain temperatures (Lin *et al.*, 2005), whereas some others consider only carbon monoxide oxidation due to the high CO selectivity (~100 per cent) of the catalyst used (Şimşek *et al.,* 2007).

Sedmak *et al.* (2003) studied the kinetics of CO oxidation over $Cu_{0.1}Ce_{0.9}O_{2-y}$ nanostructured catalyst. They found this catalyst to be 100 per cent selective in the temperature range of 318-363 K and considered two models to describe the observed reaction rate. One of the models is Mars and van Krevelen type which is derived on the basis of a redox mechanism:

$$r_{CO} = \frac{k_{CO} k_{O_2} P_{CO} P_{O_2}^n}{0.5 k_{CO} P_{CO} + k_{O_2} P_{O_2}^n} \tag{2.18}$$

Where $k_{CO} = A_{CO}.\exp(-E_{a,CO} / RT)$ and $k_{O_2} = A_{O_2}.\exp(-E_{a,O_2} / RT)$.

In Equation (2.18), k_{CO} and k_{O_2} are taken to be the reaction rate constants for the reduction of surface bu CO and reoxidation of it by O_2. Additionaly, in equation (2.19) k_L and K_L are surface reaction rate constant and CO adsorption equilibrium constant, respectively (Sedmak *et al.,* 2003). Liu and Flytzani-Stephanapoulos model is another kinetic expression that Sedmak *et al.* (2003) evaluated:

$$r_{CO} = \frac{k_L K_L P_{CO} P_{O_2}^m}{1 + K_L P_{CO}} \tag{2.19}$$

Where $k_L = A_L.\exp(-E_{a,L}/RT)$ and $K_L = B_L.\exp(Q/RT)$

The parameters of the two kinetic model calculated by Sedmak *et al.* (2003) are presented in Table 2.13.

Table 2.13. Parameters of the two kinetic models of CO oxidation in H_2-rich stream (Sedmak *et al.*, 2003)

Mars and van Krevelen model		Liu and Flytzani-Stephanapoulos model	
A_{CO} (gmol/gcat.s.bar)	1.44 x 10^5	A_L (gmol/gcat.s.bar^m)	2.64 x 10^3
$E_{a,CO}$ (J/mol)	5.72 x 10^4	$E_{a,L}$ (J/mol)	5.9 x 10^4
A_{O2} (gmol/gcat.s.bar^n)	2.39 x 10^3	B_L (1/bar)	7.53 x 10^0
$E_{a,O2}$ (kJ/mol)	6.02 x 10^4	Q (J/mol)	8.7 x 10^3
n	0.2 ± 0.05	m	0.15 ± 0.025

Kahlich *et al.* (1997) recommended a rate expression for CO oxidation over Pt/γ-Al_2O_3 catalyst for temperature range between 423 and 523 K by introducing a process parameter λ, which is defined as the concentration ratio of oxygen to carbon monoxide:

$$r_{CO} = k_1.P_{CO}^{0.4}.\lambda^{0.82} = k_{CO}.\exp(\frac{-E_A}{RT}).P_{CO}^{-0.42}.P_{O_2}^{0.82} \qquad (2.20)$$

where $\lambda = \frac{2P_{O_2}}{P_{CO_2}}$

Kahlich *et al.* (1999) also studied the selective low temperature oxidation of CO over Au/α-Fe_2O_3 and gave the parameters of the rate equation in comparison with those obtained for Pt/γ-Al_2O_3 catalyst. The parameter comparison is tabulated in Table 2.14.

Table 2.14. Power-law rate constants for Au/ α-Fe_2O_3 and Pt/γ-Al_2O_3 catalyst systems (Kahlich *et al.,* 1997; Kahlich *et al.*, 1999)

System	Au/α-Fe_2O_3 at 353 K	Pt/γ-Al_2O_3 at 473 K
$K_{0,PROX}$ (gmol/gcat.s)	9.81 x 10^{-4}	13.8 x 10^{-4}
α_{CO}	0.55	-0.42
α_{O2}	0.27	0.82
E_{PROX} (kJ/gmol)	31	71

Moreover, Özyönüm (2002) has investigated the kinetics of selective CO oxidation over Pt-Co-Ce/Al_2O_3 catalyst by studying five different reaction paths and has determined the plausible mechanisms. It is also reported that besides CO and Hydrogen oxidation in PROX unit, reverse water gas shift reaction has to be taken into consideration (Choi and Stenger, 2004).

3. FUEL PROCESSOR DESIGN AND MOLE BALANCE CALCULATIONS

3.1. Fuel Processor Design

3.1.1. Fuel Processor System

Fuel Processor system is a process that produces hydrogen and electricity via a fuel cell. At the inlet, hydrocarbons such as natural gas, LPG, gasoline, ethanol and methanol are used as a fuel source to produce hydrogen, which is then used in a fuel cell to produce electricity. A flowsheet of this system is shown in Figure 3.1.

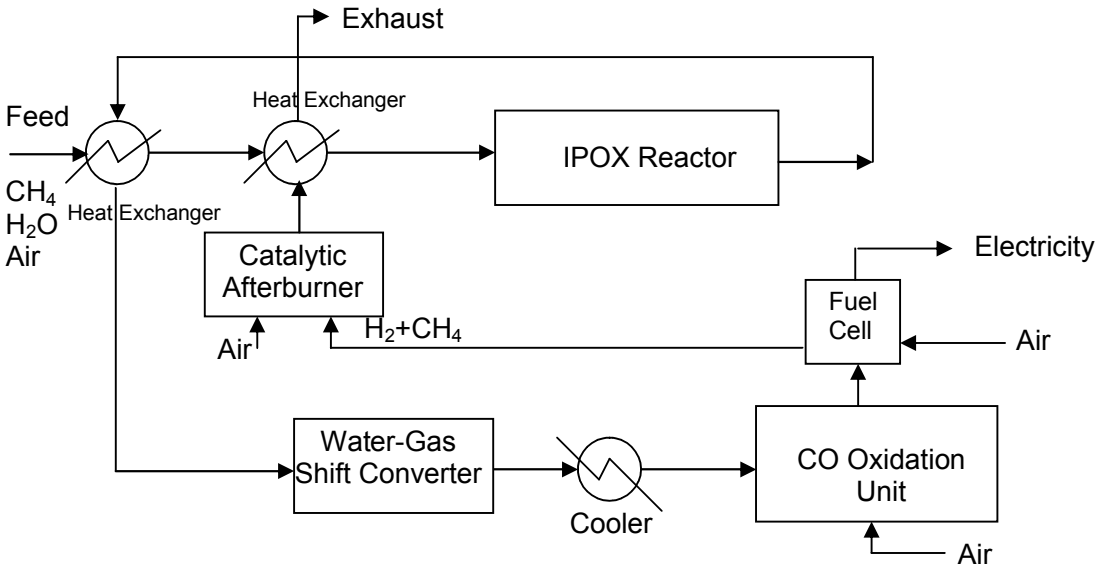

Figure 3.1 Fuel Processor system

This system contains three major reactors, which are indirect partial oxidation reactor (IPOX), water gas shift reactor (WGS) and preferential CO oxidation reactor (PROX). In this study, methane has been selected as the hydrocarbon to be processed. In the IPOX reactor, methane is converted to hydrogen by indirect partial oxidation which is a combination Total Oxidation (TOX), Steam-Reforming (SR) and Water-gas Shift (WGSS) reactions (side reaction of SR). IPOX is autothermal in character, that is, heat released by

exothermic total oxidation is used by endothermic steam reforming reaction. This scheme reduces the external energy demand (Ma and Trimm, 1996).

In total oxidation, methane is partially oxidized and converted to carbon dioxide and water:

$$CH_4 + 2O_2 \longrightarrow CO_2 + 2H_2O, \qquad \Delta H^{o}_{298} = -802 \text{ kJ/mol} \qquad (2.9)$$

Heat and steam produced in total oxidation is utilized by the steam reforming of the remaining methane to produce the desired hydrogen:

$$CH_4 + H_2O \longleftrightarrow CO + 3H_2, \quad \Delta H^{o}_{298} = 206.2 \text{ kJ/mol} \qquad (2.4)$$

Ma (1995) has proposed to use two types of catalysts specific to the reactions given above. This approach has been utilized in this study, and Pt/δ-Al_2O_3 and Ni/MgO-Al_2O_3 catalysts are considered to be packed into the same reactor in a uniformly mixed scheme to drive total oxidation (Reaction (2.9)) and steam reforming (Reaction (2.4)), respectively. The major difficulty associated with steam reforming is coke formation. In order to eliminate catalyst coking, it is reported that steam to carbon ratio has to be kept around 2.5 (Rostrup-Nielsen, 1984).

Water demand in steam reforming is greater than steam produced in total oxidation. Avcı and co-workers (2002) show that for maximum TOX conversion, steam to carbon ratio reaches maximum 1.77 value which is lower than 2.5. Thus, additional water has to be fed to the IPOX reactor. By introducing additional water in the feed, catalyst bed temperature can be controlled and also carbon formation can be minimized (Avcı *et al.,* 2000).

In this process, water gas shift reaction runs as a side reaction in which carbon monoxide treated with steam is converted to carbon dioxide and hydrogen:

$$CO + H_2O \longrightarrow CO_2 + H_2, \qquad \Delta H^{o}_{298} = -41.2 \text{ kJ/mol} \qquad (2.5)$$

Addition of extra water into the feed changes the water gas shift equilibrium in the direction of products, therefore, CO level decreases in the IPOX reactor. However, this is insufficient, and the use of a separate WGS converter is needed for further removal of CO (Avcı *et al.,* 2002). This reaction takes places at temperatures between 473 and 673K, and runs typically on Cu/ZnO based catalysts. Amount of carbon monoxide at the exit of this reactor is typically around 1-2 mol percent (Zalc and Löffler, 2002; Avcı *et al.,* 2002). However, such a CO concentration is much higher than the level that a PEM fuel cell can tolerate (ca. 10 ppm) (Kamarudin *et al.,* 2004). Therefore another step is needed for further removal of CO.

Preferential carbon monoxide oxidation (PROX) is the reactor following water-gas shift (Figure 3.1). This method is reported to be the optimum option for CO removal in a hydrogen-rich stream (Choi and Stenger, 2004):

$$CO + \tfrac{1}{2} O_2 \longleftrightarrow CO_2, \quad \Delta H^{o}_{298} = -283 \text{ kJ/mol} \tag{2.15}$$

$$H_2 + \tfrac{1}{2} O_2 \longleftrightarrow H_2O, \quad \Delta H^{o}_{298} = -242 \text{ kJ/mol} \tag{2.16}$$

One alternative method, reaction of CO with hydrogen to produce methane (methanation) is not feasible due to the significant hydrogen loss (Avcı *et al.,* 2002). Another alternative method is to diffuse hydrogen through a Pd/Ag membrane; however this route causes requires high temperatures and high-pressure differentials (Trimm and Önsan, 2001). In PROX reaction, some amount of hydrogen is also oxidized in the reactor. However, based on the recent experimental studies, this loss is minimal and it is neglected in this study (Choi and Stenger, 2004). In other words, constant selectivity of 100 per cent is assumed for CO.

Use of a heat exchanger at the exit of the IPOX reactor is needed since WGS inlet temperature is nearly 350 K smaller than the exit of the IPOX reactor (Figure 3.1). In addition, as IPOX inlet temperature is 627 K (for 1.89 & 1.56 feed ratio), another heat exchanger is needed before IPOX for heating the feed stream from ambient conditions to the light-off temperature of methane (Figure 3.1). The hot inlet stream of this heat exchanger is the exit stream of the catalytic afterburner containing the exothermal heat

released by the combustion of unconverted methane and rejected hydrogen. Apart from these, PROX inlet temperature (ca. 353 K) is smaller than WGS outlet temperature (ca. 473 K), requiring the use of another heat exchanger to decrease temperature of the stream (Figure 3.1).

Since PEMFC operates at 333-363 K temperature range, CO oxidation reaction should run at efficiently low temperatures. To reach optimal performance for CO oxidation several metal-based catalysts have been investigated such as Pt-Co-Ce/Al_2O_3 (Özyönüm, 2002). In addition, Sedmak and co-workers (2003) has investigated nanostructred $Cu_{0.1}Ce_{0.9}O_{2-y}$ catalyst. Some other alternative methods involve carrying out water-gas shift and preferential oxidation reactions simultaneously in the WGS converter by feeding oxygen into the reactor (Utaka 2000). PROX unit reduces CO concentration (Reaction (2.15)) down to nearly purified hydrogen level (~10ppm of carbon monoxide).

$$H_2 \longleftrightarrow 2H^+ + 2e^- \qquad (3.1)$$

$$1/2O_2 + 2H^+ + 2e^- \longleftrightarrow H_2O \qquad (3.2)$$

It is proposed that PEMFC rejects about 25 per cent of hydrogen that is fed into it (Avcı, *et al.,* 2002). On the anode side, hydrogen decomposition reaction (Reaction (3.1)) is occurring, while Reaction (3.2) is occurring on the cathode side (Austin, 1984). During the whole operation, some unconverted materials are also fed into the fuel cell. These components, including unconverted methane and rejected hydrogen are sent to a catalytic afterburner unit packed with a Pt-based catalyst to perform energy recovery by oxidation of rejected H_2 and unconverted CH_4 after the fuel cell (Figure 3.1). In the afterburner unit, following reactions occur:

$$H_2 + 1/2O_2 \longleftrightarrow H_2O, \quad \Delta H^o_{298} = -241.8 \text{ kJ/mol} \qquad (3.3)$$

$$CH_4 + 2O_2 \longleftrightarrow CO_2 + 2H_2O, \ \Delta H^o_{298} = -802.3 \text{ kJ / mol} \qquad (3.4)$$

In addition, part of the sensible heat of the catalytic afterburner outlet stream is harnessed to provide additional heat to the feed stream of IPOX, in order to trigger the partial oxidation reaction (Avcı *et al.,* 2002).

3.1.2. Temperatures and Stream Properties

The main function of total oxidation (Reaction 2.9) is to generate necessary heat required by the endothermic steam reforming reaction. In this study, TOX is considered to run on a Pt/δ-Al_2O_3 catalyst as proposed by Ma and co-workers (1996). As mentioned in Section 3.1.1, the IPOX reactor is considered to be packed with a physical mixture of Pt/δ-Al_2O_3 and Ni/MgO-Al_2O_3 catalysts, specific for total oxidation and steam reforming, respectively (Ma, 1995; Ma and Trimm, 1996). Both catalysts can safely operate at temperatures up to 1100 K, but catalyst bed temperature has to be controlled carefully to be below the maximum temperature, since thermal sintering of the catalysts can be significant at temperatures above ca. 1100 K (Avcı *et al.,* 2002). Moreover, in order to trigger the whole operation by initiating TOX, the catalyst bed temperature should be raised to the light-off value of methane. Light-off temperature is defined as the temperature at which approximately 10 per cent of the hydrocarbon is oxidized (Ma *et al.,* 1996).

Light-off temperature of methane depends on CH_4/O_2 ratio and is investigated by Ma and co-workers (1996) on Pt/Al_2O_3. The results given in Table 3.1 show that at a CH_4/O_2 ratio consideration is 2.5, the light-off temperature is close to 620 K. Since the CH_4/O_2 ratio at the inlet will be considered around 2.5, the inlet temperature of the IPOX reactor is assumed to be equal to 620 K. Thus IPOX reactor inlet temperature is considered 620 K for CH_4/O_2=1.89. However, in this work, another ratio fuel:oxygen ratio is used as well, i.e. CH_4/O_2=2.24. For this ratio, inlet temperature of IPOX is calculated as 627K using linear regression method. In addition, Ma (1995) has compared light-off temperatures of hydrocarbons over Pt/Al_2O_3 and Ni/MgO catalysts. The Pt catalyst was found to be more active than Ni (Trimm and Önsan, 2001).

Table 3.1. Light-off temperatures of methane oxidation at different CH_4/O_2 ratios over Pt/Al_2O_3 catalysts (Ma *et al.,* 1996)

CH_4/O_2	Light-off Temperature (K)
0.27	724
0.9	641
2.53	623
5.04	589

WGS converter in the system is considered to operate at low temperature shift (LTS) conditions (i.e. at ca. 453-523 K) using a $Cu/ZnO-Al_2O_3$ catalyst (Choi and Stenger, 2003). Based on this information, temperature at the inlet of the reactor is taken as 473 K. Temperature of the IPOX reactor exit stream is around 800K and is higher than the inlet stream of the WGS reactor. Thus, a heat exchanger must be placed before WGS reactor (Figure 3.1).

Another major reactor of the system is PROX, which is placed before PEM fuel cell to reduce the amount of CO to the levels that the PEM fuel cell can tolerate (<10 ppm). Since typical operating temperature of PEM fuel cells is around 353 K, temperature of the PROX inlet stream is considered to be equal to this value.

3.2. Mole Balance Calculations

In this study, hydrogen production rates corresponding to 10, 50 and 100 W of PEMFC power outputs are of interest. The hydrogen flow rate required for a PEMFC is reported as 37-40 mol h^{-1} kW^{-1} in the literature (Brown, 2001; Zalc and Löffler, 2002). It is also reported that a 27 L min^{-1} H_2 at standard temperature and pressure can operate a 1.5 kW PEMFC (Karakaya, 2006). Using this set of information, molar hydrogen flows are selected as given in Table 3.4 for the three power sizes of PEMFC.

Four compounds are fed to the IPOX reactor, which are CH_4, H_2O, O_2, N_2. Ma (1996) has investigated several carbon-to-oxygen and steam-to-carbon ratio combinations. Two ratio combinations, CH_4/O_2=2.24 with H_2O/CH_4=1.17 and CH_4/O_2=1.89 with

H_2O/CH_4=1.56 have been selected by taking maximum temperatures into consideration. Ma and Trimm (1996) have investigated different ratio couples, i.e. CH_4/O_2 and H_2O/CH_4 which yield base conditions for feed streams of IPOX (Table 3.2). For all ratio couples maximum temperature reached in the reactor has been presented. Using these ratio combinations, oxygen and steam flow rates can be calculated once the methane flow rate is known. Methane flow rate can be back-calculated starting from the desired hydrogen flow rate and by using assumed conversion values for every reaction that occurs in the system. The assumed conversion values are based on the data from the literature and are given in Section 3.2.1. For this purpose an MS Excel code has been prepared which gives methane flow rates for different feed ratios and fuel cell power output capacities.

Using conversion rates and stream numbers, which are defined in Table 3.3, mole balance equations used to calculated methane feed flow rate needed to give the desired hydrogen production rate (i.e. the desired electrical power) are given in Equations (3.5)-(3.55).

Table 3.2. Feed conditions (Ma and Trimm, 1996)

Feed conditions		T_{max} (K)	CH_4 converted (mol per cent)	Product Yields (mol/100 mol CH_4 admitted)		
CH_4/O_2	H_2O/CH_4			H_2	CO_2	CO
2.24	0	855	38.1	37.9	25.7	12.1
2.24	1.17	839	39.5	47.8	33.3	6.3
1.89	1.17	888	53.3	74.9	41.6	11.7
1.89	2.34	851	54.9	82.9	45.0	9.9
1.55	1.56	931	69.1	105.7	54.2	15.0
1.55	2.34	908	70.1	107.1	50.5	19.6
1.35	2.34	953	83.6	119.5	53.3	30.3
1.16	2.34	1007	91.7	120.6	55.8	35.9

Table 3.3. Mole Balance Terms

Term	Explanation
$F_{1,j}$	Feed Stream
$F_{2,j}$	Stream just after Total Oxidation and before Steam Reforming and Water-Gas shift
$F_{3,j}$	Steam Reforming (also WGS as side reaction) exit
$F_{4,j}$	Water Gas Shift Converter exit
$F_{5,j}$	Air inlet for PROX
$F_{6,j}$	PROX exit
$F_{7,j}$	Air inlet for PEM Fuel cell
$F_{8,j}$	Fuel Cell exit
$F_{9,j}$	Air inlet for Catalytic Afterburner
$F_{10,j}$	Exhaust
CtOr	CH_4 toO_2 ratio
StCr	H_2O to CH_4 ratio
X_1	Total Oxidation conversion rate
X_2	Steam Reforming conversion rate
X_3	Water Gas Shift (as a side reaction to SR) conversion rate
X_4	Water Gas Shift conversion rate
X_5	PROX conversion rate
X_6	Fuel Cell Conversion rate
X_7	Hydrogen Conversion rate in the afterburner
X_8	Methane Conversion rate in the afterburner

Feed stream:

$$F_{1,CH_4} = unknown \tag{3.5}$$

$$F_{1,H_2O} = F_{1,CH_4} * CtOr \tag{3.6}$$

$$F_{1,O_2} = F_{1,CH_4} / CtOr \tag{3.7}$$

$$F_{1,N_2} = F_{1,O_2} * 79/21 \tag{3.8}$$

$$F_{1,CO} = F_{1,CO_2} = F_{1,H_2} = 0 \tag{3.9}$$

Total Oxidation:

$$F_{2,CH_4} = F_{1,CH_4} * (1 - X_1) \tag{3.10}$$

$$F_{2,H_2O} = F_{1,H_2O} + 2 * F_{1,CH_4} * X_1 \tag{3.11}$$

$$F_{2,O_2} = F_{1,O_2} - F_{1,O_2} \tag{3.12}$$

$$F_{2,N_2} = F_{1,N_2} \tag{3.13}$$

$$F_{2,CO} = F_{2,CO} \tag{3.14}$$

$$F_{2,CO_2} = F_{1,CH_4} * X_1 \tag{3.15}$$

$$F_{2,H_2} = F_{1,H_2} \tag{3.16}$$

Steam Reforming and Water gas shift (running as a side reaction in IPOX reactor):

$$F_{3,CH_4} = F_{2,CH_4} * (1 - X_2) \tag{3.17}$$

$$F_{3,H_2O} = F_{2,H_2O} * (1 - X_2 - X_2 * X_3) \tag{3.18}$$

$$F_{3,O_2} = 0 \tag{3.19}$$

$$F_{3,N_2} = F_{2,N_2} \tag{3.20}$$

$$F_{3,CO} = F_{2,CH_4} * (X_2 - X_2 * X_3) \tag{3.21}$$

$$F_{3,CO_2} = F_{2,CO_2} + (F_{2,CH_4} * X_2 * X_3) \tag{3.22}$$

$$F_{3,H_2} = F_{2,CH_4} (3 * X_2 + X_2 * X_3) \tag{3.23}$$

Water gas shift reactor:

$$F_{4,CH_4} = F_{3,CH_4} \tag{3.24}$$

$$F_{4,H_2O} = F_{3,H_2O} - (F_{3,CO} * X_4) \tag{3.25}$$

$$F_{4,O_2} = F_{3,O_2} \tag{3.26}$$

$$F_{4,N_2} = F_{3,N_2} \tag{3.27}$$

$$F_{4,CO} = F_{3,CO} * (1 - X_4) \tag{3.28}$$

$$F_{4,CO_2} = F_{3,CO_2} + (F_{3,CO} * X_4) \tag{3.29}$$

$$F_{4,H_2} = F_{3,H_2} + (F_{3,CO} * X_4) \tag{3.30}$$

Air inlet to PROX reactor:

$$F_{5,O_2} = F_{4,CO} * \frac{X_5}{2} \tag{3.31}$$

$$F_{5,N_2} = F_{5,O_2} * \frac{79}{21} \tag{3.32}$$

Preferential carbon monoxide reactor:

$$F_{6,CH_4} = F_{4,CH_4} \tag{3.33}$$

$$F_{6,H_2O} = F_{4,H_2O} \tag{3.34}$$

$$F_{6,O_2} = F_{5,O_2} - (F_{4,CO} * \frac{X_5}{2}) \tag{3.35}$$

$$F_{6,N_2} = F_{5,N_2} + F_{4,N_2} \tag{3.36}$$

$$F_{6,CO} = F_{4,CO} - (F_{4,CO} * X_5) \tag{3.37}$$

$$F_{6,CO_2} = F_{4,CO_2} + (F_{4,CO} * X_5) \tag{3.38}$$

$$F_{6,H_2} = F_{4,H_2} \tag{3.39}$$

Air inlet to PEM fuel cell:

$$F_{7,O_2} = F_{6,H_2} * \frac{X_6}{2} \tag{3.40}$$

$$F_{7,N_2} = F_{7,O_2} * \frac{79}{21} \tag{3.41}$$

PEM fuel cell:

$$F_{8,CH_4} = F_{6,CH_4} \tag{3.42}$$

$$F_{8,H_2O} = F_{6,H_2O} + (F_{6,H_2} * X_6) \tag{3.43}$$

$$F_{8,O_2} = 0 \tag{3.44}$$

$$F_{8,N_2} = F_{7,N_2} + F_{6,N_2} \tag{3.45}$$

$$F_{8,CO} = F_{6,CO} \tag{3.46}$$

$$F_{8,CO_2} = F_{6,CO_2} \tag{3.47}$$

$$F_{8,H_2} = F_{6,H_2} * (1 - X_6) \tag{3.48}$$

Air inlet for the catalytic afterburner:

$$F_{9,O_2} = F_{8,CH_4} * 2 * X_8 + F_{8,H_2} * \frac{X_7}{2} \tag{3.49}$$

$$F_{9,N_2} = F_{9,O_2} * \frac{79}{21} \tag{3.50}$$

Catalytic afterburner:

$$F_{10,CH_4} = F_{10,O_2} = F_{10,H_2} = 0 \tag{3.51}$$

$$F_{10,H_2O} = F_{8,H_2O} + F_{8,H_2} * X_7 + F_{8,CH_4} * X_8 \tag{3.52}$$

$$F_{10,N_2} = F_{8,N_2} + F_{9,N_2} \tag{3.53}$$

$$F_{10,CO} = F_{8,CO} \tag{3.54}$$

$$F_{10,CO_2} = F_{8,CO_2} + F_{8,CH_4} * X_8 \tag{3.55}$$

Using these equations, conversion values given in Table 3.3 and the related hydrogen flow rate requirement, it will be able to calculate flow rates of methane and other feed components to generate 10, 50 and 100W electrical power. These calculations will be done for two different combinations of methane-to-oxygen and steam-to-methane ratios.

Table 3.4 Hydrogen Requirements of PEMFC

	Fuel Cell Capacity		
	10 W	50 W	100 W
H_2 Requirement (mol/h)	0.41	2.03	4.07

3.2.1. Mole Balance Assumptions

For total oxidation (TOX) conversion, complete consumption of oxygen in the feed stream is considered. By a simple calculation from stoichiometric ratios, conversion of TOX, X_1, is calculated as:

$$X_1 = \frac{F_{1,O_2} * 0.5}{F_{1,CH_4}} \tag{3.56}$$

For methane steam reforming conversion over Ni-based catalysts, a conversion value of 60 per cent is considered (Hoang and Chan, 2003; Smet *et, al*., 2000). Degree of conversion of WGS reaction running simultaneously with steam reforming is assumed to be 77 per cent (Lee *et al.*, 2005; De Smet *et al.*, 2001, Hoang and Chan, 2004). In the light of different studies made by Shishido (2006) and Choi (2003), 60 per cent conversion is assumed for WGS reaction over a Cu/ZnO based catalyst in Water-Gas shift converter. Additionally, the requirement of presence of maximum 2 per cent of carbon monoxide concentration in WGS reactor exit stream has been taken into account (Avcı *et al.,* 2002).

It has been reported that the Pt-based PEM fuel cell catalysts are very sensitive to impurities such as carbon monoxide. In order to reduce carbon monoxide concentration below tolerable values (<10 ppm), a carbon monoxide conversion of ca. 100 percent is proposed (Kahlich *et al.,* 1996; Şimsek *et al.,* 2007; Kamarudin *et al.,* 2004). For this purpose, 99 percent conversion for CO oxidation reaction, running in the PROX unit, is assumed for the carbon monoxide conversion.

In addition, in PEM fuel cells, ca. 25 percent of hydrogen in the fuel cell feed is rejected and is sent to the catalytic afterburner (Avcı *et al.,* 2002). In the catalytic afterburner, unconverted methane and rejected hydrogen are oxidized. This oxidation process, which is considered to run over a Pt-based catalyst, is assumed to run at 100 percent. Thus methane and hydrogen conversion rates, X_7 and X_8 respectively, are considered to be equal to 1.

3.2.2. Mole Balance Results

In the light of balance equations (3.5 to 3.55), methane-to-oxygen and steam-to-methane ratio combinations, hydrogen flow rate requirements and conversion assumptions for every step of the fuel processor system (Section 3.2.1), methane quantity in the feed stream is calculated for PEM fuel cells with power outputs of 10W, 50W and 100W. Solutions of the material balance equations (3.5 – 3.55) to calculate the molar flow rates of the streams shown in Figure 3.1 and defined in Table 3.3 are given in Tables 3.5, 3.6 and 3.7 for CH_4:O_2= 1.89 and H_2O:CH_4=1.56 and in Tables 3.8, 3.9 and 3.10 for CH_4:O_2= 2.24 and H_2O:CH_4=1.17.

Table 3.5. Mole Balance Results for 10W PEMFC (CH_4:O_2= 1.89 and H_2O:CH_4=1.56)

	F_1 (mol/h)	F_2 (mol/h)	F_3 (mol/h)	F_4 (mol/h)	F_5 (mol/h)	F_6 (mol/h)	F_7 (mol/h)	F_8 (mol/h)	F_9 (mol/h)	F_{10} (mol/h)
CH_4	0.25	0.18	0.08	0.08	0.00	0.08	0.00	0.08	0.00	0.00
H_2O	0.39	0.52	0.34	0.32	0.00	0.32	0.00	0.62	0.00	0.88
O_2	0.13	0.00	0.00	0.00	0.01	0.00	0.15	0.00	0.21	0.00
N_2	0.49	0.49	0.49	0.49	0.02	0.52	0.58	1.09	0.78	1.87
CO	0.00	0.00	0.03	0.01	0.00	10×10^{-6}	0.00	10×10^{-6}	0.00	10×10^{-6}
CO_2	0.00	0.07	0.14	0.16	0.00	0.17	0.00	0.17	0.00	0.25
H_2	0.00	0.00	0.39	0.41	0.00	0.41	0.00	0.10	0.00	0.00

Table 3.6. Mole Balance Results for 50W PEMFC (CH_4:O_2= 1.89 and H_2O:CH_4=1.56)

	F_1 (mol/h)	F_2 (mol/h)	F_3 (mol/h)	F_4 (mol/h)	F_5 (mol/h)	F_6 (mol/h)	F_7 (mol/h)	F_8 (mol/h)	F_9 (mol/h)	F_{10} (mol/h)
CH_4	1.24	0.91	0.39	0.39	0.00	0.39	0.00	0.30	0.00	0.00
H_2O	1.93	2.59	1.67	1.60	0.00	1.60	0.00	3.13	0.00	4.41
O_2	0.66	0.00	0.00	0.00	0.03	0.00	0.76	0.00	1.03	0.00
N_2	2.47	2.47	2.47	2.47	0.11	2.57	2.88	5.45	3.87	9.32
CO	0.00	0.00	0.13	0.06	0.00	9.5×10^{-5}	0.00	9.5×10^{-5}	0.00	9.5×10^{-5}
CO_2	0.00	0.33	0.72	0.80	0.00	0.85	0.00	0.85	0.00	1.24
CO	0.00	0.00	1.96	2.04	0.00	2.04	0.00	0.51	0.00	0.00

Table 3.7. Mole Balance Results for 100W PEMFC (CH_4:O_2= 1.89 and H_2O:CH_4=1.56)

	F_1 (mol/h)	F_2 (mol/h)	F_3 (mol/h)	F_4 (mol/h)	F_5 (mol/h)	F_6 (mol/h)	F_7 (mol/h)	F_8 (mol/h)	F_9 (mol/h)	F_{10} (mol/h)
CH_4	2.47	1.82	0.77	0.77	0.00	0.77	0.00	0.77	0.00	0.00
H_2O	3.86	5.16	3.33	3.19	0.00	3.19	0.00	6.24	0.00	8.80
O_2	1.31	0.00	0.00	0.00	0.06	0.00	1.53	0.00	2.05	0.00
N_2	4.92	4.92	4.92	4.92	0.21	5.13	5.74	10.87	7.73	18.60
CO	0.00	0.00	0.26	0.11	0.00	1.9×10^{-4}	0.00	1.9×10^{-4}	0.00	1.9×10^{-4}
CO_2	0.00	0.65	1.44	1.59	0.00	1.70	0.00	1.70	0.00	2.47
H_2	0.00	0.00	3.92	4.07	0.00	4.07	0.00	1.02	0.00	0.00

Table 3.8. Mole Balance Results for 10W PEMFC (CH_4:O_2= 2.24 and H_2O:CH_4=1.17)

	F_1 (mol/h)	F_2 (mol/h)	F_3 (mol/h)	F_4 (mol/h)	F_5 (mol/h)	F_6 (mol/h)	F_7 (mol/h)	F_8 (mol/h)	F_9 (mol/h)	F_{10} (mol/h)
CH_4	0.23	0.18	0.08	0.08	0.00	0.08	0.00	0.08	0.00	0.00
H_2O	0.27	0.38	0.20	0.18	0.00	0.18	0.00	0.49	0.00	0.74
O_2	0.10	0.00	0.00	0.00	0.01	0.00	0.15	0.00	0.21	0.00
N_2	0.39	0.39	0.39	0.39	0.02	0.41	0.57	0.99	0.77	1.76
CO	0.00	0.00	0.03	0.01	0.00	19×10^{-6}	0.00	19×10^{-6}	0.00	19×10^{-6}
CO_2	0.00	0.05	0.13	0.15	0.00	0.16	0.00	0.16	0.00	0.23
H_2	0.00	0.00	0.39	0.41	0.00	0.41	0.00	0.16	0.00	0.00

Table 3.9. Mole Balance Results for 50W PEMFC (CH_4:O_2= 2.24 and H_2O:CH_4=1.17)

	F_1 (mol/h)	F_2 (mol/h)	F_3 (mol/h)	F_4 (mol/h)	F_5 (mol/h)	F_6 (mol/h)	F_7 (mol/h)	F_8 (mol/h)	F_9 (mol/h)	F_{10} (mol/h)
CH_4	1.17	0.91	0.39	0.39	0.00	0.39	0.00	0.39	0.00	0.00
H_2O	1.37	1.89	0.98	0.90	0.00	0.90	0.00	2.43	0.00	3.71
O_2	0.52	0.00	0.00	0.00	0.03	0.00	0.76	0.00	1.03	0.00
N_2	1.96	1.96	1.96	1.96	0.10	2.07	2.87	4.94	3.86	8.80
CO	0.00	0.00	0.13	0.06	0.00	9.5×10^{-6}	0.00	9.5×10^{-6}	0.00	9.5×10^{-6}
CO_2	0.00	0.26	0.65	0.73	0.00	0.78	0.00	0.78	0.00	1.17
H_2	0.00	0.00	1.96	2.03	0.00	2.03	0.00	0.51	0.00	0.00

Table 3.10. Mole Balance Results for 100W PEMFC (CH_4:O_2= 2.24 and H_2O:CH_4=1.17)

	F_1 (mol/h)	F_2 (mol/h)	F_3 (mol/h)	F_4 (mol/h)	F_5 (mol/h)	F_6 (mol/h)	F_7 (mol/h)	F_8 (mol/h)	F_9 (mol/h)	F_{10} (mol/h)
CH_4	2.34	1.82	0.77	0.77	0.00	0.77	0.00	0.77	0.00	0.00
H_2O	2.74	3.78	1.95	1.80	0.00	1.80	0.00	4.86	0.00	7.42
O_2	1.04	0.00	0.00	0.00	0.06	0.00	1.53	0.00	2.05	0.00
N_2	3.93	3.93	3.93	3.93	0.21	4.14	5.74	9.88	7.73	17.61
CO	0.00	0.00	0.26	0.11	0.00	19×10^{-5}	0.00	19×10^{-5}	0.00	19×10^{-5}
CO_2	0.00	0.52	1.31	1.46	0.00	1.57	0.00	1.57	0.00	2.34
H_2	0.00	0.00	3.92	4.07	0.00	4.07	0.00	1.02	0.00	0.00

The results given in Tables 3.5-3.10 give the molar flow rates of each species at the entrance and exit of each reactor. Calculated flow rate values at the inlet, given in Table 3.11, will be used as initial conditions for the one-dimensional pseudohomogeneous reactor model that will be explained in Chapter 4. This model, composed of differential material, energy and momentum balance equations, simulates the molar flow rates of species, temperature and pressure along the packed-bed reactor, once the catalyst weight is specified. Catalyst weights needed to give the desired PEMFC power outputs are estimated by a trial-and-error procedure, in which the reactor model – with the initial conditions and an assumed value of catalyst weight – is solved and the outputs, i.e. the calculated exit flow rates, are compared with the ones given in Tables 3.5-3.10. Different values of catalyst weights are then tried until a match between these flow rates are noticed. This procedure is explained in detail in Chapter 4.

Table 3.11 Calculated Flow Rates of Species in the Feed Stream

Ratio	CH_4:O_2= 1.89; H_2O:CH_4=1.56			CH_4:O_2= 2.24 H_2O:CH_4= 1.17		
Fuel Cell Capacity (W)	10	50	100	10	50	100
CH_4 (mol/h)	0.25	1.24	2.47	0.23	1.17	2.34
H_2O (mol/h)	0.39	1.93	3.86	0.27	1.37	2.74
O_2 (mol/h)	0.13	0.66	1.31	0.10	0.52	1.04
N_2 (mol/h)	0.49	2.47	4.92	0.39	1.96	3.93

4. STEADY-STATE MODELING AND SIMULATION OF REACTORS

4.1. Modeling of Fuel Processor System

Molar flow rates of every species in each stream of the fuel processor-fuel cell system (Figure 3.1) were calculated and presented in Chapter 3. This chapter outlines the techniques for evaluating the catalyst weights in the IPOX, WGS and PROX reactors and their sizes for meeting the power output requirements of the PEM fuel cells.

4.1.1. Modeling Procedure

In this section, rate expressions and model equations will be given for steam reforming, water gas shift, total oxidation, and carbon monoxide oxidation reactions.

4.1.1.1. Rate Expressions. In order to quantify the rate of total oxidation over Pt/δ-Al_2O_3 catalyst, the empirical rate expression proposed by Ma (1996) is selected. At this ponit, it is assumed that total oxidation is mainly catalyzed by the Pt-based catalyst rather than Ni/MgO-Al_2O_3, which is the other catalyst forming the physical catalyst mixture in the IPOX reactor (Ma (1996)):

$$-r_{TOX} = 1.57 * 10^5 * \exp(\frac{-21068}{1.987 * T}) * P_{CH_4}{}^{0.95} * P_{O_2}{}^{-0.17} \quad (4.1)$$

In equation (4.1), T is the reaction temperature (K), P_{CH_4} and P_{O_2} are partial pressures of methane and oxygen, respectively (bar).

For evaluating rates of steam reforming and water gas shift reactions, which are the hydrogen generating reactions of the IPOX process, rate equations proposed by Xu and Froment (1989) are used (Tables 2.4 and 2.5) which occurs over Ni/$MgAl_2O_4$. Arrhenius

equation (Equation (2.11)) is used to calculate rate constants while equilibrium constant is calculated from Van't-Hoff equation (Equation (2.12)).

$$-r_{SR} = \frac{k_{SR} / P_{H_2}^{2.5}(P_{CH_4}P_{H_2O} - P_{H_2}^3 P_{CO} / K_{eq,SR})}{(1 + K_{CO}P_{CO} + K_{H_2}P_{H_2} + K_{CH_4}P_{CH_4} + K_{H_2O}P_{H_2O} / P_{H_2})^2} \tag{4.2}$$

In Equation (4.2), k_{SR} is the rate constant (kmol kgcat^{-1} h^{-1}), K_{CO}, K_{H_2}, K_{CH_4} and K_{H_2O} are the adsorption constant for indexed species in (bar^{-1}), $K_{eq,SR}$ is the equilibrium constant for steam reforming reaction in (bar^2), P_{CH_4}, P_{CO}, P_{H_2O} and P_{H_2} are the partial pressures of indexed species (bar). The temperature dependence of rate and adsorption constants is expressed by Arrhenius and Van't Hoff type equations respectively, whose parameters given in Table 2.7 and including gas constant, R, which has been taken as 8.3145 kJ kmol^{-1}K^{-1} for Equations (4.2) and (4.3).

$$-r_{WGSS} = \frac{k_{WGSS} / P_{H_2}(P_{CO}P_{H_2O} - P_{H_2}P_{CO2} / K_{eq,WGSS})}{(1 + K_{CO}P_{CO} + K_{H_2}P_{H_2} + K_{CH_4}P_{CH_4} + K_{H_2O}P_{H_2O} / P_{H_2})^2} \tag{4.3}$$

In Equation (4.3), $K_{eq,WGSS}$ is the equilibrium constant for water-gas shift side reaction (bar^2), k_{WGSS} is the rate constant (kmol kgcat^{-1} h^{-1}) and other variables are defined to be the same with those of steam reforming given above.

Table 4.1. Adsorption constants used in Van't-Hoff equation

Adsorption Constants		
Species	$K_{0,j}$ (bar^{-1})	ΔH_j (kJ/gmol)
CH_4	6.65 x 10^{-4}	38.3
H_2O	1.77 x 10^{5}	88.7
CO	8.23 x 10^{-5}	70.7
H_2	6.12 x 10^{-9}	- 82.9

The second step of the fuel processing system is the water-gas shift reactor (Figure 3.1). This reactor is considered to operate at temperatures between 393 and 523K over Cu/ZnO-Al_2O_3 type of catalyst (Choi and Stenger, 2003). Reaction rate at these conditions can be quantified by the power-law model type proposed by Choi and Stenger (2003):

$$r_{WGS} = 2.96x10^5 \exp\left(-\frac{47{,}400}{RT}\right)\left(P_{CO}P_{H_2O} - \frac{P_{CO_2}P_{H_2}}{K_{eq,WGS}}\right) \tag{4.4}$$

In Equation (4.4), r_{WGS} is the rate of water-gas shift reaction in (kmol kgcat^{-1} h^{-1}). Equilibrium constant of WGS, $K_{eq,WGS}$ has the same temperature dependency with that of $K_{eq,WGSS}$ given in Eqation (4.3). R is the gas constant (8.3144 kJ kmol^{-1} K^{-1}), P_{CO_2}, P_{CO}, P_{H_2O} and P_{H_2} are the partial pressures of the indexed species (bar).

For the last reactor of the fuel processor system which is carbon monoxide oxidation unit, one of the propositions of Sedmak *et. al.* (2003) has been selected due to the high selectivity of CO. This rate expression is valid at a temperature interval of 318 to 363 K and derived for $Cu_{0.1}Ce_{0.9}O_{2-y}$ nanostructured catalyst (Sedmak *et. al.* (2003):

$$r_{CO} = \frac{k_{CO}k_{O_2}P_{CO}P_{O_2}^n}{0.5k_{CO}P_{CO} + k_{O_2}P_{O_2}^n} \tag{4.5}$$

In Equation (4.5) r_{CO} is the rate of preferential carbon monoxide oxidation reaction in (kmol kgcat^{-1} h^{-1}). k_{CO} is the rate constant for the reduction of surface by CO (kmol kgcat^{-1} h^{-1} bar^{-1}) and k_{O_2} is the rate constant for the re-oxidation of surface by O_2 (kmol kgcat^{-1} h^{-1} bar^{-n}) and are represented with Arrhenius-type temperature dependency as $k_{CO} = A_{CO}.\exp(-E_{a,CO}/RT)$ and $k_{O_2} = A_{O_2}.\exp(-E_{a,O_2}/RT)$. Parameters of Equation 4.5 are given in Table 2.13. P_{CO} and $P_{O_2}^n$ are the partial pressures of indexed species (bar).

4.1.1.2. Model Equations. The working equations for the one-dimensional pseudohomogeneous, steady-state reactor model are listed below. The model is aiming to find catalyst weight of reactors with a trial-error procedure using preliminary results calculated in Chapter 3.

For IPOX reactor there are eight model equations describing flow rate change of each species (Equations (4.6)-(4.12)), temperature change and pressure drop. The equation which describes pressure drop in reactors is given in Equation (4.26).

$$\frac{dF_{CH_4}}{dW} = r_{TOX} + r_{SR} \tag{4.6}$$

$$\frac{dF_{CO}}{dW} = -r_{SR} + r_{WGSS} \tag{4.7}$$

$$\frac{dF_{CO_2}}{dW} = -r_{TOX} - r_{WGSS} \tag{4.8}$$

$$\frac{dF_{H_2}}{dW} = -3r_{SR} - r_{WGSS} \tag{4.9}$$

$$\frac{dF_{H_2O}}{dW} = -2r_{TOX} + r_{SR} + r_{WGSS} \tag{4.10}$$

$$\frac{dF_{O_2}}{dW} = 2r_{TOX} \tag{4.11}$$

$$\frac{dT_{IPOX}}{dW} = \frac{\left[\left(-\Delta H_{TOX} \times -r_{TOX}\right) + \left(-\Delta H_{SR} \times -r_{SR}\right) + \left(-\Delta H_{WGSS} \times -r_{WGSS}\right)\right]}{DEN} \tag{4.12}$$

$$DEN_1 = F_{CH_4} cp_{CH_4} + F_{CO} cp_{CO} + F_{CO_2} cp_{CO_2} + F_{H_2} cp_{H_2} + F_{H_2O} cp_{H_2O} + F_{O_2} cp_{O_2} + F_{N_2} cp_{N_2}$$

Model equations used to calculate flow rates of the species and fluid temperature along the water-gas shift converter are given below:

$$\frac{dF_{CO}}{dW} = \frac{dF_{H_2O}}{dW} = -r_{WGS} \tag{4.13}$$

$$\frac{dF_{CO2}}{dW} = \frac{dF_{H_2}}{dW} = r_{WGS} \tag{4.14}$$

$$\frac{dT_{WGS}}{dW} = \frac{-DH_{WGS} \times -r_{WGS}}{F_{CH_4}cp_{CH_4} + F_{CO}cp_{CO} + F_{H_2}cp_{H_2} + F_{H_2O}cp_{H_2O} + F_{O_2}cp_{O_2} + F_{N_2}cp_{N_2}} \tag{4.15}$$

Model equations for simulating component flow and temperature profiles along the PROX unit are given below:

$$\frac{dF_{CO}}{dW} = \frac{-dF_{CO_2}}{dW} = r_{PROX} \tag{4.16}$$

$$\frac{dF_{O_2}}{dW} = 0.5r_{PROX} \tag{4.17}$$

$$\frac{dT_{PROX}}{dW} = \frac{-\Delta H_{PROX} \times -r_{PROX}}{DEN_1} \tag{4.18}$$

Obtained equations have been evaluated using ode15s technique on Matlab program. Ode 15s is a variable-order solver based on the numerical differentiation formulas (NDFs) which are related to but are more efficient than the backward differentiation formulas, BDFs (also known as Gear's method). Among the other solving methods in Matlab, Ode 15s has been chosen for its stiff-type solving techniques. Peak points have been expected on the temperature profiles of the reactors, thus, ode15s is selected, as it uses variable step sizes (Shampine and Reichelt, 1997; Shampine *et al.,* 1999).

4.1.1.3. Equations for Heat and Mass Transfer Criteria. During the solution of the model equations described above, criteria to evaluate external (fluid-to-solid) heat transfer (Mears' criterion) and internal (intraparticle) mass transfer (Weisz-Prater criterion) resistances have also been calculated to quantify the significance of these transport resistances. Weisz-Prater criterion uses rate of reaction to determine if internal diffusion is limiting the reaction. The Mears' criterion uses also rate of reaction to specify if bulk fluid temperature will be the same as the temperature at the external surface of the pellet (Fogler, 1999). The other possible transport resistances, internal heat transfer and external mass transfer are not taken into account. It is assumed that catalyst particle is isothermal, also interfacial mass transfer is neglected due to the sufficiently rapid diffusion assumption of reactants.

According to the Mear's criterion given in Equation (4.19), left-hand-side of the external heat transfer criterion, *ehtc*, has to be smaller than 0.3 in order to obtain no temperature gradient between bulk fluid temperature and external surface of the pellet (Rase, 1990).

$$ehtc = \frac{\sum \Delta H_i r_i D_p \rho_b E_i}{h_s T^2 R} \tag{4.19}$$

In Equation (4.19), D_p is particle size, ρ_b is bulk density, E_i is the activation energy of reaction i, and h_s is heat transfer coefficient between bulk and particle, which has been calculated using the correlation given in Equation (4.20) (Rase, 1990):

$$h_s = \frac{\lambda_f}{D_p}(2 + 1.1\,\mathrm{Pr}^{1/3})\,\mathrm{Re}^{0.6} \tag{4.20}$$

In Equation (4.20), λ_f is the thermal conductivity of the bulk fluid (kJ m^{-1} h^{-1} K^{-1}), Pr is Prandtl number and Re is Reynolds number. Prandtl number can be estimated from Perry (1997) for nitrogen as 0.7 and Reynolds number can be evaluated from the well-known relationship:

$$\mathrm{Re} = \frac{D_t \rho_m v}{\mu} \tag{4.21}$$

In Equation (4.21), D_t is the tube diameter (m), ρ_m the density of the gas mixture (kg m^{-3}), v the velocity of the gas mixture (m s^{-1}) and μ viscosity of the mixture (kg m^{-1} s^{-1}). The gas mixture is assumed to behave like nitrogen in evaluating its physical properties, since the gas mixture contains mostly nitrogen (~ 35 per cent by volume) (Avcı, 2003).

$$\lambda_{N_2} = 1.295 * 10^{-2} + 5.223 * 10^{-5} * T \tag{4.22}$$

where T is in K and λ_{N_2} is in W m^{-1} K^{-1}.

Void fraction, in the catalyst bed has been assumed as 0.3. In order to obtain a flat velocity profile in a packed-bed tubular reactor, a well-arranged ratio of tube diameter to particle size diameter must be selected. For this purpose, Rase (1990) has proposed an average value:

$$\frac{D_T}{D_P} \geq 30 \tag{4.23}$$

In addition it is proposed that, for gases, axial dispersion and axial heat conduction effects in a packed bed generally have no effect on reactor operation, and can therefore be neglected if the criterion given in Equation (4.24) is satisfied (Rase, 1990). It has also been reported that plug-flow assumption can be made if the tube length to tube diameter ratio meets the criterion given in Equation (4.25) (Rase, 1990):

$$\frac{L}{D_P} \geq 50 \tag{4.24}$$

$$\frac{L}{D_T} \geq 5 \tag{4.25}$$

During the reactor simulations, pressure drop have been estimated for each reactor operation using Ergun equation (Rase, 1990):

$$\frac{dP}{dW} = \frac{(\frac{-G}{\rho_m D_p})(\frac{1-\phi}{\phi^3})\left[(\frac{150(1-\phi)\mu}{D_p}) + 1.75G\right]}{\frac{\rho_b \pi D_t^{\,2}}{4}} \tag{4.26}$$

In Equation (4.26), G is superficial mass velocity (kg m^{-2} s^{-1}) and equals to $\rho_m v$, ϕ the porosity (volume of void / total bed volume = void fraction), A_c the cross-sectional area of the pipe (m^2). Note that this equation is solved simultaneously with the differential mole and energy balance equations given in Section 4.1.1.2.

Internal mass transfer resistance in all reactors has been estimated using Weisz-Prater criterion (internal mass transfer criterion, *imtc*). According to this criterion, if *imtc* is much greater than one internal diffusion limits the reaction severely, and if is much smaller than one, it can be said that there is no diffusion limitations, thus no concentration gradient assumption can be made (Fogler, 1999):

$$imtc = \frac{F_{Specie}\rho_c D_p^{\,2}}{4 D_e C_{aj}} \leq\leq 1 \tag{4.27}$$

$$D_e = \frac{D_{km}\varepsilon_p \sigma}{\tau} \tag{4.28}$$

In Equations (4.27) and (4.28), D_{km} is the diffusivity of the chosen species k in mixture m in cm^2 sec^{-1}, τ is tortuosity which is defined as the ratio of actual distance a molecule travels between two points to shortest distance between those two points, σ the constriction factor which is equal to unity if the cross-section area of the reactor tube remains constant and D_{km} the multicomponent gas mixture diffusivity which is defined by Rase (1990) is shown in (Equation (4.29)).

$$D_{km} = \left(\sum_{j=1}^{n} \frac{Y_j}{D_{kj}} \right)^{-1} \tag{4.29}$$

$$D_{kj} = \frac{0.00143 T^{1.75}}{P M_{kj}^{0.5} \left[(\sum v_a)_k^{1/3} + (\sum v_a)_j^{1/3} \right]} \tag{4.30}$$

D_{kj} is the binary diffusion of component k diffusing into j present at a mole fraction of Y_j. The M_{kj} term in Equation (4.30) is defined as follows:

$$M_{kj} = 2\left[M_k^{-1} + M_j^{-1} \right]^{-1} \tag{4.31}$$

In Equations (4.30) and (4.31), P is pressure in atm, M_k and M_j are molecular weight of the components k and j, respectively, v_i is the atomic diffusion volume of species i (Rase, 1990). In calculating binary diffusivities for evaluating *imtc* in all reactors, methane is assumed to diffuse into other components.

4.1.2. Computational Results

Simulations have been made for three PEM fuel cell power outputs – 10, 50 and 100W – and for two feed ratio combinations: inlet methane-to-oxygen ratio, which are 2.24 and 1.89 and inlet steam-to-methane ratio which are 1.17 and 1.56. For all power output values of the fuel cell system and for all reactions, the methane-to-oxygen, steam-to-methane combinations of 2.24, 1.17 and 1.89, 1.56 have been studied.

4.1.2.1. Results for 10W Fuel Cell system.

Table 4.2. Simulation results for 10W PEMFC system (CH_4/O_2=1.89, H_2O/CH_4=1.56)

	Flow rates at the feed (mol/h)	Flow rates at IPOX exit (mol/h)	Flow rates at WGS exit (mol/h)	Flow rates at PROX exit (mol/h)
CH_4	0.247	0.093	0.093	0.093
H_2O	0.386	0.302	0.265	0.265
O_2	0.131	0.00	0.00	0.00
N_2	0.492	0.490	0.490	0.5269
CO	0.00	0.056	0.0196	0.0000052
CO_2	0.00	0.099	0.135	0.154
H_2	0.00	0.391	0.427	0.427
Temperature (K)	627	846	inlet 473 outlet 503	inlet 353 outlet 470
Catalyst weight (g)	-	4.35	3.00	0.7424
CO concentration	-	3.9*	1.4 *	3.5 **

* CO concentration: mol percent
** CO concentration: ppm

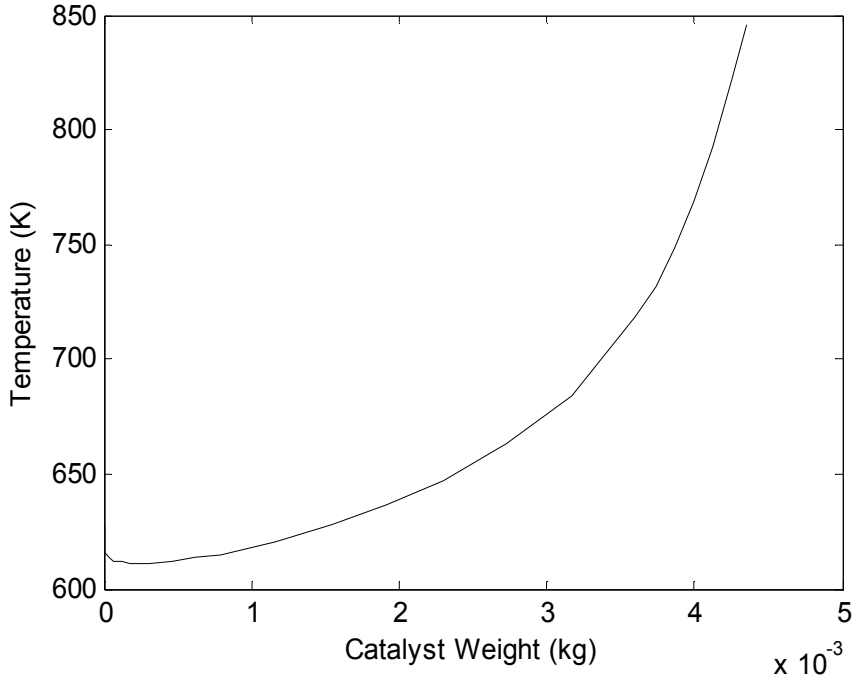

Figure 4.1. Temperature profile along IPOX reactor for CH_4/O_2=1.89, H_2O/CH_4=1.56 at 10W PEMFC

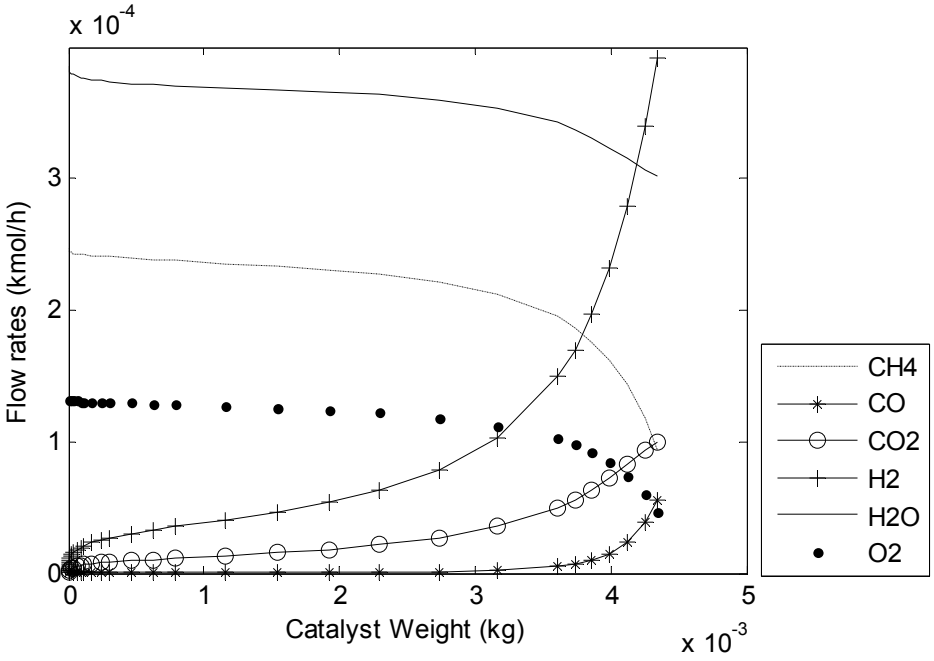

Figure 4.2. Flow rates along IPOX reactor for CH_4/O_2=1.89, H_2O/CH_4=1.56 at 10W PEMFC system

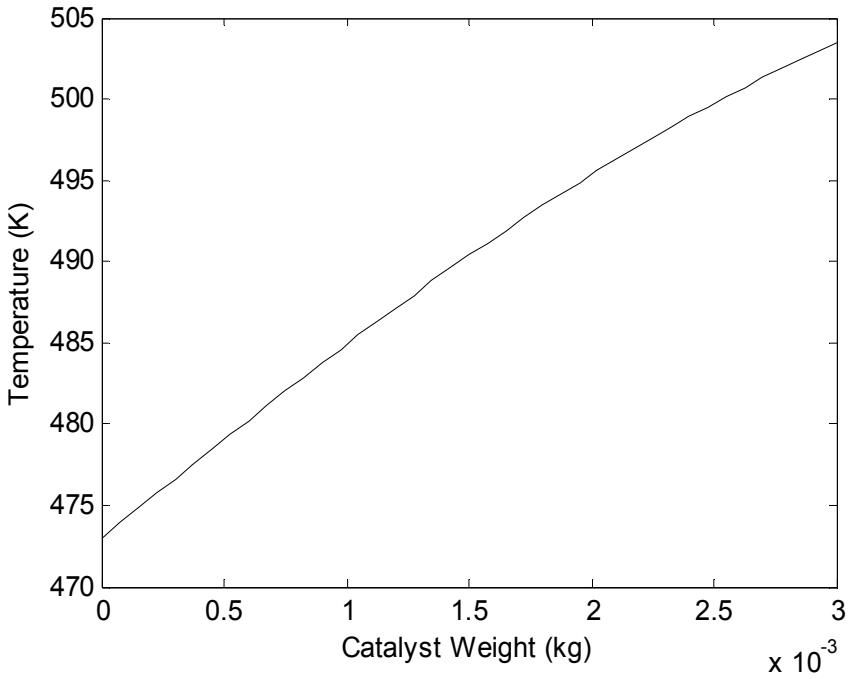

Figure 4.3. Temperature profile along WGS reactor for CH_4/O_2=1.89, H_2O/CH_4=1.56 at 10W PEMFC system

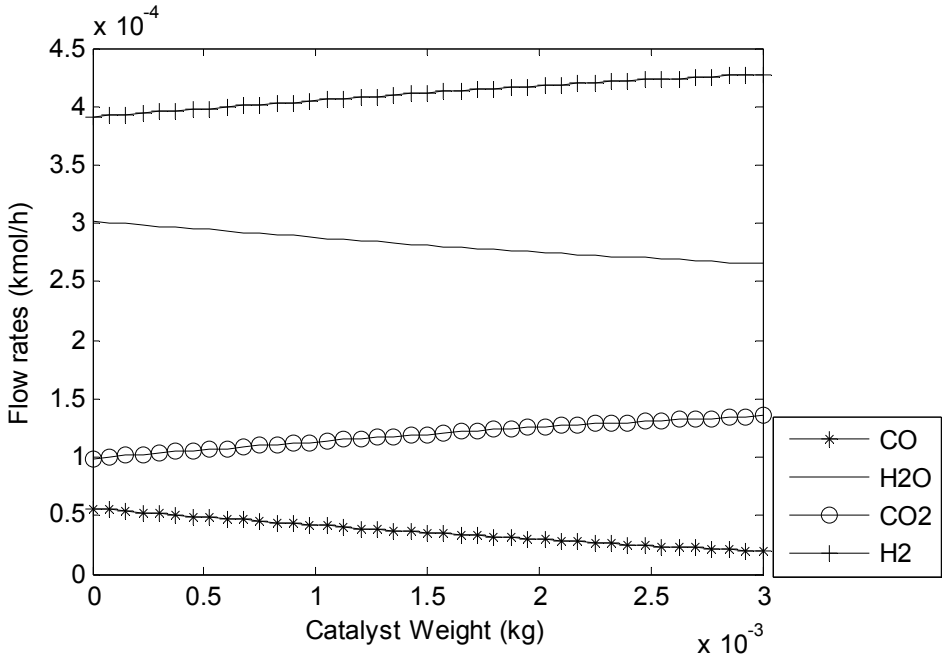

Figure 4.4. Flow rates along WGS reactor for CH_4/O_2=1.89, H_2O/CH_4=1.56 at 10W PEMFC system

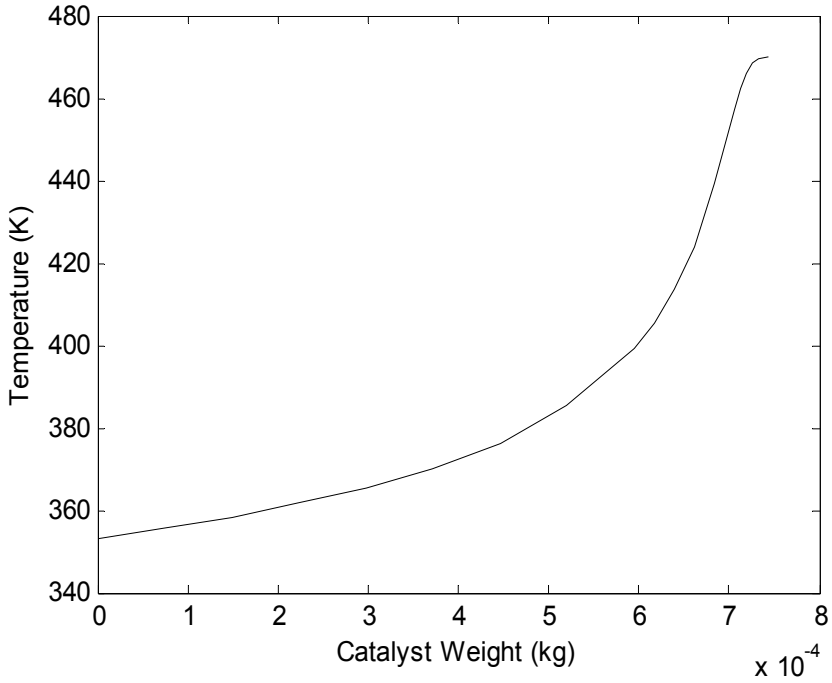

Figure 4.5. Temperature profile along PROX reactor for CH_4/O_2=1.89, H_2O/CH_4=1.56 at 10W PEMFC system

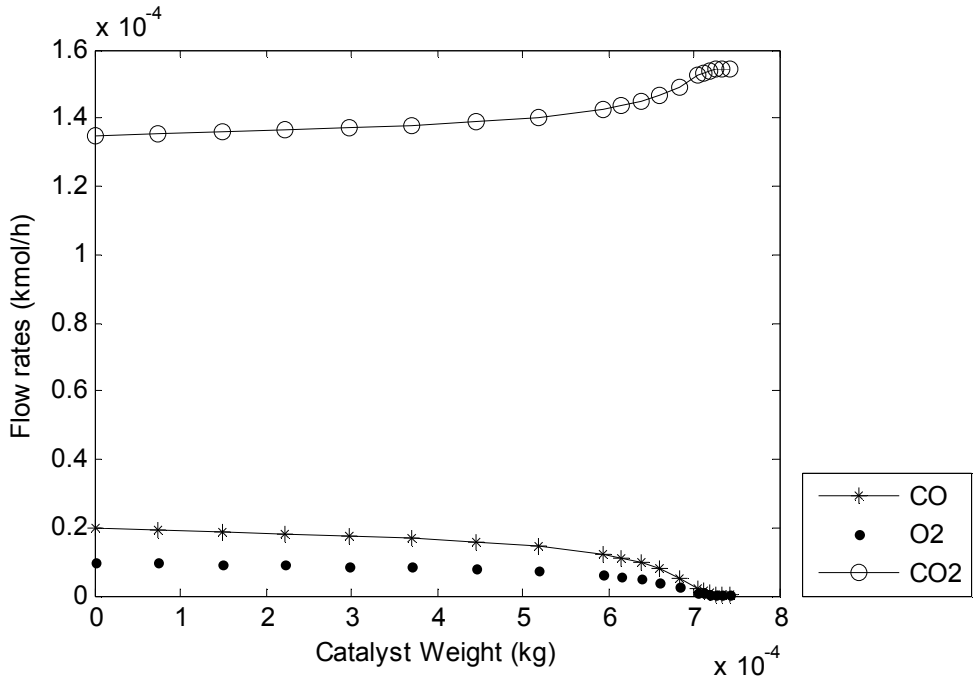

Figure 4.6. Flow rates along PROX reactor for CH_4/O_2=1.89, H_2O/CH_4=1.56 at 10W PEMFC system

Table 4.3. Simulation results of 10W PEMFC system (CH_4/O_2=2.24, H_2O/CH_4=1.17)

	Flow rates at the feed (mol/h)	Flow rates at IPOX exit (mol/h)	Flow rates at WGS exit (mol/h)	Flow rates at PROX exit (mol/h)
CH_4	0.23	0.07	0.07	0.07
H_2O	0.27	0.20	0.141	0.141
O_2	0.10	0.00	0.00	0.00
N_2	0.39	0.39	0.39	0.4295
CO	0.00	0.08	0.021	0.000017
CO_2	0.00	0.08	0.139	0.159
H_2	0.00	0.392	0.45	0.45
Temperature (K)	620	884	inlet 473 outlet 531	inlet 353 outlet 500
Catalyst Weight (g)		3.28	3.50	0.54989
CO concentration		6.7	1.7 *	13 **

* CO concentration: mol percent
** CO concentration: ppm

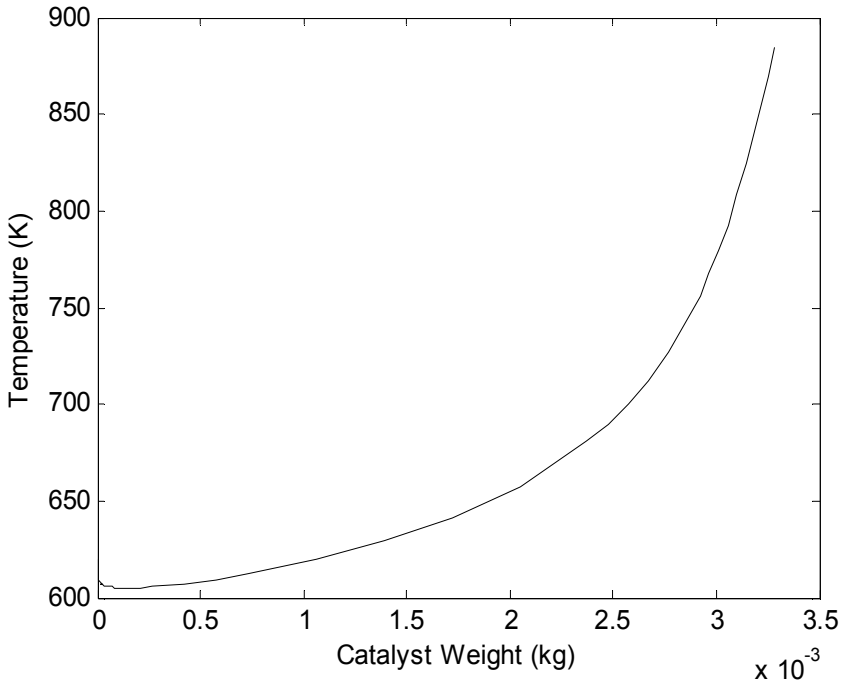

Figure 4.7. Temperature profile along IPOX reactor for CH_4/O_2=2.24, H_2O/CH_4=1.17 at 10W PEMFC system

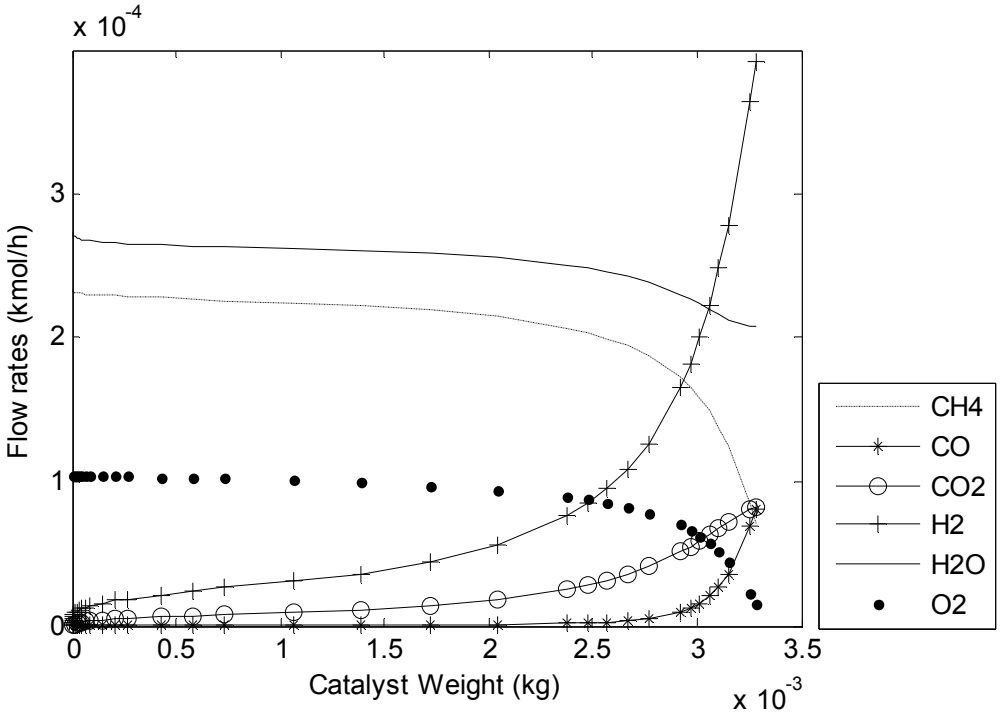

Figure 4.8. Flow rates along IPOX reactor for CH_4/O_2=2.24, H_2O/CH_4=1.17 at 10W PEMFC system

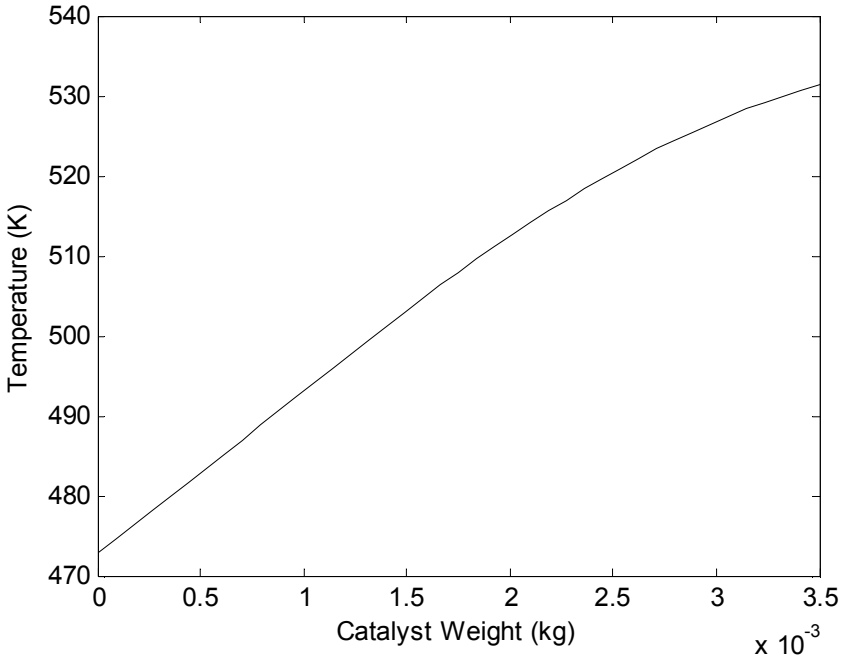

Figure 4.9. Temperature profile along WGS reactor for CH_4/O_2=2.24, H_2O/CH_4=1.17 at 10W PEMFC system

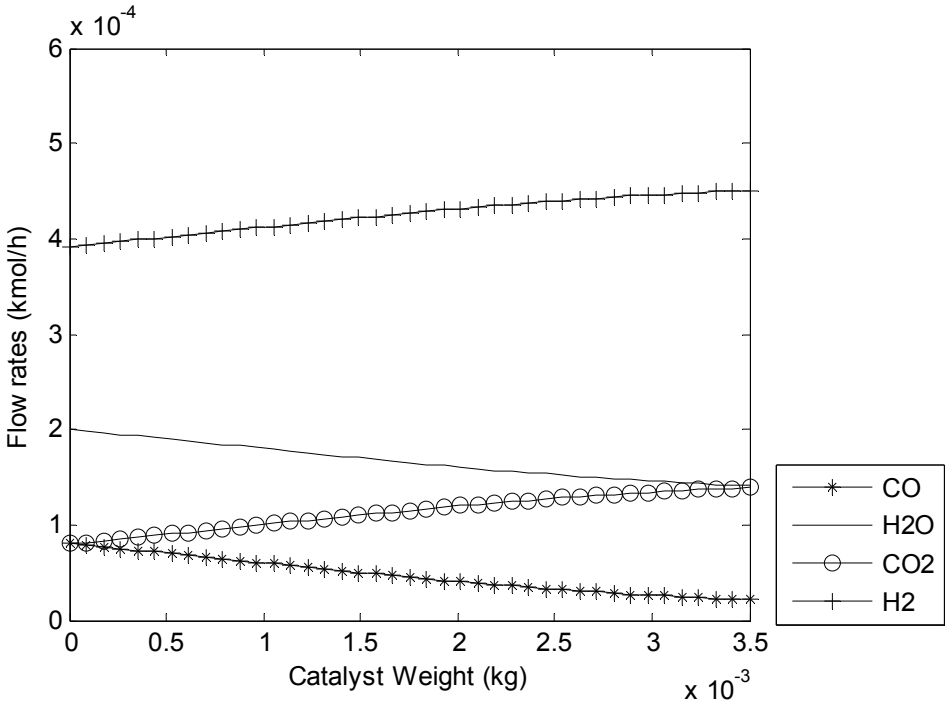

Figure 4.10. Flow rates along WGS reactor for CH_4/O_2=2.24, H_2O/CH_4=1.17 at 10W PEMFC system

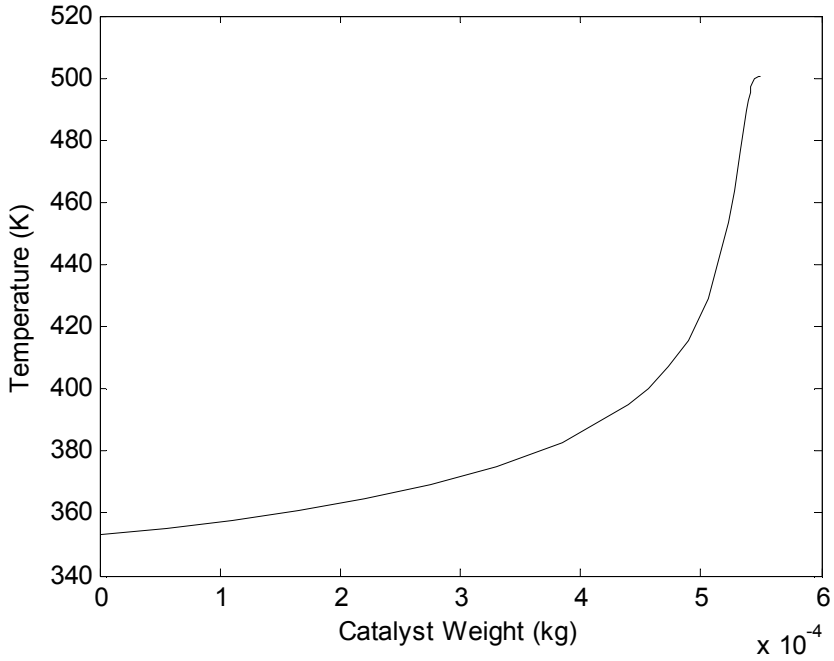

Figure 4.11. Temperature profile along PROX reactor for CH_4/O_2=2.24, H_2O/CH_4=1.17 at 10W PEMFC system

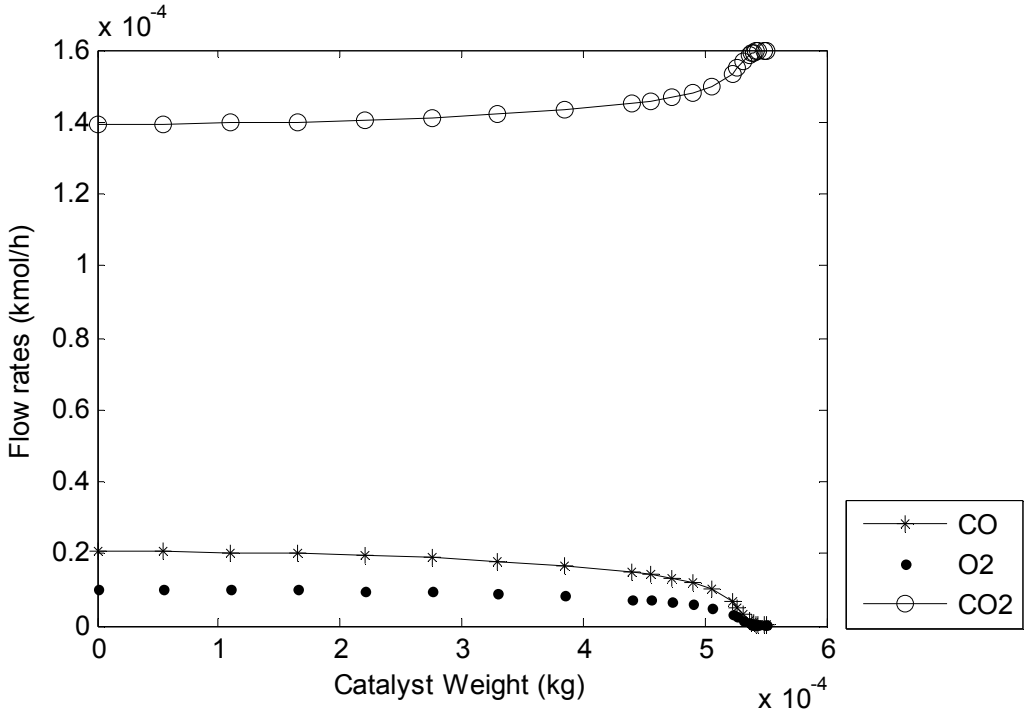

Figure 4.12. Flow rates along PROX reactor for CH_4/O_2=2.24, H_2O/CH_4=1.17 at 10W PEMFC system

4.1.2.2. Results for 50W Fuel Cell system.

Table 4.4. Simulation results of 50W PEMFC system (CH_4/O_2=1.89, H_2O/CH_4=1.56)

	Flow rates at the feed (mol/h)	Flow rates at IPOX exit (mol/h)	Flow rates at WGS exit (mol/h)	Flow rates at PROX exit (mol/h)
CH_4	1.240	0.468	0.468	0.468
H_2O	1.930	1.510	1.338	1.338
O_2	0.650	0.00	0.00	0.00
N_2	2.460	2.460	2.460	2.663
CO	0.00	0.286	0.108	0.00003
CO_2	0.00	0.504	0.672	0.778
H_2	0.00	1.972	2.142	2.142
Temperature (K)	627	847	inlet 473 outlet 501	inlet 353 outlet 481
Catalyst Weight (g)		20.85	14	3.41
CO concentration			1.5 *	4 **

* CO concentration: mol percent
** CO concentration: ppm

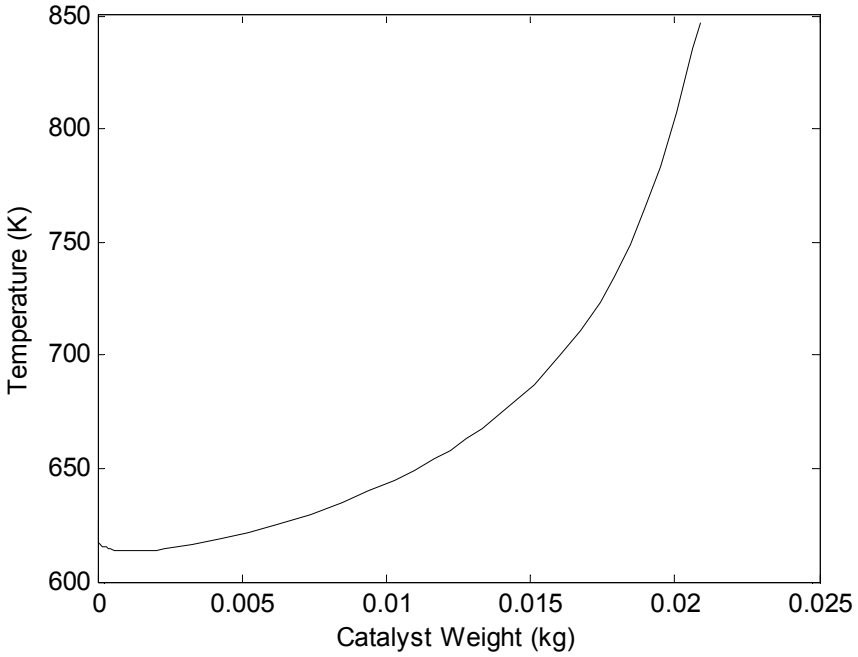

Figure 4.13. Temperature profile along IPOX reactor for CH_4/O_2=1.89, H_2O/CH_4=1.56 at 50W PEMFC

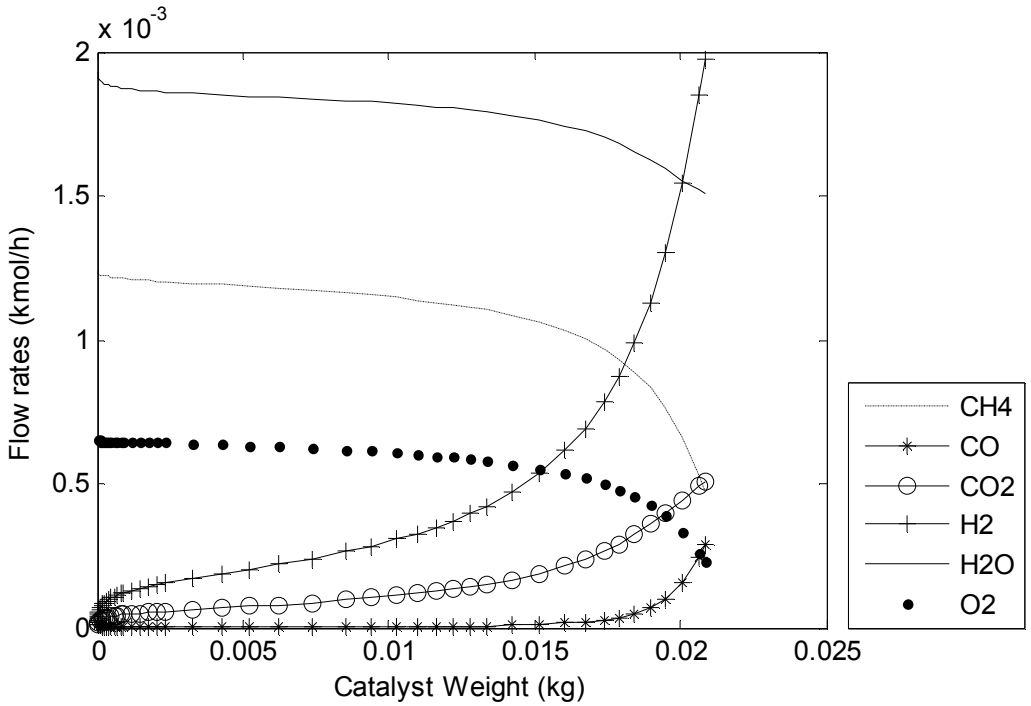

Figure 4.14. Flow rates along IPOX reactor for CH_4/O_2=1.89, H_2O/CH_4=1.56 at 50W PEMFC system

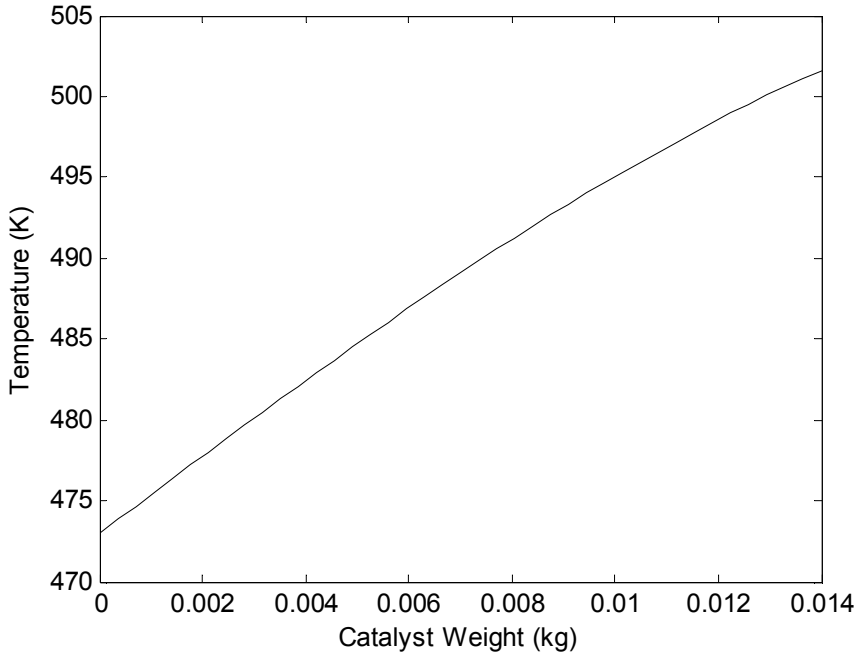

Figure 4.15. Temperature profile along WGS reactor for CH_4/O_2=1.89, H_2O/CH_4=1.56 at 50W PEMFC system

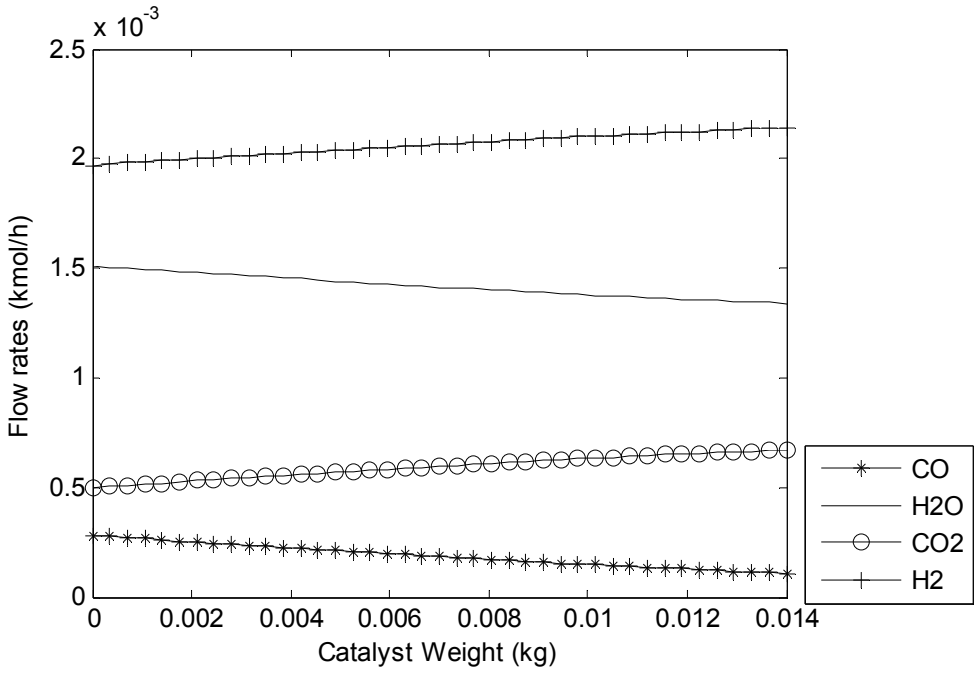

Figure 4.16. Flow rates along WGS reactor for CH_4/O_2=1.89, H_2O/CH_4=1.56 at 50W PEMFC system

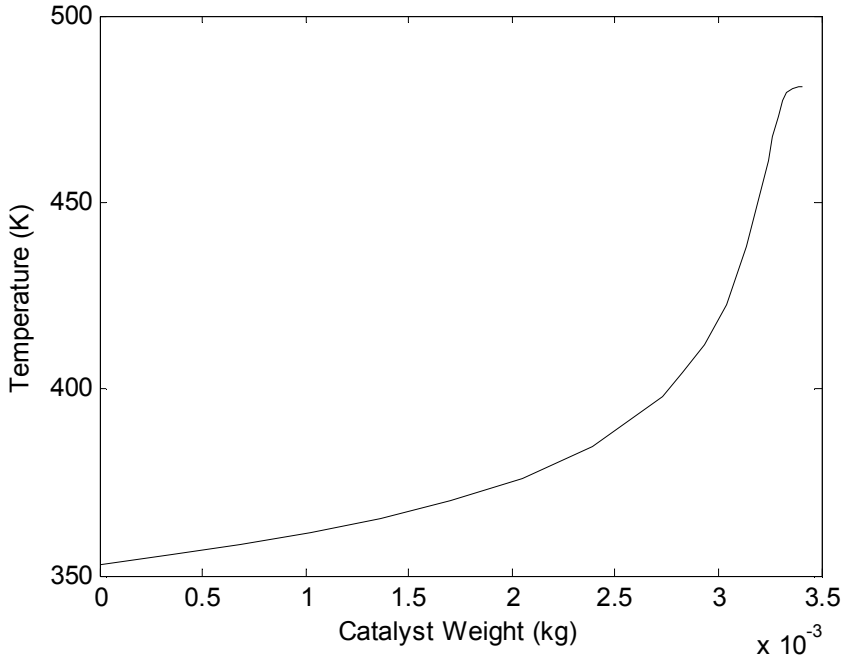

Figure 4.17. Temperature profile along PROX reactor for CH_4/O_2=1.89, H_2O/CH_4=1.56 at 50W PEMFC system

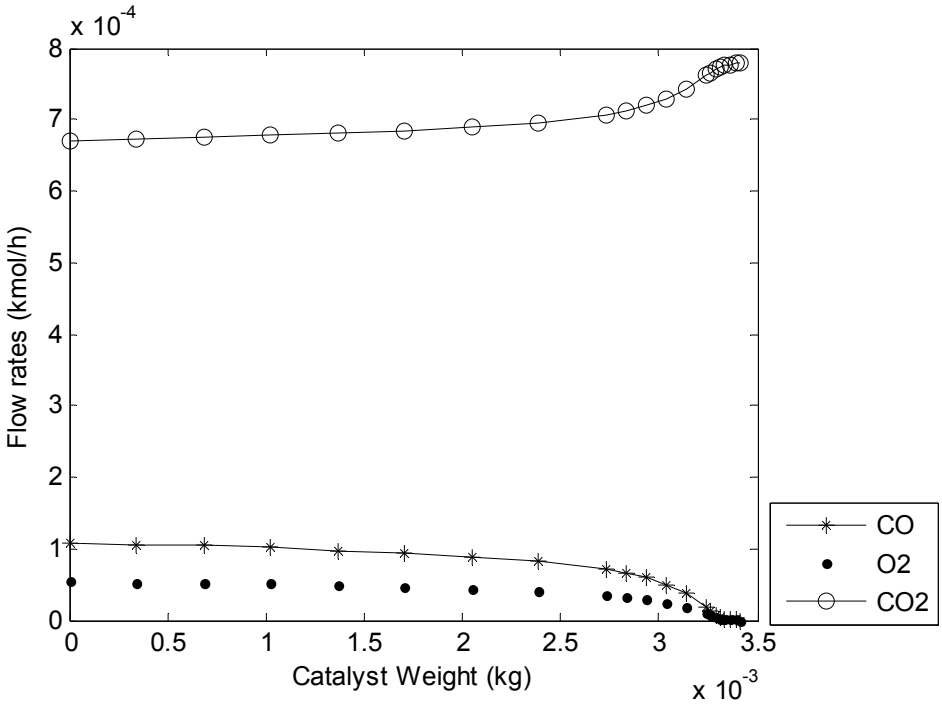

Figure 4.18. Flow rates along PROX reactor for CH_4/O_2=1.89, H_2O/CH_4=1.56 at 50W PEMFC system

Table 4.5. Simulation results of 50W PEMFC system (CH_4/O_2=2.24, H_2O/CH_4=1.17)

	Flow rates at the feed (mol/h)	Flow rates at IPOX exit (mol/h)	Flow rates at WGS exit (mol/h)	Flow rates at PROX exit (mol/h)
CH_4	1.170	0.378	0.378	0.38
H_2O	1.370	1.043	0.762	0.76
O_2	0.520	0.00	0.00	0.00
N_2	1.960	1.960	1.960	2.167
CO	0.00	0.395	0.112	0.0000164
CO_2	0.00	0.416	0.687	0.789
H_2	0.00	1.919	2.197	2.19
Temperature (K)	620	880	inlet 473 outlet 527	inlet 353 outlet 505
Catalyst Weight (g)		14.9	16	2.76
CO concentration		6.4 *	1.8 *	3.0 *

* CO concentration: mol percent
** CO concentration: ppm

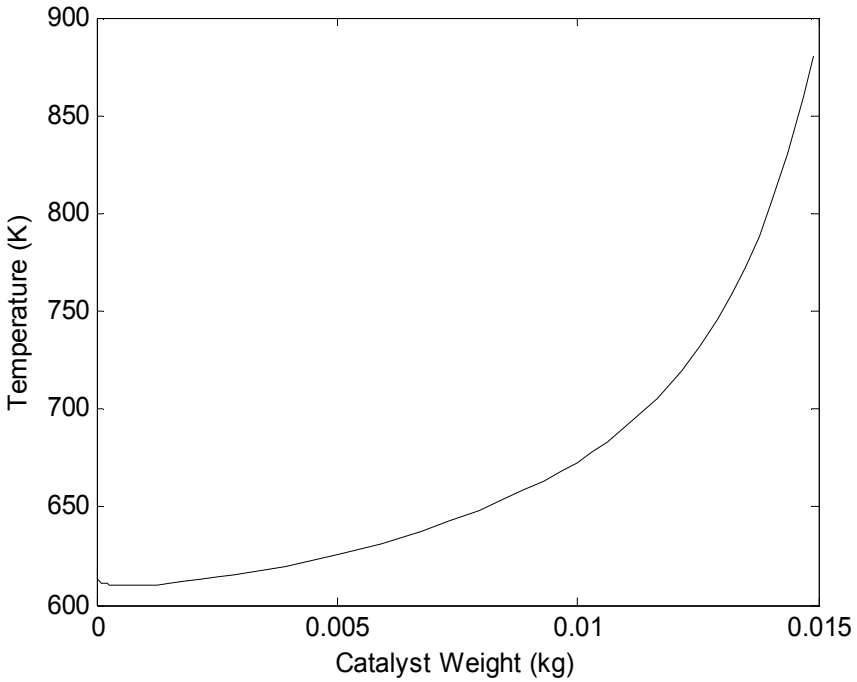

Figure 4.19. Temperature profile along IPOX reactor for CH_4/O_2=2.24, H_2O/CH_4=1.17 at 50W PEMFC system

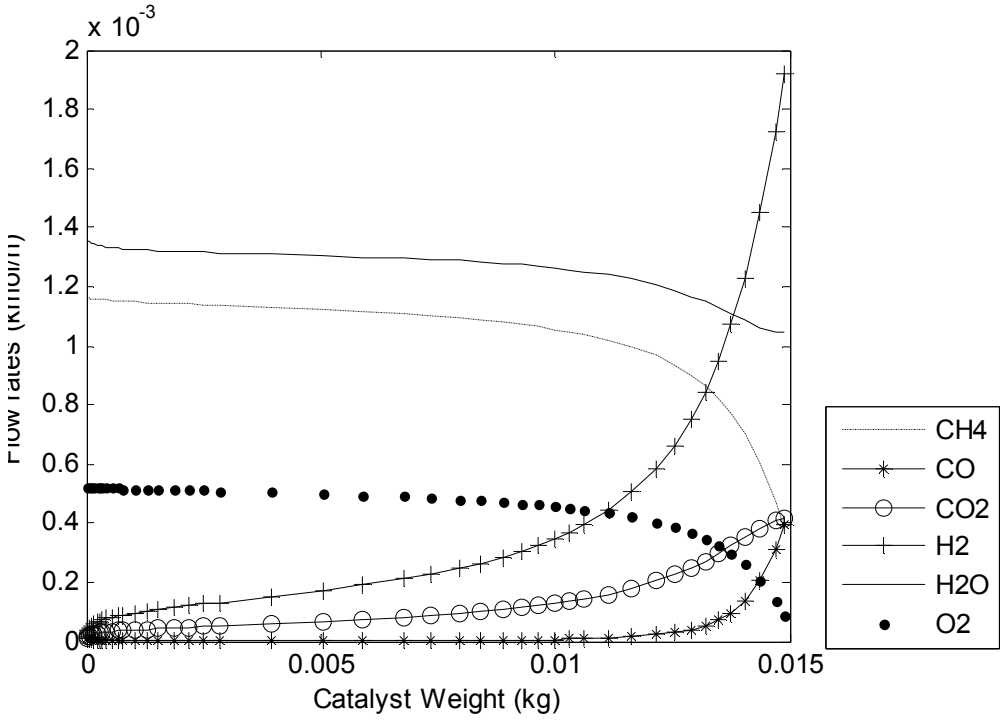

Figure 4.20. Flow rates along IPOX reactor for CH_4/O_2=2.24, H_2O/CH_4=1.17 at 50W PEMFC system

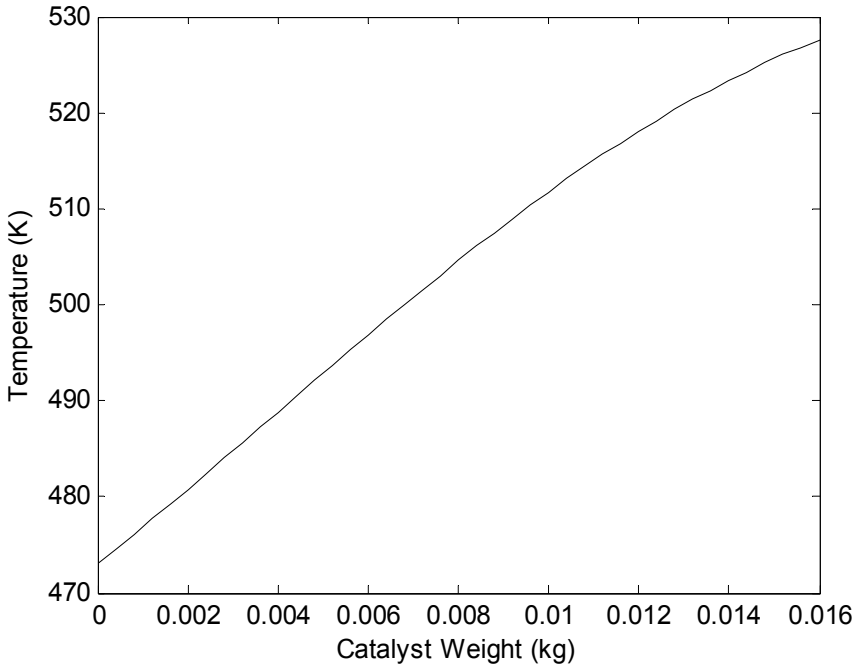

Figure 4.21. Temperature profile along WGS reactor for CH_4/O_2=2.24, H_2O/CH_4=1.17 at 50W PEMFC system

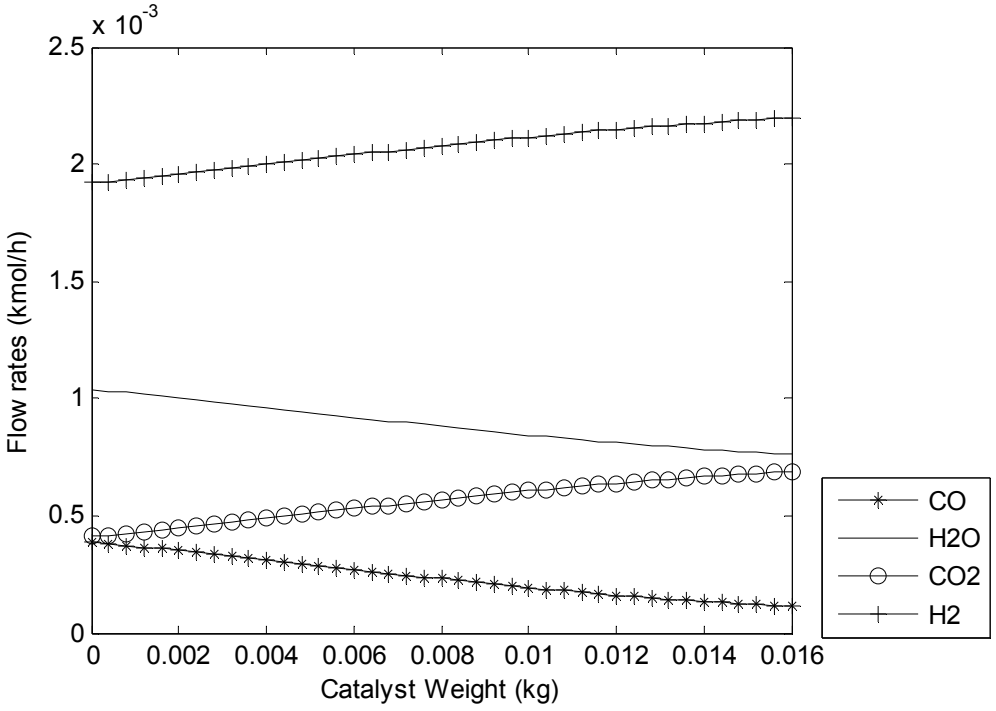

Figure 4.22. Flow rates along WGS reactor for CH_4/O_2=2.24, H_2O/CH_4=1.17 at 50W PEMFC system

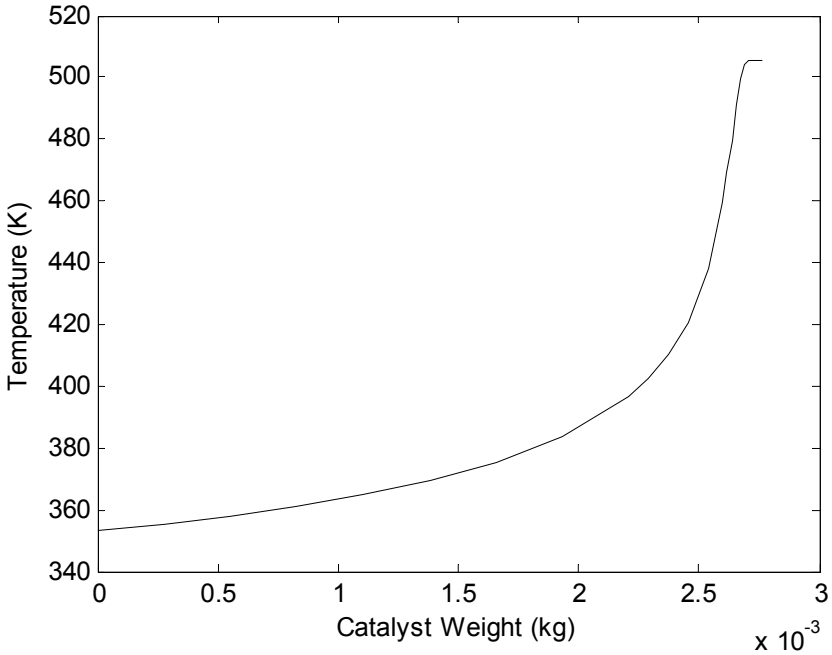

Figure 4.23. Temperature profile along PROX reactor for CH_4/O_2=2.24, H_2O/CH_4=1.17 at 50W PEMFC system

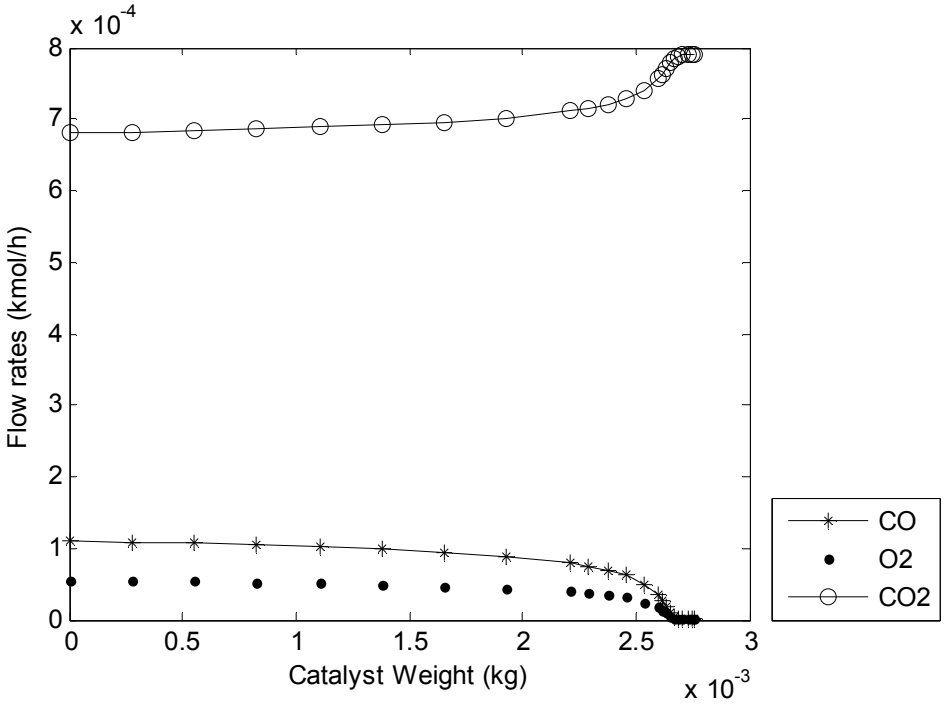

Figure 4.24. PROX stream compositions throughout the reactor for 2.24 & 1.17 ratio couple on 50W PEMFC system

4.1.2.3. Results for 100 W PEMFC.

Table 4.6. Simulation results of 100W PEMFC system (CH_4/O_2=1.89, H_2O/CH_4=1.56)

	Flow rates at the feed (mol/h)	Flow rates at IPOX exit (mol/h)	Flow rates at WGS exit (mol/h)	Flow rates at PROX exit (mol/h)
CH_4	2.47	0.94	0.94	0.94
H_2O	3.86	3.02	2.63	2.63
O_2	1.31	0.00	0.00	0.00
N_2	4.92	4.92	4.92	5.22
CO	0.00	0.55	0.16	0.0014
CO_2	0.00	1.00	1.39	1.54
H_2	0.00	3.89	4.28	4.28
Temperature (K)	627	845	inlet 473 outlet 505	inlet 353 outlet 449
Catalyst Weight (g)		44	35	8.5
CO concentration		3.8 *	1.1 *	9.5 **

* CO concentration: mol percent
** CO concentration: ppm

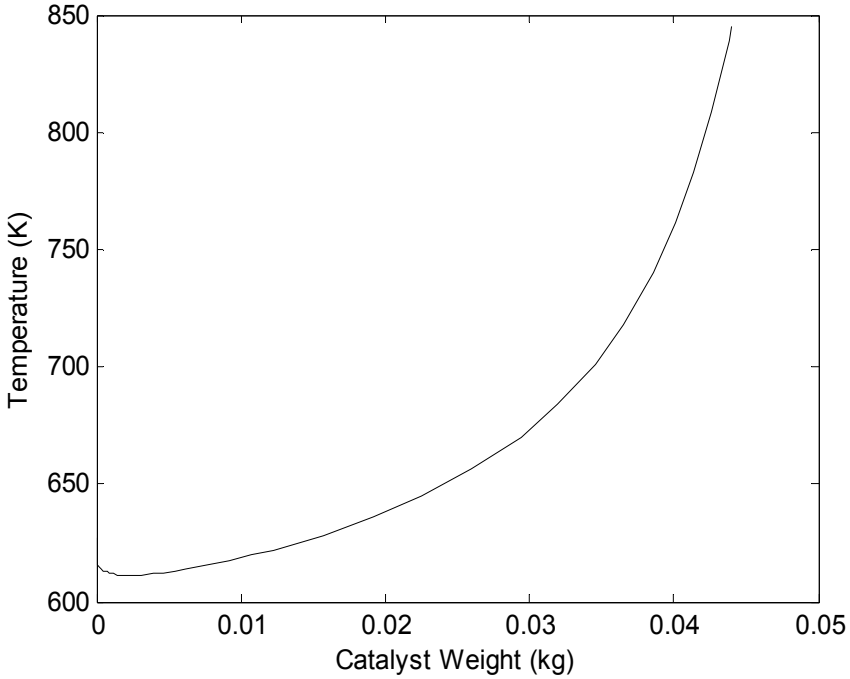

Figure 4.25. Temperature profile along IPOX reactor for CH_4/O_2=1.89, H_2O/CH_4=1.56 at 100W PEMFC system

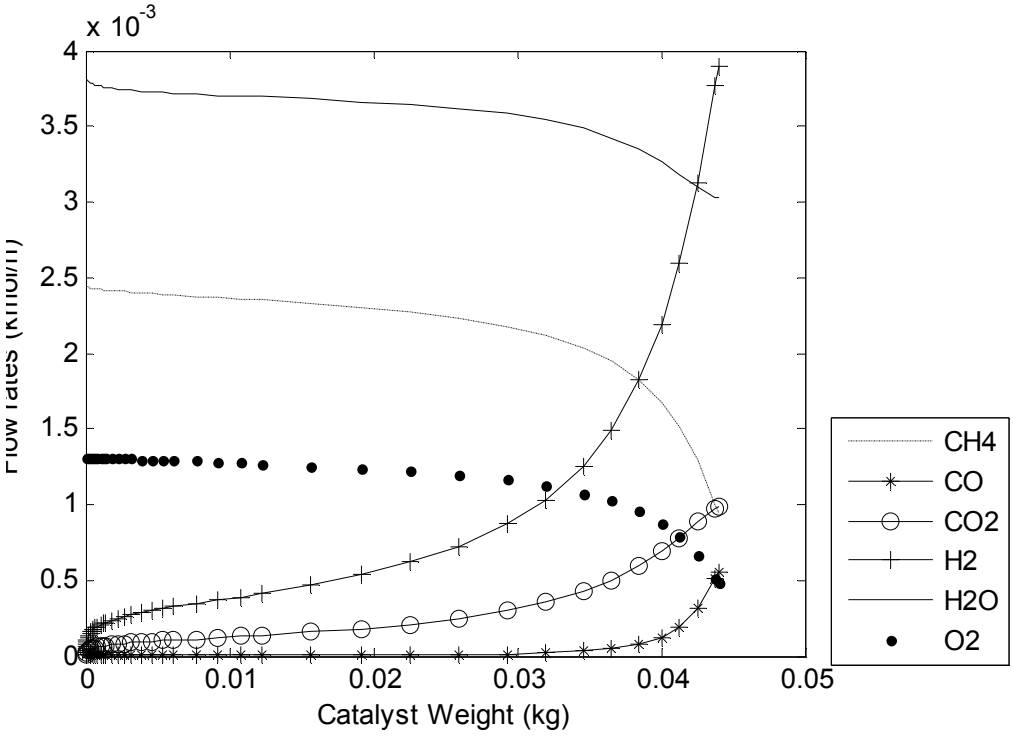

Figure 4.26. Flow rates along IPOX reactor for CH_4/O_2=1.89, H_2O/CH_4=1.56 at 100W PEMFC system

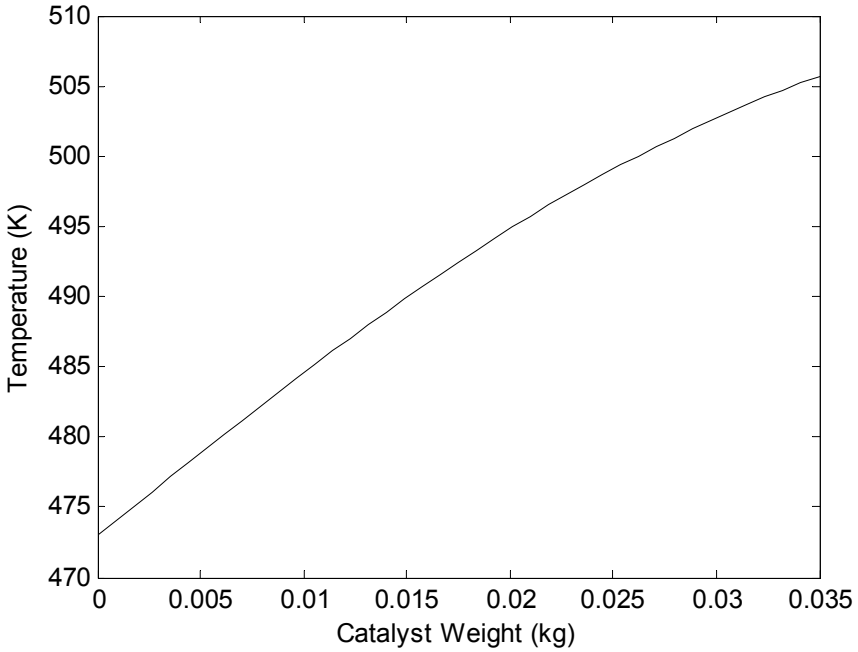

Figure 4.27. Temperature profile along WGS reactor for CH_4/O_2=1.89, H_2O/CH_4=1.56 at 100W PEMFC system

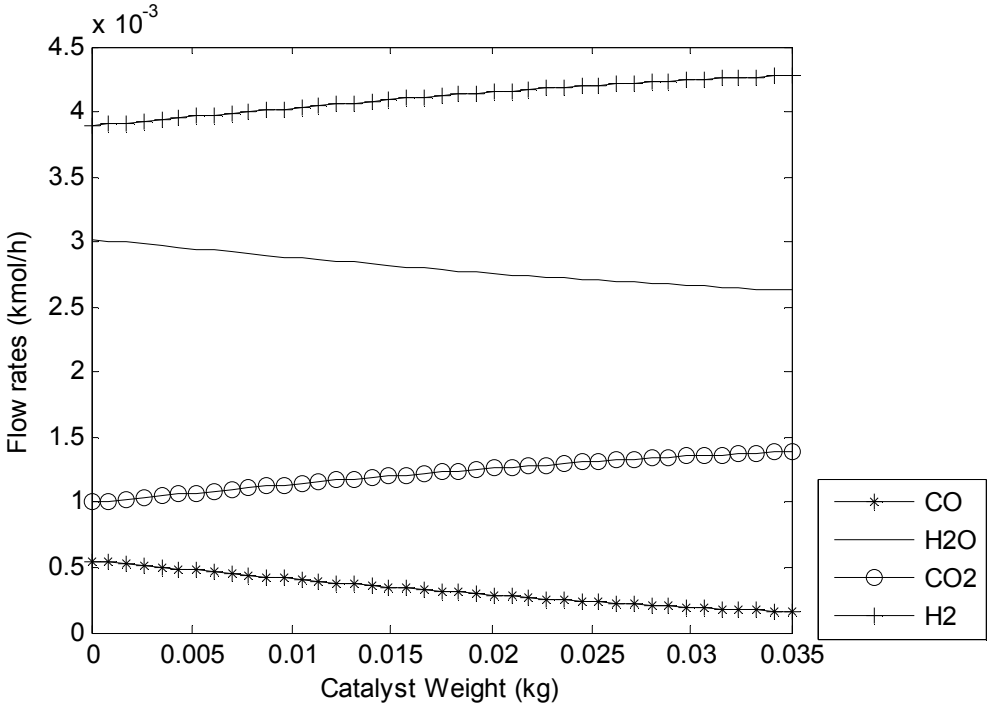

Figure 4.28. Flow rates along WGS reactor for CH_4/O_2=1.89, H_2O/CH_4=1.56 at 100W PEMFC system

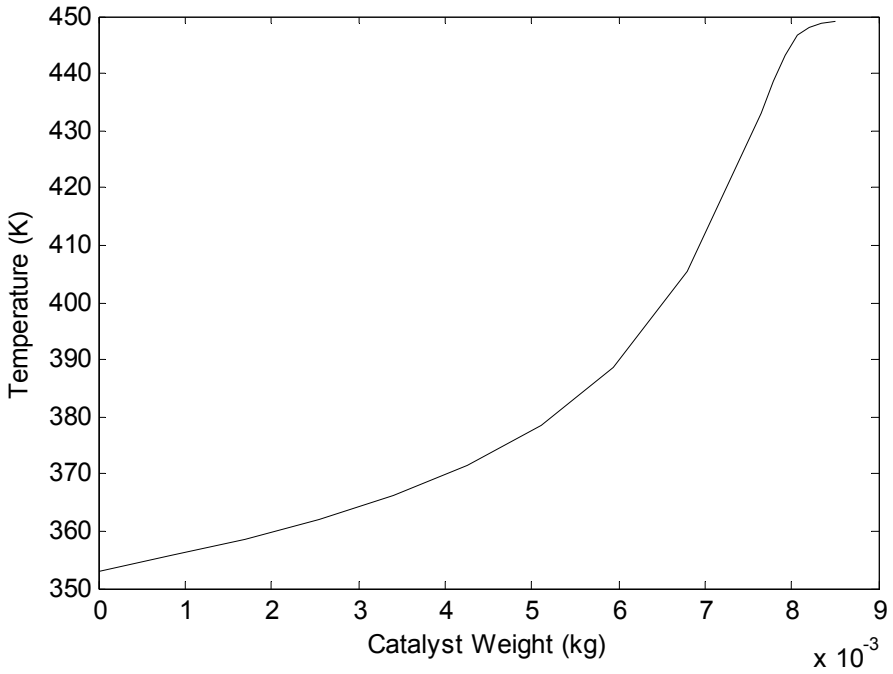

Figure 4.29. Temperature profile along PROX reactor for CH_4/O_2=1.89, H_2O/CH_4=1.56 at 100W PEMFC system

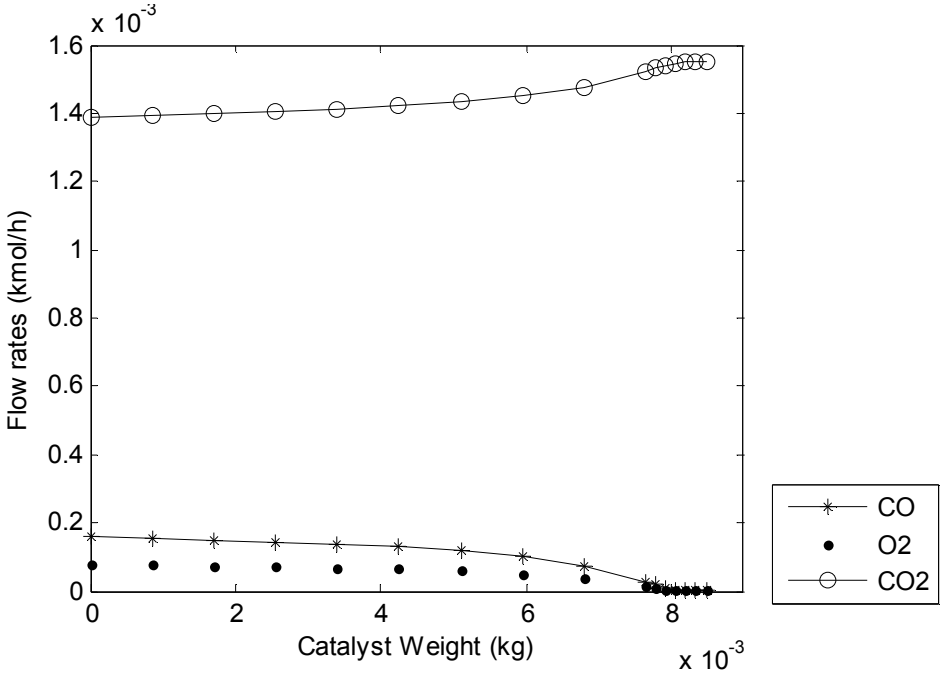

Figure 4.30. Flow rates along PROX reactor for CH_4/O_2=1.89, H_2O/CH_4=1.56 at 100W PEMFC system

Table 4.7. Simulation results of 100W PEMFC system (CH_4/O_2=2.24, H_2O/CH_4=1.17)

	Flow rates at the feed (mol/h)	Flow rates at IPOX exit (mol/h)	Flow rates at WGS exit (mol/h)	Flow rates at PROX exit (mol/h)
CH_4	2.34	0.63	0.63	0.63
H_2O	2.74	2.10	1.44	1.44
O_2	1.05	0.00	0.00	0.00
N_2	3.93	3.93	3.93	4.36
CO	0.00	0.89	0.23	0.0000012
CO_2	0.00	0.83	1.48	1.71
H_2	0.00	4.08	4.73	4.73
Temperature (K)	620	893	inlet 473 outlet 536	inlet 353 outlet 509
Catalyst Weight (g)		31.7	34	5.457
CO concentration		7.1 *	1.8 *	0.1 **

* CO concentration: mol percent
** CO concentration: ppm

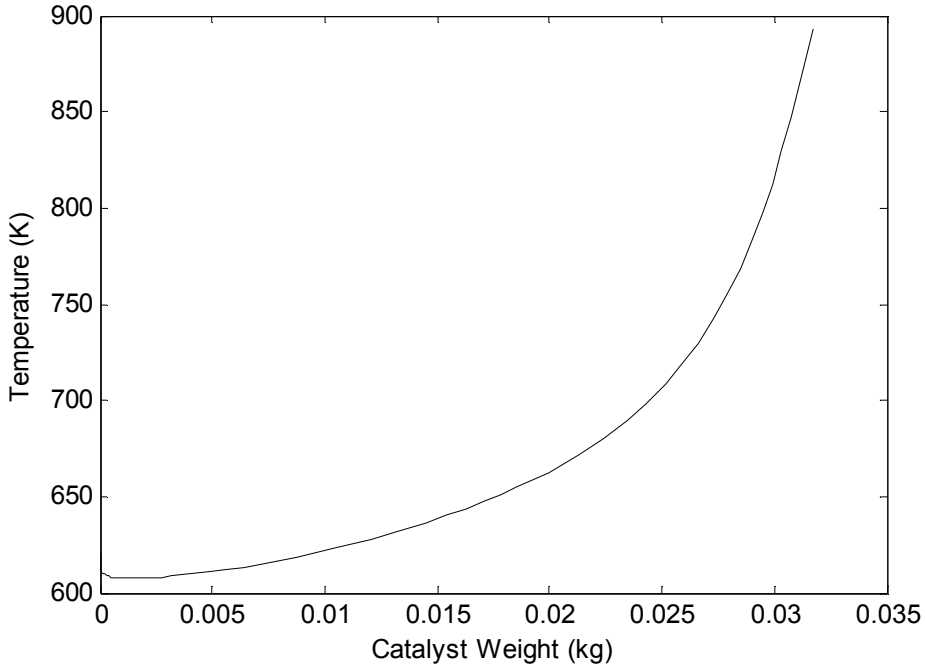

Figure 4.31. Temperature profile along IPOX reactor for CH_4/O_2=2.24, H_2O/CH_4=1.17 at 100W PEMFC system

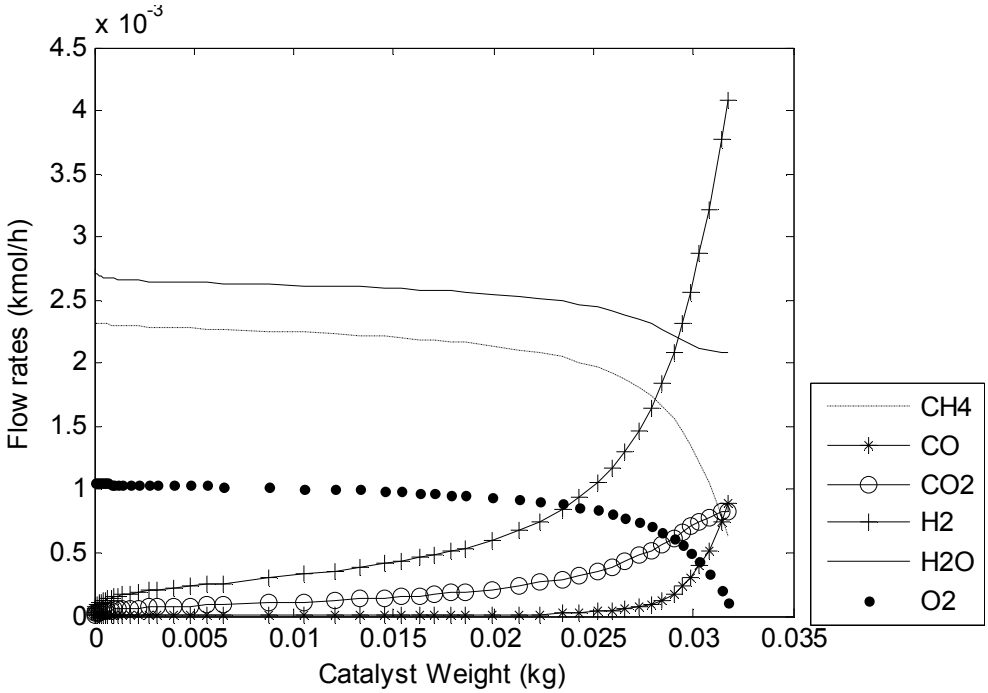

Figure 4.32. Flow rates along IPOX reactor for CH_4/O_2=2.24, H_2O/CH_4=1.17 at 100W PEMFC system

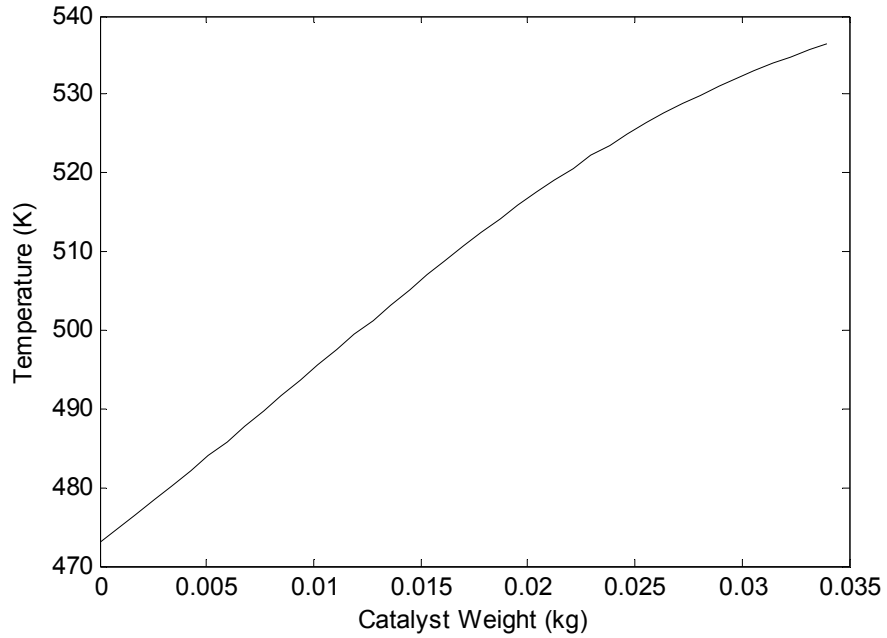

Figure 4.33. Temperature profile along WGS reactor for CH_4/O_2=2.24, H_2O/CH_4=1.17 at 100W PEMFC system

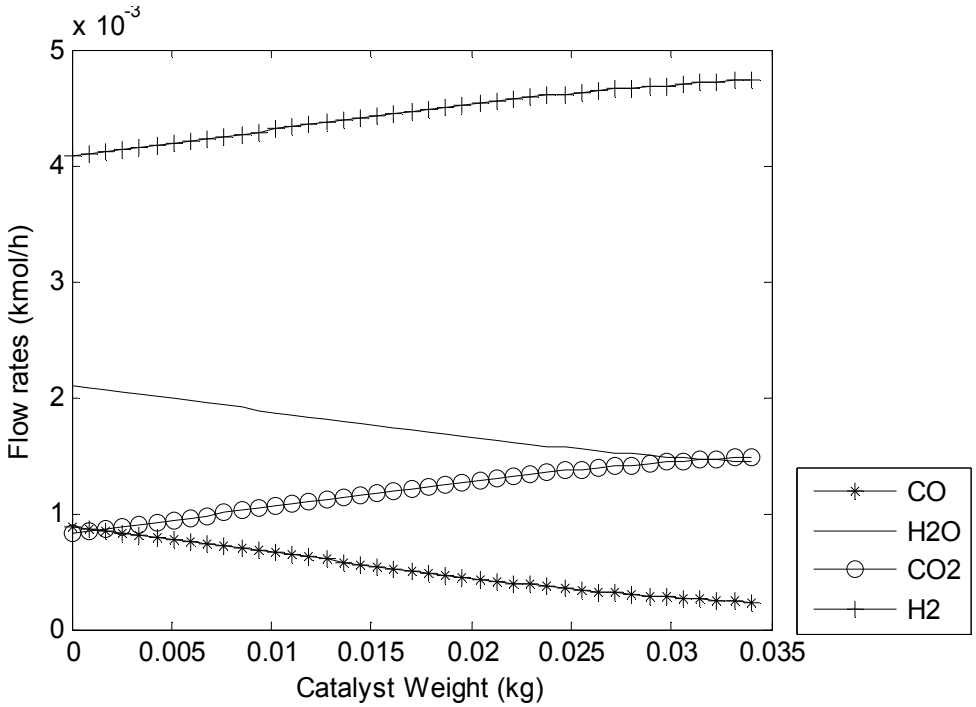

Figure 4.34. Flow rates along WGS reactor for CH_4/O_2=2.24, H_2O/CH_4=1.17 at 100W PEMFC system

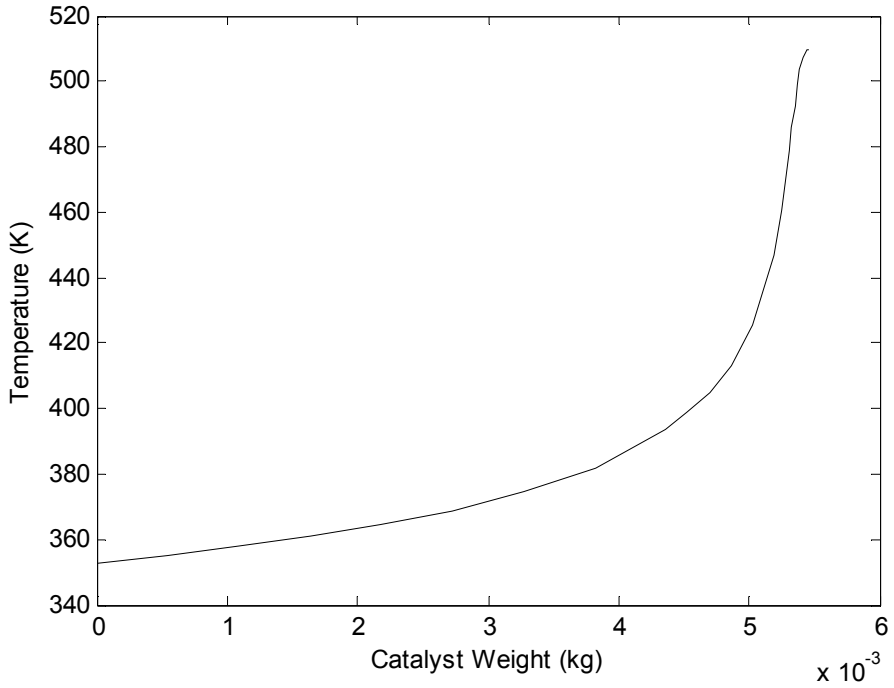

Figure 4.35. Temperature profile along PROX reactor for CH_4/O_2=2.24, H_2O/CH_4=1.17 at 100W PEMFC system

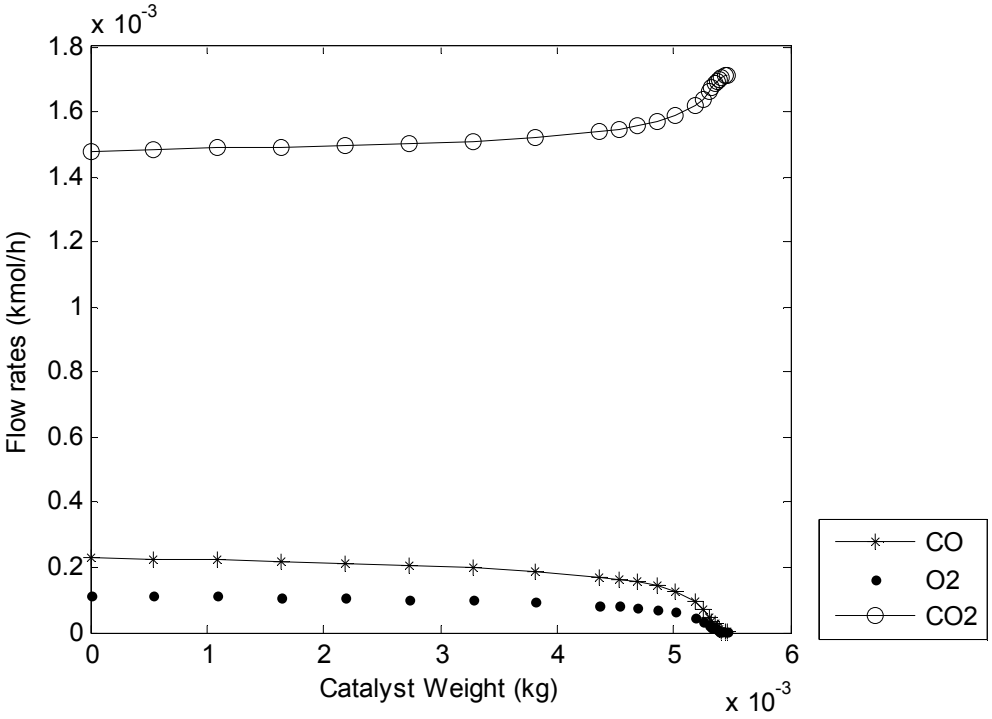

Figure 4.36. Flow rates along PROX reactor for CH_4/O_2=2.24, H_2O/CH_4=1.17 at 100W PEMFC system

4.1.3. Discussion

Catalyst weight requirements for each reactor type are presented in Table 4.8 for every fuel cell power output and feed ratio values. The results show that catalyst weight for changes almost linearly with the power output requirement of the fuel cell.

Table 4.8. Catalyst weight requirements for all reactors and feed ratio combinations

	CH_4/O_2=1.89, H_2O/CH_4=1.56			CH_4/O_2=2.24, H_2O/CH_4=1.17		
PEMFC power output (W)	10	50	100	10	50	100
IPOX catalyst (g)	4.35	20.85	44.00	3.28	14.90	31.70
WGS catalyst (g)	3.00	14.00	35.00	3.50	16.00	34.00
PROX catalyst (g)	0.74	3.41	8.50	0.55	2.76	5.46
Total catalyst weight (g)	8.09	38.26	87.5	7.33	33.66	71.16

It can be clearly seen that, for every power output, total catalyst quantity needed for 1.89 & 1.56 combination are higher than 2.24 & 1.17 for all reactors except WGS reactor. When carbon-to-oxygen ratio is smaller and steam-to-carbon ratio is bigger, higher flow rates of oxygen and steam are needed. This situation leads to the requirement of bigger reactor volumes and catalyst weight. For example, in order to operate 10W fuel cell system eight grams of catalyst is used in total for 1.89 & 1.56 feed ratio combination, while approximately seven grams is used for 2.24 & 1.17. However, for WGS reactor, in 10 and 50W fuel processor system, catalyst use is higher in 2.24 & 1.17 than in 1.89 & 1.56.

When the reactor simulation results (SR) are compared with the preliminary results (PR), i.e. component flow rates obtained from material balances (Chapter 3), some

differences can be observed. These comparisons are given in Tables 4.9 and 4.10 for 10W and 100W fuel cell systems, respectively. For a certain reactor, a simulation is conducted using the initial conditions obtained from the material balance results (Chapter 3) and a catalyst weight specified arbitrarily. The simulation result, i.e. the solution of the reactor model, is then compared with the exit flow rates of that reactor obtained from the material balance results given in Chapter 3. Here the objective is to find a catalyst weight that will give a hydrogen exit flow rate that will match with the value obtained from the material balance and to compare all streams between simulation results and material balance results. The differences observed in simulation results and preliminary results are mainly due to assumptions made in material balance calculations and rate equations behavior used in simulation calculations.

Table 4.9. Comparison between PR and SR for 1.89 & 1.56 ratio combination at 10W fuel system

	Flow rates at the Feed (mol/h)	Flow rates at IPOX exit (mol/h)		Flow rates at WGS exit (mol/h)		Flow rates at PROX exit (mol/h)	
		PR	SR	PR	SR	PR	SR
CH_4	0.247	0.08	0.093	0.08	0.093	0.08	0.093
H_2O	0.386	0.34	0.302	0.32	0.265	0.32	0.265
O_2	0.131	0.00	0.00	0.00	0.00	0.00	0.00
N_2	0.492	0.49	0.490	0.49	0.490	0.52	0.5269
CO	0.00	0.03	0.056	0.01	0.0196	10×10^{-6}	5.2×10^{-6}
CO_2	0.00	0.14	0.099	0.16	0.135	0.17	0.154
H_2	0.00	0.39	0.391	0.41	0.427	0.41	0.427

PR: Material Balance/Preliminary Results

SR: Simulation Results

Table 4.10. Comparison between PR and SR for 2.24 & 1.17 ratio combination on 100W fuel system

	Flow rates at the Feed (mol/h)	Flow rates at IPOX exit (mol/h)		Flow rates at WGS exit (mol/h)		Flow rates at PROX exit (mol/h)	
		PR	SR	PR	SR	PR	SR
CH_4	2.34	0.77	0.63	0.77	0.63	0.77	0.63
H_2O	2.74	1.95	2.10	1.80	1.44	1.80	1.44
O_2	1.05	0.00	0.00	0.00	0.00	0.00	0.00
N_2	3.93	3.93	3.93	3.93	3.93	4.14	4.36
CO	0.00	0.26	0.89	0.11	0.23	19×10^{-5}	12×10^{-7}
CO_2	0.00	1.31	0.83	1.46	1.48	1.57	1.71
H_2	0.00	3.92	4.08	4.07	4.73	4.07	4.73

PR: Material Balance/Preliminary Results

SR: Simulation Results

4.2. Reactor Sizing

Reactor sizing has been made by taking a set of criteria, such as external heat transfer resistance, internal mass transfer resistance, axial dispersion and pressure drop into account. Equations used to quantify these criteria were presented in Section 4.1.1.3. These criteria are evaluated by assigning different combinations of tube diameter, tube length and particle diameter. The objective is to find a combination such that the reactor operates at a 'pseudohomogeneous' behavior, i.e. free of transport resistances with minimal axial dispersion and pressure drop. Thus, sizing procedure has been calculated five times for each reactor, for different catalyst particle size and tube length.

4.2.1. Sizing for 10 W PEMFC

In this section, design (reactor sizing) calculations will be shown for IPOX, WGS and PROX reactors for the feed ratio combinations of 2.24 & 1.17 and 1.89 & 1.56 to operate a 10W PEM fuel cell.

Table 4.11. IPOX reactor sizing for 10W PEMFC system (CH_4/O_2=1.89, H_2O/CH_4=1.56)

	CH_4/O_2=1.89, H_2O/CH_4=1.56				
Run	1	2	3	4	5
Catalyst Weight (g)	4.35	4.35	4.35	4.35	4.35
D_p (μm)	300	300	275	200	180
D_t (cm)	1.2	0.9	0.825	0.9	0.9
L (cm)	1.5	2.74	3.26	2.7	2.74
Mears' criterion	0.37	0.32	0.26	0.14	0.11
L/D_p	51	91	118	137	152
D_t/D_p	40	30	30	45	50
Weisz-Prater criterion	0.16	0.16	0.13	0.07	0.059
Outlet Pressure (bar)	0.93	0.75	0.58	0.44	0.3

Table 4.12. IPOX reactor sizing for 10W PEMFC system (CH_4/O_2=2.24, H_2O/CH_4=1.17)

	CH_4/O_2=2.24, H_2O/CH_4=1.17				
Run	1	2	3	4	5
Catalyst Weight (g)	3.28	3.28	3.28	3.28	3.28
D_p (μm)	250	250	250	200	200
D_t (cm)	1.05	0.775	0.875	0.9	0.84
L (cm)	3.27	6	4.71	4.45	5.1
Mears' criterion	0.42	0.37	0.39	0.25	0.24
L/D_p	131	240	188	222	255
D_t/D_p	42	31	35	45	42
Weisz-Prater criterion	0.2	0.20	0.20	0.13	0.13
Outlet Pressure (bar)	0.89	0.61	0.76	0.67	0.56

Table 4.13. WGS reactor sizing for 10W PEMFC system (CH_4/O_2=1.89, H_2O/CH_4=1.56)

	CH_4/O_2=1.89, H_2O/CH_4=1.56				
Run	1	2	3	4	5
Catalyst Weight (g)	3	3	3	3	3
D_p (μm)	300	250	250	200	300
D_t (cm)	1.05	0.875	1	0.8	1.05
L (cm)	3.85	5.54	4.2	6.63	3.85
Mears' criterion	0.0059	0.00037	0.0004	0.00023	0.0059
L/D_p	128	222	169	331	128
D_t/D_p	35	35	40	40	35
Weisz-Prater criterion	0.0055	0.0039	0.0038	0.0024	0.0055
Outlet Pressure (bar)	0.94	0.81	0.89	0.56	0.94

Table 4.14. WGS reactor sizing for 10W PEMFC system (CH_4/O_2=2.24, H_2O/CH_4=1.17)

CH_4/O_2 & H_2O/CH_4	2.24 & 1.17				
Run	1	2	3	4	5
Catalyst Weight (gr)	3.5	3.5	3.5	3.5	3.5
D_p (μm)	300	300	250	250	200
D_t (cm)	1.05	0.9	1	0.875	0.8
L (cm)	4.49	6.11	4.9	6.4	7.74
Mears' criterion	0.0006	0.0005	0.0004	0.00036	0.00022
L/D_p	149	204	198	258	387
D_t/D_p	35	30	40	35	40
Weisz-Prater criterion	0.005	0.005	0.0038	0.0038	0.0024
Outlet Pressure (bar)	0.94	0.88	0.896	0.81	0.57

Table 4.15. PROX reactor sizing for 10W PEMFC system (CH_4/O_2=1.89, H_2O/CH_4=1.56)

	CH_4/O_2=1.89, H_2O/CH_4=1.56				
Run	1	2	3	4	5
Catalyst Weight (g)	0.74	0.74	0.74	0.74	0.74
D_p (μm)	200	175	175	150	150
D_t (cm)	0.6	0.525	0.5775	0.6	0.495
L (cm)	2.25	2.94	2.43	2.25	3.31
Mears' criterion	0.015	0.01	0.011	0.0084	0.007
L/D_p	118	168	139	150	221
D_t/D_p	30	30	33	40	33
Weisz-Prater criterion	0.21	0.16	0.16	0.12	0.12
Outlet Pressure (bar)	0.84	0.63	0.75	0.71	0.36

Table 4.16. PROX reactor sizing for 10W PEMFC system (CH_4/O_2=2.24, H_2O/CH_4=1.17)

	CH_4/O_2=2.24, H_2O/CH_4=1.17				
Run	1	2	3	4	5
Catalyst Weight (g)	0.55	0.55	0.55	0.55	0.55
D_p (μm)	180	160	150	150	140
D_t (cm)	0.54	0.528	0.525	0.495	0.495
L (cm)	2.06	2.15	2.18	2.44	2.44
Mears' criterion	0.003	0.0023	0.002	0.0019	0.0017
L/D_p	114	134	145	163	174
D_t/D_p	30	33	35	33	35.35
Weisz-Prater criterion	0.003	0.0023	0.002	0.002	0.0017
Outlet Pressure (bar)	0.81	0.73	0.68	0.59	0.53

4.2.2. Sizing for 50 W PEMFC

In this section, design (reactor sizing) calculations will be shown for IPOX, WGS and PROX reactors for the feed ratio combinations of 2.24 & 1.17 and 1.89 & 1.56 to operate a 50W PEM fuel cell.

Table 4.17. IPOX reactor sizing for 50W PEMFC system (CH_4/O_2=1.89, H_2O/CH_4=1.56)

	CH_4/O_2=1.89, H_2O/CH_4=1.56				
Run	1	2	3	4	5
Catalyst Weight (g)	20.85	20.85	20.85	20.85	20.85
D_p (μm)	500	500	450	400	320
D_t (cm)	1.65	1.5	1.575	1.6	1.6
L (cm)	8.38	10.13	9.19	8.9	8.9
Mears' criterion	0.55	0.53	0.44	0.35	0.22
L/D_p	167	202	204	223	278
D_t/D_p	33	30	35	40	50
Weisz-Prater criterion	0.46	0.46	0.37	0.29	0.188
Outlet Pressure (bar)	0.81	0.71	0.71	0.65	0.46

Table 4.18. IPOX reactor sizing for 50W PEMFC system (CH_4/O_2=2.24, H_2O/CH_4=1.17)

	CH_4/O_2=2.24, H_2O/CH_4=1.17				
Run	1	2	3	4	5
Catalyst Weight (g)	14.9	14.9	14.9	14.9	14.9
D_p (μm)	400	350	400	300	500
D_t (cm)	1.6	1.575	1.8	1.5	1.5
L (cm)	6.62	6.83	5.23	7.53	7.53
Mears' criterion	0.64	0.48	0.68	0.34	0.96
L/D_p	165	195	131	251	150
D_t/D_p	40	45	45	50	30
Weisz-Prater criterion	0.51	0.39	0.51	0.29	0.80
Outlet Pressure (bar)	0.81	0.73	0.88	0.55	0.84

Table 4.19. WGS reactor sizing for 50W PEMFC system (CH_4/O_2=1.89, H_2O/CH_4=1.56)

	CH_4/O_2=1.89, H_2O/CH_4=1.56				
	1	2	3	4	5
Catalyst Weight (g)	14	14	14	14	14
D_p (μm)	500	500	450	400	300
D_t (cm)	1.75	1.5	1.575	1.6	1.5
L (cm)	6.47	8.80	7.99	7.74	8.80
Mears' criterion	0.001	0.0009	0.0008	0.00062	0.00034
L/D_p	129	176	177	194	293
D_t/D_p	35	30	35	40	50
Weisz-Prater criterion	0.016	0.016	0.013	0.01	0.0059
Outlet Pressure (bar)	0.94	0.87	0.87	0.84	0.63

Table 4.20. WGS reactor sizing for 50W PEMFC system (CH_4/O_2=2.24, H_2O/CH_4=1.17)

	CH_4/O_2=2.24, H_2O/CH_4=1.17				
Run	1	2	3	4	5
Catalyst Weight (g)	16	16	16	16	16
D_p (μm)	600	500	450	400	400
D_t (cm)	1.86	1.5	1.575	1.6	1.4
L (cm)	6.98	10.06	9.12	8.84	11.5
Mears' criterion	0.0016	0.001	0.0008	0.00067	0.0006
L/D_p	116	201	202	221	288
Dt/Dp	30	30	35	40	35
Weisz-Prater criterion	0.024	0.017	0.014	0.0109	0.01
Outlet Pressure (bar)	0.97	0.88	0.87	0.85	0.73

Table 4.21. PROX reactor sizing for 50W PEMFC system (CH_4/O_2=1.89, H_2O/CH_4=1.56)

	CH_4/O_2=1.89, H_2O/CH_4=1.56				
Run	1	2	3	4	5
Catalyst Weight (g)	3.41	3.41	3.41	3.41	3.41
D_p (μm)	300	300	250	250	200
D_t (cm)	0.96	1.05	1.12	1	0.9
L (cm)	4.2	3.51	3.06	3.86	4.77
Mears' criterion	0.0039	0.004	0.003	0.0028	0.0017
L/D_p	140	117	122	154	239
D_t/D_p	32	35	45	40	45
Weisz-Prater criterion	0.020	0.024	0.017	0.017	0.011
Outlet Pressure (bar)	0.73	0.82	0.80	0.67	0.21

Table 4.22. PROX reactor sizing for 50W PEMFC system (CH_4/O_2=2.24, H_2O/CH_4=1.17)

	CH_4/O_2=2.24, H_2O/CH_4=1.17				
Run	1	2	3	4	5
Catalyst Weight (g)	2.76	2.76	2.76	2.76	2.76
D_p (μm)	200	300	300	250	285
D_t (cm)	0.8	0.9	1.05	0.875	0.855
L (cm)	4.7	3.72	2.73	3.94	4.12
Mears' criterion	0.017	0.041	0.045	0.28	0.036
L/D_p	236	124	91	157	145
D_t/D_p	40	30	35	35	30
Weisz-Prater criterion	0.0309	0.069	0.069	0.48	0.063
Outlet Pressure (bar)	0.77	0.75	0.87	0.59	0.65

4.2.3. Sizing for 100 W PEMFC

In this section, design (reactor sizing) calculations will be shown for IPOX, WGS and PROX reactors for the feed ratio combinations of 2.24 & 1.17 and 1.89 & 1.56 to operate a 100W PEM fuel cell.

Table 4.23. IPOX reactor sizing for 100W PEMFC system (CH_4/O_2=1.89, H_2O/CH_4=1.56)

	CH_4/O_2=1.89, H_2O/CH_4=1.56				
Run	1	2	3	4	5
Catalyst Weight (g)	44	44	44	44	44
D_p (μm)	700	600	600	500	450
D_t (cm)	2.10	2.10	2.4	2	2.025
L (cm)	10.9	10.9	8.3	12	11.73
Mears' criterion	0.83	0.61	0.65	0.41	0.33
L/D_p	156	181	139	240	260
D_t/D_p	30	35	40	40	45
Weisz-Prater criterion	0.86	0.63	0.63	0.43	0.35
Outlet Pressure (bar)	0.80	0.78	0.88	0.61	0.54

Table 4.24. IPOX reactor sizing for 100W PEMFC system (CH_4/O_2=2.24, H_2O/CH_4=1.17)

	CH_4/O_2=2.24, H_2O/CH_4=1.17				
Run	1	2	3	4	5
Catalyst Weight (g)	31.7	31.7	31.7	31.7	31.7
D_p (μm)	500	450	400	375	400
D_t (cm)	2	1.8	1.8	2.0625	2
L (cm)	8.67	10.7	10.7	8.15	8.67
Mears' criterion	0.77	0.59	0.47	0.44	0.49
L/D_p	173	237	267	217	216
D_t/D_p	40	40	45	55	50
Weisz-Prater criterion	0.98	0.79	0.63	0.55	0.63
Outlet Pressure (bar)	0.85	0.58	0.46	0.65	0.66

Table 4.25. WGS reactor sizing for 100W PEMFC system (CH_4/O_2=1.89, H_2O/CH_4=1.56)

	CH_4/O_2=1.89, H_2O/CH_4=1.56				
Run	1	2	3	4	5
Catalyst Weight (g)	35	35	35	35	35
D_p (μm)	700	600	600	500	500
D_t (cm)	2.10	2.10	1.8	2	2.25
L (cm)	11.23	11.23	15.2	12.4	9.78
Mears' criterion	0.0011	0.0008	0.0007	0.00055	0.0006
L/D_p	160	187	254	247	195
D_t/D_p	30	35	30	40	45
Weisz-Prater criterion	0.024	0.0175	0.017	0.012	0.012
Outlet Pressure (bar)	0.91	0.88	0.76	0.78	0.87

Table 4.26. WGS reactor sizing for 100W PEMFC system (CH_4/O_2=2.24, H_2O/CH_4=1.17)

	CH_4/O_2=2.24, H_2O/CH_4=1.17				
Run	1	2	3	4	5
Catalyst Weight (g)	34	34	34	34	34
D_p (μm)	700	600	600	500	500
D_t (cm)	2.10	2.10	1.8	2	2.25
L (cm)	10.91	10.91	14.8	12	0.95
Mears' criterion	0.0015	0.0011	0.001	0.00074	0.0008
L/D_p	156	181	248	240	190
D_t/D_p	30	35	30	40	45
Weisz-Prater criterion	0.037	0.027	0.027	0.019	0.019
Outlet Pressure (bar)	0.93	0.90	0.80	0.82	0.89

Table 4.27. PROX reactor sizing for 100W PEMFC system (CH_4/O_2=1.89, H_2O/CH_4=1.56)

	CH_4/O_2=1.89, H_2O/CH_4=1.56				
Run	1	2	3	4	5
Catalyst Weight (g)	8.5	8.5	8.5	8.5	8.5
D_p (μm)	450	400	400	350	300
D_t (cm)	1.35	1.4	1.2	1.4	1.35
L (cm)	4.8	4.46	6.08	4.46	4.8
Mears' criterion	0.0009	0.0007	0.0006	0.0005	0.0004
L/D_p	107	111	152	128	160
D_t/D_p	30	35	30	40	45
Weisz-Prater criterion	0.003	0.002	0.002	0.002	0.001
Outlet Pressure (bar)	0.85	0.83	0.67	0.78	0.65

Table 4.28. PROX reactor sizing for 100W PEMFC system (CH_4/O_2=2.24, H_2O/CH_4=1.17)

	CH_4/O_2=2.24, H_2O/CH_4=1.17				
Run	1	2	3	4	5
Catalyst Weight (g)	5.46	5.46	5.46	5.46	5.46
D_p (μm)	400	400	350	350	300
D_t (cm)	1.4	1.2	1.05	1.225	1.2
L (cm)	3.04	4.1	5.4	3.97	4.14
Mears' criterion	0.043	0.039	0.028	0.03	0.022
L/D_p	76	103	154	113	138
D_t/D_p	35	30	30	35	40
Weisz-Prater criterion	0.1	0.0103	0.79	0.079	0.058
Outlet Pressure (bar)	0.91	0.82	0.56	0.78	0.68

4.3. Results and Discussion

In this study, several trial runs have been conducted to search for optimum values of reactor length, diameter and particle size for minimizing interfacial/intraparticle heat/mass transfer, axial dispersion and mechanical energy loss due to the pressure drop. These runs have been conducted for every PEM fuel cell power output/feed ratio combination and presented in Tables 4.11-4.28. In every trial run, length/diameter ratio (Equation (4.25)), Mears' criterion (Equation (4.19)) and Weisz-Prater criterion (Equation (4.27)) have been calculated using assigned values of reactor length, diameter and particle size to quantify the significance of the related phenomenon. Five different trial runs have been calculated and one single run, which seemed to be optimal, has been selected and presented in Tables 4.29, 4.30 and 4.31 for 10W, 50W and 100W power outputs, respectively.

While choosing the optimized design parameters for every reactor, L/D_t and pressure drop values has been considered as the primary selection criteria since gas phase components are significantly pressure dependent. L/D_t ratio must have a value of 5 or greater for ensuring plug flow assumption (Rase, 1990). However in most of the reactors, this value could not be achieved due to serious pressure drop along the tubes. For selection purposes, 30 percent of pressure drop has been assumed to be acceptable, i.e. pressure drop is considered as negligible if the exit pressure is higher than 0.7 bar. In addition, L/D_t value of 3 or higher is considered as acceptable.

Mears' and Weisz-Prater criteria have also been considered to investigate the significance of external heat transfer and internal mass transfer resistances. However, these criteria can hardly be met together with the pressure drop and plug flow criteria, especially in the IPOX reactor sizing. Therefore, in order to make a decision for the reactor and particle size, pressure drop and plug flow phenomena have been checked on primary basis due to the reasons explained above. In several cases of IPOX reactor sizing (Table 4.17, 4.18, 4.23 and 4.24), Mears' and Weisz-Prater criteria have not been proven in the selected options.

Table 4.29. Design parameters for 10W fuel cell system

	CH_4/O_2=1.89, H_2O/CH_4=1.56			CH_4/O_2=2.24, H_2O/CH_4=1.17		
Reactor	IPOX	WGS	PROX	IPOX	WGS	PROX
D_t(cm)	0.9	0.875	0.5775	0.875	0.9	0.528
D_p (μm)	300	250	175	250	300	160
D_t/D_p	30	53	33	35	30	33
Length (cm)	2.74	5.54	2.45	4.71	6.11	2.15
L/D_t	3.04	6.33	4.2	5.38	6.79	4.07
Pressure (bar)	0.93	0.81	0.75	0.76	0.88	0.73
Mears' criterion	0.37	0.00037	0.011	0.39	0.0005	0.0023
Weisz-Prater criterion	0.16	0.0039	0.16	0.20	0.005	0.0023

Table 4.30. Design parameters for 50W fuel cell system

	CH_4/O_2=1.89, H_2O/CH_4=1.56			CH_4/O_2=2.24, H_2O/CH_4=1.17		
Reactor	IPOX	WGS	PROX	IPOX	WGS	PROX
D_t(cm)	1.65	1.5	0.96	1.6	1.5	0.8
D_p (μm)	500	500	300	400	500	200
D_t/D_p	33	30	32	40	30	40
Length (cm)	8.38	8.80	4.2	6.62	10.06	4.7
L/D_t	5.08	5.87	4.375	4.1375	6.71	5.875
Pressure (bar)	0.81	0.87	0.73	0.81	0.88	0.77
Mears' criterion	0.55	0.0009	0.0039	0.64	0.001	0.017
Weisz-Prater criterion	0.46	0.016	0.024	0.39	0.014	0.031

Table 4.31. Design parameters for 100W fuel cell system

	CH_4/O_2=1.89, H_2O/CH_4=1.56			CH_4/O_2=2.24, H_2O/CH_4=1.17		
Reactor	IPOX	WGS	PROX	IPOX	WGS	PROX
D_t(cm)	2.1	2.1	1.35	2.0	2.10	1.2
D_p (μm)	600	700	450	500	700	400
D_t/D_p	35	30	30	40	30	30
Length (cm)	10.9	11.23	4.8	8.67	10.91	4.1
L/D_t	5.2	5.35	3.55	4.34	5.19	3.41
Pressure (bar)	0.78	0.91	0.85	0.85	0.93	0.78
Mears' criterion	0.61	0.0011	0.0009	0.77	0.0015	0.03
Weisz-Prater criterion	0.63	0.024	0.003	0.98	0.037	0.079

Catalyst weight requirements, selected tube lengths, diameters, particle diameters and calculated tubular reactor volumes are presented in Table 4.33 for three types of PEM fuel cell power outputs. In addition Table 4.32 shows that which feed ratio is selected for optimum system design since for every reactor and power size a different feed ratio is selected due to achieve maximum reactor length.

Table 4.32. Feed ratios for reactor design

Reactor	10W	50W	100W
IPOX	1.89 & 1.56	1.89 & 1.56	1.89 & 1.56
WGS	2.24 & 1.17	2.24 & 1.17	1.89 & 1.56
PROX	1.89 & 1.56	1.89 & 1.56	1.89 & 1.56

Table 4.32. Design parameters for the fuel processing reactors

		IPOX	WGS	PROX
10W PEMFC system	Catalyst weight (g)	3.28	3.50	0.7424
	Reactor length (cm)	4.71	6.11	2.45
	Reactor diameter (cm)	0.875	0.9	0.5775
	Reactor Volume (cm^3)	2.83	3.89	0.64
	Particle Diameter (μm)	250	300	175
50W PEMFC system	Catalyst weight (g)	20.85	16	2.76
	Reactor length (cm)	8.38	10.06	4.7
	Reactor diameter (cm)	1.65	1.5	0.8
	Reactor Volume (cm^3)	17.91	17.78	2.36
	Particle Diameter (μm)	500	500	200
100W PEMFC system	Catalyst weight (g)	44	35	8.5
	Reactor length (cm)	10.9	11.23	4.8
	Reactor diameter (cm)	2.1	2.1	1.35
	Reactor Volume (cm^3)	37.75	38.90	6.87
	Particle Diameter (μm)	700	600	450

Temperature profiles obtained for the IPOX reactor in all power output/feed ratio combinations shows a decreasing-increasing behavior, i.e., first, temperature decreases rapidly; then, a continuous temperature rise has been observed (Figures 4.1, 4.7, 4.13, 4.19, 4.25, 4.31). This is believed to be due to the fact that at the entrance of the reactor, steam reforming is faster than total oxidation which causes also a rapid increase in hydrogen production at the inlet of IPOX reactors (Figures 4.2, 4.8, 4.14, 4.20, 4.26, 4.32). Since in WGS and PROX reactors takes place one reaction each, show a classical temperature-rising behavior due to the exothermic reaction behavior.

5. PROPOSAL FOR BENCH SCALE LABORATORY PROTOTYPE

In this section a fuel processor prototype which can be used in bench-scale studies will be proposed using the results obtained in Chapter 4. This proposal study is conducted at feed ratios of CH_4/O_2 = 2.24 and H_2O/CH_4=1.17 for a PEM fuel cell of 10W power output. The laboratory scale fuel processor system is composed of IPOX, WGS, PROX reactors, a water reservoir, heating and cooling facilities, thermocouples, differential pressure transmitters, mass flow controllers, valves, and line filters.

5.1. Description of the Prototype System

On the fuel processor system simulation, a physical mixture of Pt/δ-Al_2O_3 and Ni/MgO-Al_2O_3 is assumed in the IPOX reactor which can be used also in bench-scale prototype. Cu/ZnO (for WGS unit) and $Cu_{0.1}Ce_{0.9}O_{2-y}$ (for PROX unit) have been considered as the catalysts in the simulations. However, preparation of the $Cu_{0.1}Ce_{0.9}O_{2-y}$ catalyst is more complex than typical metal based catalyst due to its nanostructural type (Sedmak *et al.,* 2003). Hence, a metal based catalyst such as Pt-Co-Ce/Al_2O_3 for PROX unit can be used which can be much more easy to prepare. Özyönüm (2002) reported that Pt based catalysts are commonly used to reach optimal performance for CO oxidation. Catalyst weights determined in Chapter 4 have been shown in Table 5.1.

Table 5.1. Calculated Catalyst weights for 10W fuel processor system

Reactor	Catalyst	Weight (g)
IPOX	Pt/δ-Al_2O_3 & Ni/MgO-Al_2O_3	3.28
WGS	Cu/ZnO	3.50
PROX	$Cu_{0.1}Ce_{0.9}O_{2-y}$	0.55

Feed flow rates and stream temperatures calculated at feed ratios of CH_4/O_2 = 2.24 and H_2O/CH_4=1.17 for a 10W fuel cell system (Chapter 4) are given in Tables 5.2 and 5.3, respectively. In Table 5.2, molar feed flow rates are converted to volumetric flow rates at conditions which have been described in Section 4.2.1. Feed temperatures used to calculate

molar flow rates are shown in Table 5.3. In addition, pressure drop in the simulation has been neglected during volumetric flowrate calculations. In table 5.4., expected flowrates through the system have been described, these values have been calculated using temperatures given in table 5.4., and results obtained in Section 4.1.2.1.

Table 5.2. Flow rates at the inlet of IPOX reactor for 10W fuel processor system (Feed conditions: CH_4/O_2 = 2.24, H_2O/CH_4=1.17)

Component	Molar Flowrate (mmol/min)	Flowrate (ml min^{-1}) 620K & 1 atm	Molar composition (per cent)
CH_4	3.90	94.14	23.28
H_2O	4.56	0.082	27.24
O_2	1.74	42.03	10.39
N_2	6.55	158.10	39.09
Total	16.75	294.36	100

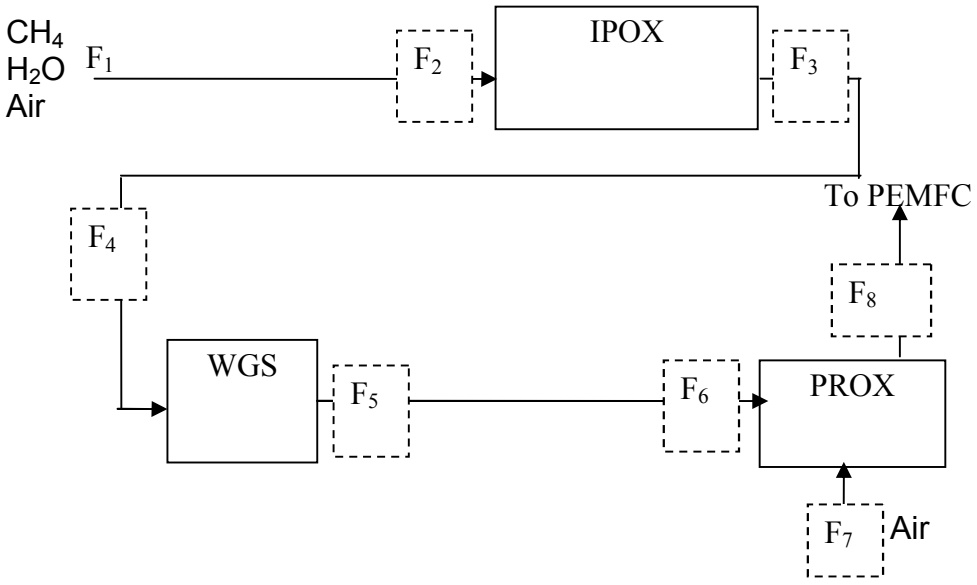

Figure 5.1. Basic block diagram for fuel processor system prototype

Table 5.3. Stream temperatures for 10W fuel cell processor prototype

Stream	Temperature (K)
F_2	620
F_3	884
F_4	473
F_5	531
F_6	353
F_8	500

Figure 5.1 shows a basic flowsheet of the bench scale prototype. In such a prototype, heating tapes are used instead of heat exchangers to heat the streams. In order to demonstrate temperature differences in the streams of prototype, an alternative stream numbering is used. For example, F_3 and F_4 have the same molar compositions; but, the temperature is decreased from 884K to 473K by water bath, which causes change in the volumetric flow rates. Similarly, F_1 and F_2 contain the same molar flow rates, but different volumetric flowrates. Also F_5 and F_6 show the same characteristic behavior.

Table 5.4. Volumetric flowrates along the 10W fuel cell processor prototype

	Volumetric flowrates (ml/min at 1 atm and at given temperature)							Temperature
	CH_4	H_2O	O_2	N_2	CO	CO_2	H_2	(K)
F_1	94.14	0.082	42.03	158.10	0	0	0	298
F_2	195.86	229.16	87.44	328.94	0	0	0	620
F_3	83.06	236.40	0	465.45	93.09	93.09	465.44	884
F_4	44.44	126.44	0	249.04	49.81	49.81	249.05	473
F_5	49.89	101.08	0	279.58	15.05	99.36	322.59	531
F_6	33.17	67.20	0	185.86	10.00	66.05	214.44	353
F_7	0	0	42.24	158.90	0	0	0	298
F_8	46.98	95.18	0	289.99	0.012	107.33	303.76	500

5.2. Proposed Bench-Scale Fuel Processor System

The prototype flow diagram has been presented in Figure 5.3. In this prototype proposal three packed-bed tubular reactors are used. Three different feed streams, i.e. methane, air and water enter to the system. Flow rates of these streams are controlled by two mass flow controllers and one HPLC pump (MFC_1, MFC_2, $HPLC_1$). Heated lines are used to increase temperature of the streams. For cooling purposes, temperature controlled lines are used as well; heat given in the lines is reduced when a cooling operation is needed. Alternatively, a water bath can be placed in order to decrease stream temperature. Water entering at 298 K has to be vaporized in order to merge uniformly with gas mixture. This can be achieved before merging with gas mixture by heating tapes. The feed streams are then mixed homogeneously in a mixer and then fed to the IPOX reactor. Heated stream goes to the IPOX reactor which has two thermocouples at two edges in order to observe temperature change in the reactor. In addition, one pressure controller is also placed for the reactor in order to observe pressure change in the reactor. In the IPOX reactor, stream is heated to the light-off temperature of methane (i.e. 620K) with the help of the furnace in which the reactor will be placed. The furnace is insulated from top and bottom ends to prevent heat loss from the furnace. Outlet streams of the IPOX go to the WGS reactor. Temperature decrease from 884 K to 473 K is provided by reducing heat given from the tape and by using a water bath. A mass flow controller (MFC_3), is placed in a parallel line at the inlet of WGS with thermocouples on two edges to observe temperature change in the reactor, and the pressure controller. Outlet stream has to be cooled from 531K to 353K in the same way of WGS and IPOX cooling. Before the PROX reactor, a mass flow controller (MFC_4) is placed in parallel to the feed line in order to control the flow into the reactor. Extra air stream is also controlled by MFC_5. Outlet stream of the PROX reactor is at ca. 500K. This stream is then fed to the series of gas chromatographs for qualitative and quantitative analyses. Two gas chromatographs are placed in the system in order to observe flowrates at the outlet of three reactors. Carrier gas of the GC-1 is helium, which can distinguish only hydrocarbons in this system due to the similar thermal conductivity values of hydrogen and helium. GC-2 is placed in order to observe hydrogen flowrate at the outlet of the streams. CO concentration should be less than 10 ppm. Since GC-1 and GC-2 are unable to measure CO concentration at ppm level, a mass spectrometer, MS-1, is placed to determine CO concentration at the outlet of PROX reactor. MS-1 operating pressure and

temperature ranges are 200 mbar - 2 bar and maximum 523K respectively. Figure 5.2 shows the elements used in Figure 5.3. In addition, Table 5.5 gives specifications required for mass flow controller used in the system while in Table 5.6, specifications of gas chromatographers are presented.

Table 5.5. Maximum flow rates for mass flow controllers on the fuel processor system

Mass Flow Controller	Flow Rate (ml/min) at 1 atm	MFC range to be selected (ml/min)	Temperature (K)
MFC_1	94.14	0-100	298
$HPLC_1$	0.082 (water)	0-10	298
MFC_2	200.13	0-1000	298
MFC_3	768.60	0-1000	473
MFC_4	576.45	0-1000	353
MFC_5	201.14	0-1000	298

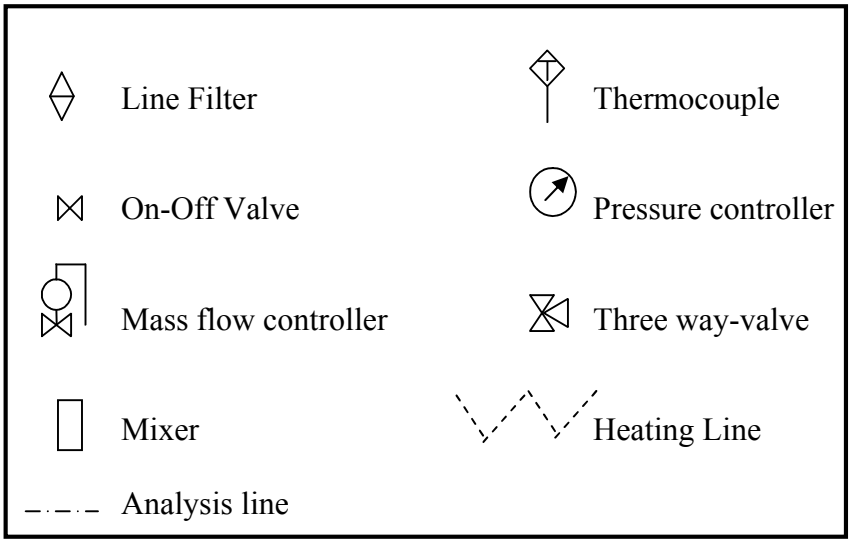

Figure 5.2. Elements Used in Figure 5.3

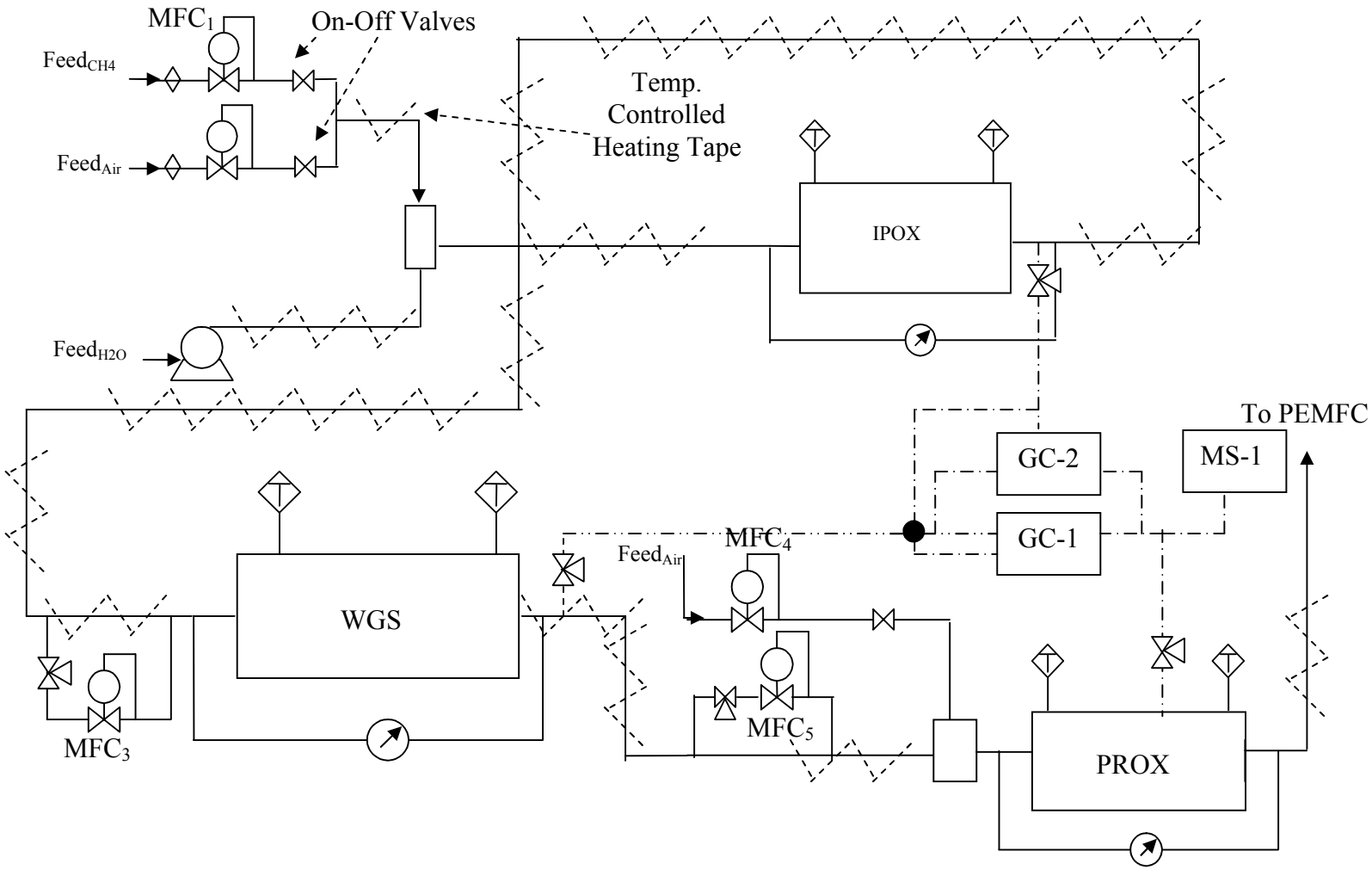

Figure 5.3. Bench scale prototype for the fuel processor system

Table 5.6. Specifications of gas chromatographs

GC Parameter	GC-1	GC-2
Detector type	TCD	TCD
Column temperature, K	363	333
Injector temperature, K	423	363
Detector temperature, K	423	363
TCD temperature, K	423	363
TCD current, μA	120	60
Carrier gas (CG)	He	Ar
Column flowrate, ml min^{-1}	25	50
Column packing material	Porapak Q, 80-100mesh	MS 5A, 60-80 mesh
Column tuing material	Stainless steel	Stainless steel
Column length & ID	3 m x 3mm	2 m x 3mm
Sample loop	1 ml kept at 398	1 ml kept at 298

6. CONCLUSIONS AND RECOMMENDATIONS

6.1. Conclusions

The main goal of this study is to estimate the sizes of the three catalytic reactors of the fuel processor system – indirect partial oxidation (packed with a mixture of Ni/MgO-Al_2O_3 and Pt/δ-Al_2O_3 catalysts), water-gas shift (packed with a Cu/ZnO catalyst) and preferential carbon monoxide oxidation (packed with a nanostructured $Cu_{0.1}Ce_{0.9}O_{2-y}$ catalyst) reactors – starting from a desired level of fuel cell electrical power output. For this purpose, material balance calculations have been conducted to solve the process flow sheet and a one-dimensional pseduhomogeneous reactor model has been employed to find out the catalyst weight requirements. Detailed sizing of the reactors have then been conducted to minimize heat and mass transport resistances, pressure drop and axial dispersion. Finally, an experimental fuel processing system at bench-scale is proposed to test hydrogen production for driving a 10 W PEM fuel cell. Major conclusions of this study can be summarized as follows:

- Results obtained from simulations show that catalyst weight increase linearly with power size output of PEMFC (i.e 10, 50 100 W) for both feed ratio combination ((CH_4/O_2, H_2O/CH_4)=(1.89, 1.56),(2.24, 1.17)).

- For CH_4/O_2 = 1.89 and H_2O/CH_4 = 1.56 and for IPOX, WGS and PROX reactors, estimated catalyst quantities are 4.35, 3 and 0.74 g for 10 W, 20.85, 14 and 3.41 g for 50 W and 44, 35 and 8.5 g for 100 W PEMFC operation.

- For CH_4/O_2 = 2.24 and H_2O/CH_4 = 1.17 and for IPOX, WGS and PROX reactors, estimated catalyst quantities are 3.28, 3.5 and 0.55 g for 10 W, 14.90, 16 and 2.76 g. for 50 W and 31.70, 34 and 5.46 g for 100 W PEMFC operation.

- In IPOX reactor, temperature shows a decreasing-increasing behavior, i.e., first, temperature decreases rapidly; then, a continuous temperature rise has been

observed, which can be explained by the phenomena that endothermic SR reaction occurs faster than exothermic TOX reaction. In WGS and PROX reactors, temperature shows a classical exothermic reaction behavior, i.e. temperature increase is observed.

- 2.24&1.17 feed ratio needs smaller amount of catalyst than 1.89&1.56 in all reactors except WGS converter. The small difference of WGS catalyst demands is because of difference in conversions. More catalyst demand of 1.89&1.56 in IPOX and PROX is because of high steam reforming and water-gas shift conversion in IPOX and occurrence of reverse water-gas shift reaction in PROX.

- Total reactor sizes, i.e. the sum of the IPOX, WGS and PROX reactor volumes, have been calculated as 7.36 cm^3, 38.05 cm^3, 83.52 cm^3 for 10, 50, 100 W of PEM fuel cell outputs, respectively.

6.2. Recommendations

The following improvements can be suggested in order to enhance the ability of the fuel processor system:

- Further studies can be done with different feed ratio combinations to understand the effect of CH_4/O_2 and H_2O/CH_4 ratios on the estimated catalyst weights. These investigations would give a more reliable idea about the size of the fuel processor system.

- Same simulation method can be investigated using other fuel types than methane to determine the effects on the size of the fuel processing system.

- Simulation and design calculations can be investigated using a dynamic model to analyze the process regarding to its start-up and to its response against changes. In addition, a heterogeneous model can be developed and its outcomes can be compared with the existing results based on a pseudohomogeneous model to

evaluate the validity of the criteria used to quantify the significance of transport resistances.

- More realistic results in terms of catalyst weight requirements can be achieved with the addition of peripheral units such as heat exchangers and coolers in to the mathematical model.

- Proposed bench-scale fuel processor prototype in Section 5 can be tested through setting-up an experimental system in order to determine the validity of the results obtained in this work.

APPENDIX A: TEMPERATURE-DEPENDENT HEAT CAPACITIES OF THE SPECIES

Table A.1. Constants of the heat capacity equation (Sinnot, 1993)

Species	α_j	β_j (x 10^2)	γ_j (x 10^5)	δ_j (x 10^9)
CH_4	19.251	5.2126	1.1974	-11.32
H_2O	32.243	0.19238	1.0555	-3.596
CO	30.869	-1.285	2.7892	-12.72
CO_2	19.795	7.3436	-5.602	17.153
H_2	27.143	0.92738	-1.381	7.6451
O_2	28.106	-0.00037	1.7459	-10.65
N_2	31.15	-1.357	2.6796	-11.68

$$c_{p,j} = \alpha_j + \beta_j T + \gamma_j T^2 + \delta_j T^3 \qquad [\text{kJ kmol}^{-1}\ \text{K}^{-1}] \qquad \text{(A.1)}$$

REFERENCES

Abanades S. and G. Flamant, 2006, “Experimental Study and Modeling of a High-Temperature Solar Chemical Reactor for Hydrogen Production from Methane Cracking”, *International Journal of Hydrogen Energy*, doi:10.1016 /j.ijhydene.2006.10.038.

Ahmed S. and M. Krumpelt, 2001, “Hydrogen from Hydrocarbon Fuels for Fuel Cells”, *International Journal f Hydrogen Energy*, Vol. 26, pp. 291-301.

Amadeo, N. E. and M. A. Laborde, 1995, “Hydrogen Production from the Low-Temperature Water-Gas Shift Reaction: Kinetics and Simulation of the Industrial Reactor”, *International Journal of Hydrogen Energy*, Vol. 20, pp. 949-956.

Andreeva, D., V. Idakiev, T. Tabakova, L. Ilieva, P. Falaras, A. Bourlinos and A. Travlos, 2002, “Low-Temperature Water-Gas Shift Reaction Over Au/CeO_2 Catalysts”, *Catalysis Today*, Vol. 72, pp. 51-57.

Armor, J. N., 1999, “The Multiple Roles for Catalysis in the Production of H2”, *Applied Catalysis A: General,* Vol. 176, pp. 159-176.

Avcı, A. K., 2003, *Computational and Experimental Investigation of Catalytic Hydrocarbon Fuel Processing for Autothermal Hydrogen Production*, Ph.D. Dissertation, Boğaziçi University.

Avcı, A. K., D. L. Trimm, Z. I. Önsan, 2000, "Simulation of alternative catalyst bed configurations in autothermal hydrogen production", *Studies in Surface Science and Catalysis,* Vol. 130, pp. 2753-2758.

Avcı, A. K., D. L. Trimm and Z. İ. Önsan, 2001a, "Heterogeneous Reactor Modeling for Simulation of Catalytic Oxidation and Steam Reforming of Methane", *Chemical Engineering Science*, Vol.56, pp. 641-649.

Avcı, A. K., Z. İ. Önsan and D. L. Trimm, 2001b, "On-board Fuel Conversion for Hydrogen Fuel Cells: Comparison of Different Fuels by Computer Simulations", *Applied Catalysis A: General*, Vol. 216, pp. 243-256.

Avcı, A. K., D. L. Trimm, Z. İ. Önsan, 2002, "Quantitative Investigation of Catalytic Natural Gas Conversion for Hydrogen Fuel Cell Applications", *Chemical Engineering Journal*, Vol. 90, pp. 77-87.

Avcı, A. K., D. L. Trimm, A. E. Aksoylu and Z. İ. Önsan, 2003, "Ignition characteristics of Pt, Ni and Pt–Ni catalysts used for autothermal fuel processing", *Catalysis Letters*, Vol. 88, pp. 17-22.

Bharadwaj, S. S. and L. D. Schmidt, 1995, "Catalytic Partial Oxidation of Natural Gas to Syngas", *Fuel Processing Technology*, Vol. 42, pp. 109-127.

Bradford, M. C. J. and M. A. Vannice, 1996, "Catalytic Reforming of Methane with Carbon Dioxide over Nickel Catalysts II. Reaction Kinetics", *Applied Catalysis A: General*, Vol. 142, pp. 97-122.

Brown, L. F., 2001, "A Comparative Study of Fuels for On-board Hydrogen Production for Fuel-Cell-Powered Automobiles", *International Journal of Hydrogen Energy*, Vol. 26, pp. 381-397.

Burch, R., D. J. Crittle and M. J. Hayes, 1999, "C-H Bond Activation in Hydrocarbon Oxidation on Heterogeneous Catalysts", *Catalysis Today*, Vol. 47, pp. 229-234.

Cheng, X., Z. Shi, N. Glass, L. Zhang, J. Zhang, D. Song, Z.S. Liu, H. Wang and J. Shen, 2007, "A Review of PEM Hydrogen Fuel Cell Contamination: Impacts, Mechanisms and Mitigation", *Journal of Power Sources*, Vol. 165, pp. 739-756.

Chin, S. Y., O. S. Alexeev and M. D. Amiridis, 2005, "Preferential Oxidation of CO under Excess H_2 Conditions over Ru Catalysts", *Applied Catalysis A: General*, Vol. 286, pp. 157-166.

Cho, Y.-H., B. Choi, Y.-H. Cho, H.-S. Park and Y.-E. Sung, "Pd-Based PdPt(19:1)/C Electrocatalyst as an Electrode in PEM Fuel Cell", 2007, *Electrochemistry Communications*, Vol. 9, pp. 378-381.

Choi, Y. and H. G. Stenger, 2003, "Water Gas Shift Reaction Kinetics and Reactor Modeling for Fuel Cell Grade Hydrogen", *Journal of Power Sources*, Vol. 124, pp. 432-439.

Choi, Y. and H. G. Stenger, 2004, "Kinetics, Simulation and Insights for CO Selective Oxidation in Fuel Cell Applications", *Journal of Power Sources*, Vol. 129, pp. 246-254.

Ciaparlu, D. and Pfefferle L., 2001, "Methane Combustion Activity of Supported Palladium catalysts After Partial Reduction", *Applied Catalysis A: General*, Vol. 218, pp. 197-209.

Cipiti, F., V. Recupero, L. Pino, A. Vita and M. Lagana, 2006, "Experimental Analysis of a 2kWe LPG-based Fuel Processor for Polymer Electrolyte Fuel Cells", *Journal of Power Sources*, Vol. 157, pp. 914-920.

Golunski, S., 1998, "HotSpot^{TM} Fuel Processor", *Platinum Metals Review*, Vol. 42, pp. 2-7.

Farias, A. M. D. de, A. P. M. G. Barandas, R. F. Perez and M. A. Fraga, 2007, "Water-Gas Shift reaction over Magnesia-Modified Pt/CeO_2 catalysts", *Journal of Power Sources*, Vol. 165, pp. 854-860.

Fogler, H. S., 1999, *Elements of Chemical Reaction Engineering*, Prentice Hall, New Jersey.

Galvita, V. and K. Sundmacher, 2005, "Hydrogen Production from Methane by Steam Reforming in a Periodically Operated Two-Layer Catalytic Reactor", *Applied Catalysis A: General,* Vol. 289, pp. 121- 127.

Grigoriev, S. A., E. K. Lyutikova, S. Martemianov and V.N. Fateev, 2007, "On the Possibility of Replacement of Pt by Pd in a Hydrogen Electrode of PEM Fuel Cells", *International Journal of Hydrogen Energy*, doi:10.1016/j.ijhydene.2007.02.005.

Hickman, D. A. and L. D. Schmidt, 1992, "Synthesis Gas Formation by Direct Oxidation of Methane over Pt Monoliths", *Journal of Catalysis*, Vol. 138, pp. 267-282.

Hickman, D. A. and L. D. Schmidt, 1993, "Production of Syngas by Direct Catalytic Oxidation of Methane", *Science*, Vol. 259, pp.343-346.

Hirschenhofer, J. H., D. B. Stauffer, R. R. Engleman and M. G. Klett, 1998, *Fuel Cell Handbook*, 4th ed., DOE/FETC-99/1076, US Department of Energy, Federal Energy Technology Center, Morgantown, WV.

Hoang, D. L., S. H. Chan and O. L. Ding, 2006, Hydrogen Production for fuel cells by autothermal reforming of methane over sulfide nickel catalyst on a gamma alumina support", *Journal of Power Sources*, Vol. 159, pp. 1248-1257.

Idakiev, V., T. Tabakova, Z.-Y, Huan, B.-L, Su, 2004, "Gold Catalysts Supported on Mesoporous Titania for Low-Temperature Water-Gas Shift Reaction", *Applied Catalysis:A General*, Vol. 270, pp. 135-141.

Jamal, Y. and M. L. Wyszynski, 1994, "On-Board Generation of Hydrogen-Rich Gaseous Fuels-a Review", *International Journal of Hydrogen Energy*, Vol. 19, pp. 557-572.

Jin, R., Y. Chen, W. Li, W. Cui, Y. Ji, C. Yu and Y. Jiang, 2000, "Mechanism for Catalytic Partial Oxidation of Methane to Syngas over a Ni/Al2O3 Catalyst", *Applied Catalysis A:General*, Vol. 201, pp. 71-80.

Jun, H. J., T. H. Lim, S.-W. Nam, S.-A. Hong and K. J. Yoon, 2006, "Mechanism of Partial Oxidation of Methane Over a Nickel-Calcium Hydroxyapatite catalyst", *Applied Catalysis A: General*, Vol. 312, pp. 27-34.

Kahlich, M. J., H. A. Gasteiger and R. J. Behm, 1997, "Kinetics of the Selective CO Oxidation in H_2-Rich Gas on Pt/Al_2O_3", *Journal of Catalysis*, Vol. 171, pp. 93–105.

Kahlich, M. J., H. A. Gasteiger and R. J. Behm, 1999, "Kinetics of the Selective CO Oxidation in H_2-Rich Gas on $Au/\alpha\text{-}Fe_2O_3$", *Journal of Catalysis*, Vol. 182, pp. 430–440.

Kamarudin, S. K., W. R. W. Daud, A. Md. Som, A. W. Mohammad, S. Takriff and M. S. Masdar, 2004, "The Conceptual Design of a PEMFC System via Simulation", *Chemical Engineering Journal*, Vol. 103, pp. 99-113.

Karakaya, M., 2006, *Dynamic Simulation of Indirect Partial Oxidation Reactor for Methane Conversion to Hydrogen*, M.S. Thesis, Boğaziçi University.

Larentis, A.L., N. S. de Resende, V. M. M. Salim and J. C. Pinto, 2001, "Modeling and Optimization of the Combined Carbon Dioxide Reforming and Partial Oxidation of Natural Gas", *Applied Catalysis A: General*, Vol. 215, pp. 211-224.

Lei, Y., N. W. Cant and, D. L. Trimm, 2006, "The Origin of Rhodium promotion of Fe_3O_4-Cr_2O_3 catalysts for the High-Temperature Water-Gas Shift Reaction", *Journal of Catalysis*, Vol. 229, pp. 227-236.

Li, Y., B. Zhang, X. Thang, Y. Xu and W. Shen, (2006), Hydrogen Production From Methane Decomposition over Ni/CeO_2 Catalysts, *Catalysts Communications*, Vol. 7, pp. 380-386.

Lian, H. L., M. J. Jia, W. C. Pan, W. X. Zhang and D. Z. Jiang, 2006, "Copper Promoted Au/ZnO-CuO Catalysts for Low Temperature Water-gas Shift Reaction", *Chemical Research in Chinese Universities*, Vol. 22, pp. 99-102.

Lin, S.H., Y. H. Chen, C. C. Yu, Y. C. Liu and C. H. Lee, 2005, "Modelling an Experimental Methane Fuel Processor", *Journal of Power Sources*, Vol. 148, pp. 45-53.

Ma, L, 1995, *Hydrogen Production from Steam Reforming of Light Hydrocarbons in an Autothermic System,* Ph.D. Dissertation, University of New South Wales.

Ma, L. and D. L. Trimm, 1996, "Alternative Catalyst Bed Configurations for the Autothermic Conversion of Methane to Hydrogen", *Applied Catalysis A: General*, Vol. 138, pp. 265-273.

Ma, L., D. L. Trimm and C. Jiang, 1996, "The Design and Testing of an Autothermal Reactor for the Conversion of the Light Hydrocarbons to Hydrogen I. The Kinetics of the Catalytic Oxidation of Light Hydrocarbons", *Applied Catalysis A: General*, Vol 138, pp. 275-283.

Michalkiewicz, B., 2006, "The Kinetics of Homogeneous Catalytic Methane Oxidation", *Apllied Catalysis A: General*, Vol. 307, pp. 270-274.

Moretti, E., M. Lenarda, L. Storara, A. Talon, R. Frattini, S. Polizzi, E. Rodriguez-Castellon and A. Jimenez-Lopez, 2007, "Catalytic Purification of Hydrogen Streams by PROX on Cu Supported on an Organized Mesoporous Ceria-Modified Alumina", *Applied Catalysis B: Environmental*, Vol. 72, pp. 149-156.

Muradov, N., 2003, "Emission-Free Fuel Reformers for Mobile and Portable Fuel Cell Applications", 2003, *Journal of Power Sources*, Vol. 118, pp. 320-324.

Muradov, N., Z. Chen and F. Smith, 2005, "Fossil Hydrogen with Reduced CO_2 Emmission: Modeling Thermocatalytic Decomposition of Methane in a Fluidized Bed of Carbon Particles", *International Journal of Hydrogen Energy*, Vol. 30, pp. 1149-1158.

Numaguchi, T. and K. Kikuchi, 1988, "Intrinsic Kinetics and Design Simulation in a Complex Reaction Network: Steam-Methane Reforming", *Chemical Engineering Science*, Vol. 43, 2295-2301.

Örücü, E., 2005, *Computational and Experimental Investigation of Catalytic Hydrogen Production from Ethanol, M.S. Thesis*, Boğaziçi University.

Özkara, S. and A. E. Aksoylu, 2003, "Selective Low Temperature Carbon Monoxide Oxidation in H_2-rich Gas Streams over Activated Carbon Supported Catalysts", *Applied Catalysis A: General*, Vol. 251, pp. 75-83.

Özyönüm, G. N., 2002, *Kinetics of Selective CO Oxidation in Hydrogen-Rich Streams over Pt-Co- Ce/Al_2O_3 catalyst*, M.S. Thesis, Boğaziçi University.

Pena, M. A., J. P. Gomez and J. L. G. Fierro, 1996, "New Catalytic Routes for Syngas and Hydrogen Production", *Applied Catalysis A: General*, Vol. 144, pp. 7-57.

Perry, R. H. and D. W. Green, 1997, *Perry's Chemical Engineers' Handbook*, 7th ed., McGraw-Hill, USA.

Pukrushpan, J., A. Stefanopoulou, S. Varigonda, J. Eborn and C. Haugstetter, 2006, "Contol-Oriented Model of Fuel Processor for Hydrogen Generation in Fuel Cell Applications", *Control Enginering Practice*, Vol. 14, pp. 277-293.

Radhakrishnan, R., R. R. Willagan, Z. Dardas and T. H. Vanderspurt, 2006, "Water Gas Shift Activity and Kinetics of Pt/Re Catalysts Supported on Ceria-Zirconia Oxides", *Applied Catalysis B: Environmental*, Vol. 66, pp. 23-28.

Ralph, T. R. and G. A. Hards, 1998, "Powering the Cars and Homes for Tomorrow", *Chemistry & Industry,* Vol. 9, pp. 337-342.

Rase, H. F., 1990, *Fixed-Bed Reactor Design and Diagnostics*, London: Butterworths.

Reuse, P., A. Renken, K. Haas-Santo, O. Görke and K. Schubert, 2004, "Hydrogen production for fuel cell application in an autothermal micro-channel reactor", *Chemical Engineering Journal*, Vol. 101, pp. 133-141.

Rosa, F., E. Lopez, Y. Briceno, D. Sopena, R. M. Navarro, M. C. Alvarez-Galvan, J.L. G. Fierro and C. Bordons, 2006, "Design of a Diesel Reformer Coupled to a PEMFC", *Catalysis Today*, Vol. 116, pp. 324-333.

Ross, J. R. H., 1974, Surface and Defect properties of Solids, in M. W. Roberts and J. M. Thomas (Eds.), *Chemical Society*, Vol. 4, pp.34, London.

Rossignol, C., S. Arrii, F. Morfin, L. Piccolo, V. Caps and J-L. Rousset, 2005, "Selective Oxidation of CO over Model Gold-Based Catalysts in the Presence of H2", Journal of Catalysis, Vol. 230, pp. 476-483.

Rostrup-Nielsen, J. R., 1984, "Catalytic Steam Reforming", in J. R. Anderson and M. Boudart (Eds.), *Catalysis, Science & Technology*, Vol. 5, pp. 1-117, Springer-Verlag, Berlin.

Rostrup-Nielsen, J. R., 1998, "Methane Conversion", in D. M. Bibley (Eds.), Elsevier, Amsterdam.

Saito, M., K. Tomada, I. Takahara, K. Murata and M. Inaba, 2003, "Effects of Pretreatment of Cu/ZnO-based Catalysts on Their Activities for the Water-Gas Shift Reaction", *Catalysis Letters*, Vol. 89, pp. 11-13.

Satyapal, S., J. Petrovic, C. Read, G. Thomas, G. Ordaz, 2007, "The U.S. Department of Energy's National Hydrogen Storage Project: Progress Towards Meeting Hydrogen-Powered Vehicle Requirements", *Catalysis Today*, Vol. 120, pp. 240-256.

Schmidt, V. M., P. Bröcherhoff, B. Höhlein, R. Menzer and U. Stimmung, 1994, "Utilization of Methanol for Polymer Electrolyte Fuel Cells in Mobile Systems", *Journal of Power Sources*, Vol. 49, pp. 299-313.

Schubert, M. M., A. Venugopal, M. J. Kahlich, V. Plzak and R. J. Behm, 2004, "Influence of H_2O and CO_2 on the Selective CO Oxidation in H_2-rich Gases over Au/α-Fe_2O_3", *Journal of Catalysis*, Vol. 222, pp. 32-40.

Sedmak, G., S. Hocevar and J. Levec, 2003, "Kinetics of Selective CO Oxidation in Excess of H_2 over the Nanostructured $Cu_{0.1}Ce_{0.9}O_{2-y}$ Catalyst", *Journal of Catalysis*, Vol. 213, pp. 135-150.

Selen, B., 2003, *Production of Hydrogen from Light Hydrocarbons via Indirect Partial Oxidation on Bimetallic Catalysts,* M.S. Thesis, Boğaziçi University.

Seo, Y. T., D. J. Seo, J. H. Jeong and W. L. Yoon, 2006, "Design of an Integrated Fuel Processor for Residential PEMFCs Applications", *Journal of Power Sources*, Vol. 160, pp. 505-509.

Seymour, E. H., F. C. Borges, R. Fernandes, 2007, "Indicators of European Public Research in Hydrogen and Fuel Cells –An Input-Output Analysis", *International Journal of Hydrogen Energy*, doi: 10.1016/j.ijhydene.2007.02.031.

Sinnot, R. K., 1993, *Coulson's & Richardson's Chemical Engineering*, *Design*, Vol. 6., 2nd ed., Butterworth–Heinemann, London.

Shampine, L. F. and M. W. Reichelt, 1997, "The MATLAB ODE Suite," *SIAM Journal on Scientific Computing*, Vol. 18, pp 1-22.

Shampine, L. F., M. W. Reichelt, and J.A. Kierzenka, 1999 "Solving Index-1 DAEs in MATLAB and Simulink," *SIAM Review*, Vol. 41, pp 538-552.

Shao, Y., G. Yin, Z. Wang, Y. Gao, 2007, "Proton Exchange Membrane Fuel Cell From Low Temperature to High Temperature: Material Challenges", *Journal of Power Sources*, Vol. 167, pp. 235-242.

Shishido, T., M. Yamamoto, D. Li, Y. Tian, H. Moriaka, M. Honda, T. Sano and K. Takehira, 2006, "Water-Gas Shift Reaction over Cu/ZnO and Cu/ZnO/Al_2O_3 Catalysts Prepared by Homogeneous Precipitation", *Applied Catalysis A: General*, Vol. 303, pp. 62-71.

Song, C., 2002, "Fuel Processing for Low-Temperature and High-Temperature Fuel Cells. Challenges and Opportunities for Sustainable Development in the 21st Century", *Catalysis Today*, Vol. 77, pp. 17-49.

Springmann, S., M. Bohnet, A. Docter, A. Lamm and G. Eigenberger, 2004, "Cold Start Simulations of a Gasoline Based Fuel Processor for Mobile Fuel Cell Applications", *Journal of Power Sources*, Vol. 128, pp. 13-24.

Sun, J., J. DesJardins, J. Buglass and K. Liu, 2005, "Noble Metal Water Gas Shift Catalysis: Kinetic Study and Reactor Design", *International Journal of Hydrogen Energy*, Vol. 30, pp. 1259-1264.

Şimşek, E., Ş. Özkara, A. E. Aksoylu and Z. İ., Önsan, 2007, "Preferential CO Oxidation over Activated Carbon Supported Catalysts in H_2-Rich Gas Streams Containing CO_2 and H_2O", *Applied Catalysis A: General*, Vol. 316, pp. 169-174.

Tabakova, T., V. Idakiev, D. Andreeva and I. Mitov, 2000, "Influence of the Microscopic Properties of the Support on the Catalytic Activity of Au/ZnO, Au/ZrO_2, Au/Fe_2O_3, Au/Fe_2O_3–ZnO, Au/Fe_2O_3–ZrO_2 Catalysts for the WGS Reaction", *Applied Catalysis A: General*, Vol. 202, pp. 91-97.

Thomas, C. E., B. D. James, F. D. Lomax Jr. and I. F. Kuhn Jr, 2000, "Fuel Options for the Fuel Cell Vehicle: Hydrogen, Methanol or Gasoline?", *International Journal of Hydrogen Energy*, Vol. 25, pp. 551-567.

Trimm, D. L., 1999, "Catalysts for the Control of Coking During Steam Reforming", *Catalysis Today*, Vol. 49, pp. 3-10.

Trimm, D. L. and C. W. Lam, 1980, "The Combustion of Methane on Platinum-Alumina Fibre Catalysts", *Chemical Engineering Science*, Vol. 35, pp. 1405-1413.

Trimm, L. and Z. İ. Önsan, 2001, "On-board Fuel Conversion for Hydrogen-Fuel-Cell-Driven Vehicles", *Catalysis Reviews: Science and Engineering*, Vol.43, pp. 31-84.

Trimm, L. and Z. İ. Önsan, 2001, "On-board Fuel Conversion for Hydrogen-Fuel-Cell-Driven Vehicles", *Catalysis Reviews: Science and Engineering*, Vol.43, pp. 31-84.

Twigg, M. V. (editor), 1989, *Catalyst Handbook*, Wolf Scientific Text: London.

Utaka, T. K., K. Sekizawa and K. Eguchi, 2000, "CO Removal by Oxygen-Assisted Water Gas Shift Reaction over Supported Cu Catalysts", *Applied Catalysis A: General*, Vol. 194-195, pp. 21-26.

Veser, G. and L. D. Schmidt, 1996, "Ignition and Extinction in the Catalytic Oxidation of Hydrocarbons over Platinum", *AIChE Journal*, Vol. 42, pp. 1077-1087.

Watanabe, M., H. Igarashi M. Suzuki, Y. Sasaki and H. Uchida, 1997, "Removal of Carbon Monoxide from Hydrogen-Rich Fuels by Selective Oxidation Over Platinum Catalyst Supported on Zeolite", Applied Catalysis A: General, Vol. 159, pp. 159-169.

Xu, J. and G. F. Froment, 1989, "Methane Steam Reforming, Methanation and Water-Gas Shift: I. Intrinsic Kinetics", *AIChE Journal*, Vol. 35, pp. 88-96.

Yan, Q. G., T. H. Wu, W. Z. Weng, H. Toghiani, R. K. Toghiani, H. L. Wan and C. U. Pittman Jr., 2004, "Partial Oxidation of Methane to H_2 and CO over Rh/SiO_2 and Ru/SiO_2 catalysts", *Journal of Catalysis*, Vol. 226, pp. 247-259.

Zaidi, S. M. J., S. U. Rahman, H. H. Redhwi, 2007, "R&D Activities of Fuel Cell Research at KFUPM", *Desalination*, Vol. 209, pp. 319-327.

Zalc, J. M., D. G. Löffler, 2002, "Fuel Processing for PEM Fuel Cells: Transport and Kinetic Issues of System Design", *Journal of Power Sources*, Vol. 111, pp. 58-64.

Zeng, R., Y. Wang, S. Wang and P. K. Shen, 2007, "Homogeneous Synthesis of PFSI/Silica Composite Membrane for PEMFC Operating at Low Humidity", *Electrochimica Acta*, Vol. 52, pp.3895-3890.